

INAUGURAL - DISSERTATION

zur
Erlangung der Doktorwürde
der
Naturwissenschaftlich - Mathematischen Gesamtfakultät
der
Ruprecht - Karls - Universität Heidelberg

vorgelegt von
Dipl.-Phys. Sabine Frink
aus **Limburg an der Lahn**

Tag der mündlichen Prüfung: 10.2.1999

KINEMATICS OF T TAURI STARS
IN NEARBY STAR FORMING REGIONS

Gutachter: Prof. Dr. Burkhard Fuchs
Prof. Dr. Joachim Krautter

Kinematik von T Tauri Sternen in nahen Sternentstehungsgebieten

Die Kinematik von T Tauri Sternen in den nahen Sternentstehungsgebieten Taurus-Auriga, Chamaeleon, Lupus und Scorpius-Centaurus wird mit Hilfe von Eigenbewegungen aus den Hipparcos-, PPM-, ACT-, TRC- und STARNET-Katalogen untersucht. Der STARNET-Katalog eignet sich dafür besonders gut, da er genaue Eigenbewegungen für 4.3 Millionen Sterne enthält und somit auch ein Großteil der T Tauri Sterne im Katalog vorhanden ist. Hipparcos Parallaxen und Radialgeschwindigkeiten werden, soweit verfügbar, in Verbindung mit den Eigenbewegungen dazu benutzt, Raumgeschwindigkeiten und Geschwindigkeitsdispersionen abzuleiten. Die günstige Geometrie der Scorpius-Centaurus Assoziation erlaubt zusätzlich die Bestimmung von kinematischen Entfernungen.

Viele der untersuchten Sterne gehören zur umfangreichen Population von weak-line T Tauri Sternen, die mit Hilfe des Röntgensatelliten ROSAT während der letzten Jahre entdeckt worden sind. Im Gegensatz zu klassischen T Tauri Sternen, die man vorwiegend in unmittelbarer Nähe der dichtesten Wolkenstrukturen in diesen Sternentstehungsgebieten fand, sind die weak-line T Tauri Sterne über größere Gebiete im Raum verteilt. Die Prozesse, die zu diesen beobachteten Halos von weak-line T Tauri Sternen führen können, sollten sich kinematisch bemerkbar gemacht haben, und die beobachteten Bewegungen der Sterne werden im Rahmen verschiedener Sternentstehungsszenarien analysiert.

Kinematics of T Tauri Stars in nearby Star Forming Regions

The kinematics of T Tauri stars in the nearby star forming regions Taurus-Auriga, Chamaeleon, Lupus and Scorpius-Centaurus is studied using proper motions from the Hipparcos, PPM, ACT, TRC and STARNET proper motion catalogues. Especially the STARNET catalogue is very well suited for this purpose as it provides accurate proper motions for about 4.3 million stars, so that a large number of T Tauri stars is included in that catalogue. Where available, Hipparcos parallaxes and radial velocities are combined with the proper motions to calculate space velocities and velocity dispersions. In the Scorpius-Centaurus association, the favourable geometry allows for the determination of kinematical distances.

A large fraction of the stars in the samples belongs to the population of weak-line T Tauri stars discovered with the help of the X-ray satellite ROSAT during the last years. In contrast to classical T Tauri stars, which had preferentially been found very close to the densest cores of the cloud material in those star forming regions, weak-line T Tauri stars are distributed over larger regions in space. The kinematic signatures of processes producing such halos of weak-line T Tauri stars should still be visible, and the observed motions of the stars are analyzed in the framework of various star formation scenarios.

Contents

1	Introduction	1
1.1	Outline	1
1.2	T Tauri stars	1
1.3	Proper motion catalogues	5
1.3.1	Transformation of PPM and STARNET to ICRS system	6
2	Taurus-Auriga	11
2.1	Overview	11
2.2	Data	11
2.2.1	Proper motions of PMS stars	11
2.2.2	High proper motion stars	15
2.2.3	Distance to Taurus-Auriga	15
2.3	Kinematics	15
2.3.1	Velocity dispersion	15
2.3.2	Space velocities	17
2.3.3	Search for high velocity escapers	19
2.3.4	Relation of the southern stars to Taurus-Auriga	20
2.4	High proper motion stars	22
2.4.1	Verification of high proper motions	22
2.4.2	Pleiades membership	23
2.5	Summary	23
3	Chamaeleon	25
3.1	Overview	25
3.2	Data	26
3.2.1	The samples	26
3.2.2	Discordant proper motions	27
3.3	Kinematics	29
3.3.1	Proper motions	29
3.3.2	Space velocities	32

3.4	Discussion	33
3.4.1	Structure of the Chamaeleon clouds	33
3.4.2	Implications for the formation scenario of the Chamaeleon cloud complex	34
3.5	Summary	36
4	Lupus	37
4.1	Overview	37
4.2	Data	38
4.2.1	Pre-main sequence stars known before ROSAT	38
4.2.2	Pre-main sequence stars discovered with ROSAT	38
4.3	Proper motions	40
4.4	Space velocities	42
4.5	Summary	44
5	Scorpius-Centaurus	45
5.1	Overview	45
5.2	Data	46
5.2.1	Early-type stars	46
5.2.2	Late-type stars	46
5.3	Positions and proper motions	49
5.4	Derivation of kinematical distances	49
5.4.1	Method	49
5.4.2	Results	51
5.4.3	Hertzsprung-Russell diagram	55
5.5	Summary	56
6	Conclusions	57
6.1	Comparison with simulations	57
6.2	Comparison of the results in different SFR	59
6.3	Outlook	61
	References	63
A	Appendix	69

1 Introduction

1.1 Outline

With the help of the German X-ray satellite ROSAT a large population of very young stars, so-called weak-line T Tauri stars, has been discovered in and around several nearby star forming regions. Whereas the classical T Tauri stars had only been found very close to the densest cores of the cloud material in those star forming regions, it was a big surprise that the weak-line T Tauri stars discovered by ROSAT are distributed over the whole region and even further out. But where did these stars form? Did they form in the dense cloud cores and travel to their current positions? Or did they form where they are observed now, implying the need for a modification of the standard theory of star formation?

Comparisons with theoretical isochrones in the Hertzsprung-Russell diagram showed that most of the stars are really very young so that we are not dealing with a population of older post T Tauri stars which could have had enough time to travel to their current locations at moderate relative velocities. On the contrary, some of the stars of the wide-spread population of weak-line T Tauri stars are even younger than the classical T Tauri stars.

The velocities of the weak-line T Tauri stars play a crucial role in answering the question of their birthplaces. While radial velocities are accessible by direct observations, the availability of proper motion catalogues is essential to get information about the two velocity components projected on the sky. Very recently several proper motion catalogues have become available which are very well suited for the above sketched purpose: the Hipparcos, PPM, ACT, TRC and STARNET catalogues.

With these catalogues the database of stars with known proper motions is large enough to study the kinematics of each of the associations, i. e. the determination of the mean proper motion of the cluster, of members and potential escapers, the velocity dispersion and hopefully constraints on the distances. On the basis of these kinematical studies, the relation of the weak-line T Tauri stars (especially those located outside the adopted boundaries of the star forming regions) to the classical T Tauri stars will be investigated with the aim of deriving constraints on their birthplaces.

1.2 T Tauri stars

Discovery of the classical T Tauri stars

T Tauri stars (TTS) are very young ($10^5 - 10^7$ yrs) pre-main sequence (PMS) stars of late spectral types (F7–M) and masses between 0.1 and $3 M_{\odot}$. They were introduced as a separate class of stars and named after their most prominent representative, T Tauri, by Joy (1945), who characterized them as being slightly irregularly variable in the optical and in their emission line strength.

Ambartsumian (1947) deduced from their location in the Hertzsprung-Russell (HR) diagram that TTS must be of very young age and low mass and introduced the term *T association* for the T Tauri groups as low-mass counterparts to the more famous OB associations.

Objective prism surveys conducted in the following led to the discovery of a few hundred TTS which were preferentially located in the cloud cores of nearby star forming regions (SFR) (see catalogues by Herbig 1962, Herbig & Rao 1972, Schwartz 1977, Herbig & Bell 1988). Observational evidence for identification as TTS include H_{α} emission and infrared excess (for definitions of the TTS class, see Herbig (1962) and Bastian et al. (1983)). Other characteristics of the spectrum include Ca II H and K emission lines and lithium in absorption.

Earlier attempts to explain the observed correlation between TTS and dark clouds invoked accretion on field stars while flying through the cloud, but this hypothesis had to be rejected later on when it became clear that TTS are kinematically linked to the clouds, with rather small velocity dispersions (Herbig 1962). Systematic radial velocity (Herbig 1977) and proper motion surveys (Jones & Herbig 1979) supported this finding.

Discovery of the weak-line T Tauri stars

Based on a variety of different arguments it has been speculated that there might exist many more TTS with an H_α equivalent width smaller than about 5–10 Å. Jones & Herbig (1979) concluded from an analysis of the proper motions of field stars and of TTS in the Taurus-Auriga region that there are some more stars in the field star sample with kinematics similar to the TTS than expected when all the PMS were already known. Judging from the distribution of H_α equivalent widths of known TTS Herbig (1985) arrived at a similar conclusion.

Observations made with the Einstein Observatory launched in 1978 showed a clear correlation between SFR and the number of X-ray sources in the sky, some of which could be identified with known TTS (Ku & Chanan 1979, Feigelson & DeCampi 1981). Others turned out to be low-mass pre-main sequence stars as well, but without the characteristic strong emission lines and IR excesses of the TTS known until then (Feigelson & Kriss 1981, Walter & Kuhi 1981).

In contrast to the well-known classical TTS (CTTS) these were now called naked TTS (NTTS), because they have no dense matter surrounding them (Walter 1986), or more phenomenologically weak-line TTS (WTTS) (Herbig & Bell 1988). The limit between WTTS and CTTS was set at an H_α equivalent width of 10 Å. Since the distribution of line widths is smooth and line widths themselves are variable this is a bit arbitrarily, but nevertheless it turned out to be a meaningful division.

Now that it was clear that young PMS stars could be discovered by their X-ray emission, new results could be expected from the ROSAT X-ray satellite launched in 1990. ROSAT performed, besides so-called pointed observations, an All-Sky Survey (RASS) in several X-ray bands. From this large database likely PMS candidate stars could be extracted using their hardness ratios (which relate the count rates in the soft and hard energy bands) as discrimination criterium (Neuhäuser et al. 1995a, Sterzik et al. 1995), and a lot of these stars really turned out to be very young TTS in optical follow-up observations. The regions studied were chosen such that they comprised the suspected sites of star formation in the dark clouds on a large scale. However, it turned out that the chosen boundaries were too small to encompass the whole wide-spread population of WTTS, and larger study areas outside the traditional star formation regions were defined (*Taurus-Auriga*: Wichmann et al. 1996, Neuhäuser et al. 1995c, Neuhäuser et al. 1997, Magazzí et al. 1997; *Chamaeleon*: Alcalá et al. 1995, Alcalá et al. 1996, Covino et al. 1997; *Lupus*: Krautter et al. 1997, Wichmann et al. 1997a, Wichmann et al. 1997b; *Orion*: Sterzik et al. 1995, Alcalá et al. 1996, Alcalá et al. 1998; *Upper Scorpius*: Kunkel et al. 1999, Preibisch et al. 1998a).

Indeed a lot of WTTS were found also up to several tens of parsec away from the known sites of star formation. The aim of this thesis is to unravel the kinematical relation of this population of stars to the CTTS found preferentially in the dense cloud cores.

Nature of the X-ray emission

The X-ray emission from TTS is likely to be caused by a solar-like dynamo. TTS are known to rotate with periods typically smaller than 10 days (see e.g. Bouvier et al. 1997, Wichmann et al. 1998a) and to have strong magnetic fields of the order of 1–2 kG (Guenther & Lehmann 1998, Guenther et al. 1999). Initially TTS rotate slowly, because the stellar magnetic field is coupled to the magnetic field of the disk. After disk dissipation the star speeds up, and this fast rotation in turn supports and disturbs the magnetic field. 10^7 K hot gas in outbreking magnetic field tubes causes the observed X-ray emission, which is typically 1000 times stronger than that from the Sun.

Age determination

A very important parameter which enters in all the studies of star formation, the evolutionary status of CTTS and WTTS and particularly in interpreting the observed locations of these stars far from the known cloud material is the age of these stars. In principle it could be determined by placing each star in the HR diagram and by comparing its position with theoretical pre-main sequence tracks. For most of the stars however individual distances are not known, and assuming the mean distance of the corresponding SFR may introduce large errors since the depth of these regions can be expected to be similar to their observed projected distances on the sky (typical values are 10° or 26 pc at a distance of 150 pc).

Fortunately, there is another quantity easily accessible by observations which can serve as a youth indicator: the strength of the Li I absorption line ($\lambda = 6707.7 \text{ \AA}$). Since lithium is destroyed very rapidly in the stellar interior through proton capture processes at temperatures above $2.5 \cdot 10^6 \text{ K}$ (Bodenheimer 1965), its presence in the outer layers of convective stars indicates the youth of a star.

The lithium criterion, which is now very common in the literature (e.g. Neuhäuser et al. 1997), compares the lithium line widths of stars of unknown age with that of stars of the same spectral type and known age (usually stars from young clusters like the Pleiades or IC 2602). In this way the sample of stars with unknown ages can be divided at least in three parts with ages lower than, comparable to and higher than the age of the reference sample, respectively.

For some TTS (CTTS suggested to be included in the Hipparcos Input Catalogue as well as some WTTS included 'by accident') precise parallaxes have been measured by Hipparcos, so that they can reliably be placed in the HR diagram. All of them lie above the main sequence and therefore turn out to be really very young (Neuhäuser & Brandner 1998).

Pre-main sequence evolution

According to the current picture of single low-mass star formation the first stage is a class I protostar emerging from a gravitational collapsing cloud core. X-ray emission attributed to class I sources has been detected by ASCA (Koyama et al. 1996) and ROSAT (Casanova et al. 1995, Neuhäuser & Preibisch 1997).

In the subsequent evolution a disk forms from which the central object accretes further material, until it becomes a classical TTS that appears on the birthline in the HR diagram. In this stage it is fully convective and contracts down the Hayashi track in the HR diagram, turning on to the radiative tracks when a radiative core has developed. Evolutionary tracks for different opacities and convection models have been computed by D'Antona & Mazzitelli (1994).

After dissipation of the disk, the CTTS possibly evolves into a WTTS. It is not clear however whether all WTTS emerge from CTTS, or whether they could already be born as WTTS. Furthermore, there are examples for WTTS showing infrared excess, an indication for a surrounding disk (Strom et al. 1989), and age distributions from WTTS and CTTS do not differ significantly. Weaver (1983) already noticed that there is no correlation between emission line strength and age, and indeed there are examples for very young WTTS (e.g. Alcalá 1996).

If the above picture is roughly correct this would imply large variations for the disk dissipation timescales, which are of primary importance for models of planet formation (see Beckwith & Sargent 1996 for a recent review). However, most TTS seem to be binary or multiple systems without disks, with individual disks or with one common disk, and interactions may severely affect the simple model sketched above.

Binary properties

The observed overall binary frequency among main sequence stars varies from 65% to 100% (Duquennoy & Mayor 1991). Investigations of the binary frequency among pre-main sequence stars reveal no significant deviations from the main sequence value at least in the regions of Chamaeleon, Lupus, Upper Scorpius and ρ Ophiuchi (Brandner et al. 1996), so that it is concluded that binary properties are not subject to

major changes during stellar evolution. Furthermore, there are no differences between WTTS and CTTS binary distributions found in these studies.

The binary frequency among PMS stars in Taurus-Auriga however is significantly higher by a factor of about 2 than the corresponding main sequence value (Köhler & Leinert 1998). It seems likely to attribute this difference in PMS binary frequencies to environmental effects (Brandner & Köhler 1998).

The Taurus-Auriga SFR is the canonical example for the distributed mode of star formation, with relatively low density and large extent. In contrast to this, the Trapezium cluster is a representative for the clustered mode of star formation, with a very high density and a high degree of concentration. The PMS binary frequency in the Trapezium cluster is again indistinguishable from that of the main sequence (Petr et al. 1998).

Interestingly, Brandner & Köhler (1998) have found different binary distributions in adjacent parts of the Scorpius-Centaurus association and attributed it to distinctive environmental conditions as e.g. the presence or absence of early type stars.

Simulations carried out by Kroupa (1998) however suggest that this may be a consequence of dynamical interactions. Binary properties are effected significantly during the dynamical evolution of a cluster, so that an initially unique IMF and binary distribution can evolve into quite different binary distributions in rather close regions on the sky.

Nature of the ROSAT discovered WTTS population

There has been some debate in the past concerning the question whether the lithium rich stars discovered with the help of ROSAT are really very young PMS stars. Briceño et al. (1997) put forward a simple model based on the assumption of a constant star formation rate which could reproduce the observed properties of the ROSAT discovered stars like X-ray luminosity and hardness ratios, spectral characteristics, visual magnitudes and spatial distribution. The stars in their model are young active main sequence stars with typical distances of 110–120 pc, slightly nearer than most of the nearby SFR.

Indeed the lithium equivalent widths of some of the ROSAT discovered WTTS had been overestimated in earlier low resolution spectroscopy studies due to line blending with nearby iron lines and the unknown positioning of the continuum (Covino et al. 1997), which led to the derivation of smaller ages for these stars. The same argument has been used also by Favata et al. (1997), who argue for a population of young and active main sequence rather than pre-main sequence stars, similar to Briceño et al. (1997).

Post T Tauri stars

Herbig (1973, 1978) was the first who noted that there was a lack of older TTS ($> 5 - 10$ Myr) among the populations studied so far and gave this missing population the name post T Tauri stars (PTTS). Nearly two decades later, Feigelson (1996) considered the problem as even more serious than before since all search strategies to track down these mysterious stars had failed. Assuming a constant star formation rate, the number of missing stars would be of the order of hundreds or thousands in the star forming regions Chamaeleon and Taurus, respectively, which in turn would imply a much higher star formation efficiency than the canonical few percent put forward by Cohen & Kuhn in 1979.

Recently, Palla & Galli (1997) have shown that all these problems can be circumvented by a star formation efficiency which is very low initially, but steeply rises when the conditions for gravitational collapse in the cloud are established. This is achieved through redistribution of magnetic flux by ambipolar diffusion, and the timescales for typical clouds are of the order of 10 Myr or so, a large fraction of the whole cloud's lifetime.

Palla & Galli (1997) conclude that the missing PTTS no longer constitute a serious problem, since according to their theory of star formation the PTTS population should not exist at all.

1.3 Proper motion catalogues

The availability of accurate proper motion catalogues extending to faint magnitudes is essential for the type of kinematical study aimed in this thesis. The typical accuracy of the older proper motion catalogues like SAO (SAO Staff 1966) or AGK3 (Heckmann & Dieckvoss 1975) of about 10–15 mas/a was not sufficient. At a typical distance of 150 pc for the nearby SFR, this uncertainty translates to 7–10 km/s in one coordinate, which is of the order of the expected total velocity itself. On the other hand proper motions in the FK5 (Fricke et al. 1988) are rather accurate (better than 1 mas/a), but are provided only for a very small number of stars.

Usually, much better accuracies can be achieved in small areas on the sky by using relative proper motions. These relative proper motions are well suited to distinguish member from non-member stars in small-scale aggregates like open clusters, but they do not carry information on large-scale systematic motions like expansion or rotation over the whole region. Moreover the TTS and especially the weak-line TTS discovered with the help of ROSAT populate a rather large region, so that a deep all-sky catalogue of proper motions is required to study their kinematics.

Fortunately, several new proper motion catalogues have become available during the last decade. The properties of each of these catalogues used in this study are given below in more detail.

Hipparcos Catalogue

The Hipparcos Catalogue (ESA 1997) is the major outcome of the Hipparcos Space Astrometry Mission. It contains 118 218 stars and provides, among other astrometric and photometric data, proper motions with a median accuracy smaller than 1 mas/a and parallaxes with a median precision better than 1 mas for stars brighter than 9th magnitude. The International Celestial Reference Frame ICRS, of which the Hipparcos Catalogue is the optical representation, supersedes the FK5 system, and deviations from an inertial system are smaller than 0.25 mas/a in total.

The Hipparcos satellite was launched in 1988 and operated for about 3 1/2 years. Positions, proper motion and parallaxes were determined by means of a least squares fit to all the astrometric abscissae available for a particular star. At a typical distance of 150 pc for the nearby SFR investigated in this thesis, the accuracies achieved with Hipparcos parallaxes translate into 20 pc or 15 % for distances and those of the proper motions into 0.7 km/s for tangential velocities.

The proper motions for all stars solved without a specific double star treatment reflect the mean motion during these 3 1/2 years of observations. This means that the proper motion for unrecognized double or multiple systems is partly made up of orbital motion and may differ significantly from the proper motion of the centre of mass of the system (Wielen 1997). For this reason Hipparcos proper motions for suspected double stars have to be treated with great care and should be checked wherever possible with proper motions based on larger epoch differences (see Appendix).

PPM Catalogue

The PPM Catalogue (Röser & Bastian 1991, Bastian et al. 1993, Röser et al. 1994) is a compilation catalogue, which means that its positions and proper motions were calculated using the observations published in different catalogues over the past century. Typically, more than 6 observations per star could be collected. The fact that there is some redundancy present in these multiple positions avoided coarse errors like misidentifications or other errors in the source catalogues. PPM North, South, and Southern Extension contain 468 586 stars in total, and the typical proper motion error is around 3 mas/a. The PPM has been constructed in the FK5 system and has to be transformed to the ICRS for comparison with proper motions based on that system. For this work this has been done in the limited regions of the sky which are of interest here, and the procedure will be described in section 1.3.1.

In principle, the PPM is superseded by the ACT/TRC catalogues, which contain more stars with similar or slightly better accuracies already in the ICRS system. However, in the context of the double

star problem mentioned above it is always useful to have another partly independent proper motion estimate, and so the PPM proper motions are used for comparison in doubtful cases.

ACT/TRC Catalogues

The ACT Reference Catalog (Urban et al. 1997) and the Tycho Reference Catalogue (TRC, Høg et al. 1998) were both derived from the same observational material, but with a quite different reduction philosophy. For both catalogues the first epoch is provided by the Astrographic Catalogue (AC), whereas as second epoch data the Tycho Catalogue (ESA 1997) is used.

For the derivation of ACT, the Astrographic Catalogue Reference Stars (ACRS, Corbin & Urban 1991) was directly transformed to the ICRS and then matched with Tycho to derive proper motions. For the identification process the Tycho proper motions were used.

In contrast to this, for the construction of the TRC the original AC was directly transformed to the ICRS with the help of ACRS and HIP. In several intermediate steps systematic (e.g. magnitude-dependent) residuals which were found by direct comparison of preliminary TRC and HIP were removed. The identification of AC and Tycho stars did not use any astrometric quantities except for the positions, but sometimes magnitudes were used to resolve doubtful cases.

ACT contains 988 758 stars and TRC 990 182 stars, but only 950 290 stars are common to both catalogues. Proper motion accuracies are similar, around 2.5 mas/a. However, there are rather large differences between the proper motions from ACT and TRC, with the median of 2.65 mas/a being slightly larger than the internal standard errors (Høg et al. 1998).

Where available both proper motions will be given for a particular star in the Appendix, and by comparison with possible entries from other catalogues the most likely proper motion will be adopted. A slight preference however is given to TRC, as it is based on a more rigorous reduction.

STARNET Catalogue

The STARNET Catalogue (Röser 1996) is based again on the Astrographic Catalogue as first epoch. As second epoch the Guide Star Catalog (Lasker et al. 1990, Russell et al. 1990, Jenkner et al. 1990) in version GSC 1.2 (Röser et al. 1997) was used.

Its big advantage is the large number of stars that it contains, namely 4 278 947 stars up to $V \approx 12 - 13$ mag. The proper motion errors are slightly larger than in the other proper motion catalogues mentioned so far, about 5 mas/a. However, such proper motions are still useful for kinematical studies (at a distance of 150 pc 5 mas/a correspond to 3.5 km/s), and for many TTS the STARNET proper motion is the only one available.

Presently the STARNET catalogue (like the PPM catalogue) is still in the FK5 system, and so it has been transformed to ICRS as described in the next section.

1.3.1 Transformation of PPM and STARNET to ICRS system

In order to compare proper motions from different catalogues, it is essential that they refer to the same astrometric system. Otherwise at least part of the deviation will be made up of systematic differences between the two systems. The best astrometric system known to date is the so-called International Celestial Reference System ICRS which is quasi-inertial (Kovalevsky 1997). It is represented by the Hipparcos Catalogue in the optical, and a great effort has been undertaken to establish an extragalactic link, thereby minimizing possible spurious motions (Lindgren & Kovalevsky 1995).

Systematic differences to the FK5 system which was used before the Hipparcos era were shown to be quite large in some regions of the sky, up to about 250 mas in positions (Lindgren 1992). Given the epoch difference of about 37 years between the mean epochs of Hipparcos (1991.25) and FK5 (1954), this translates into proper motion differences of the order of up to 7 mas/a.

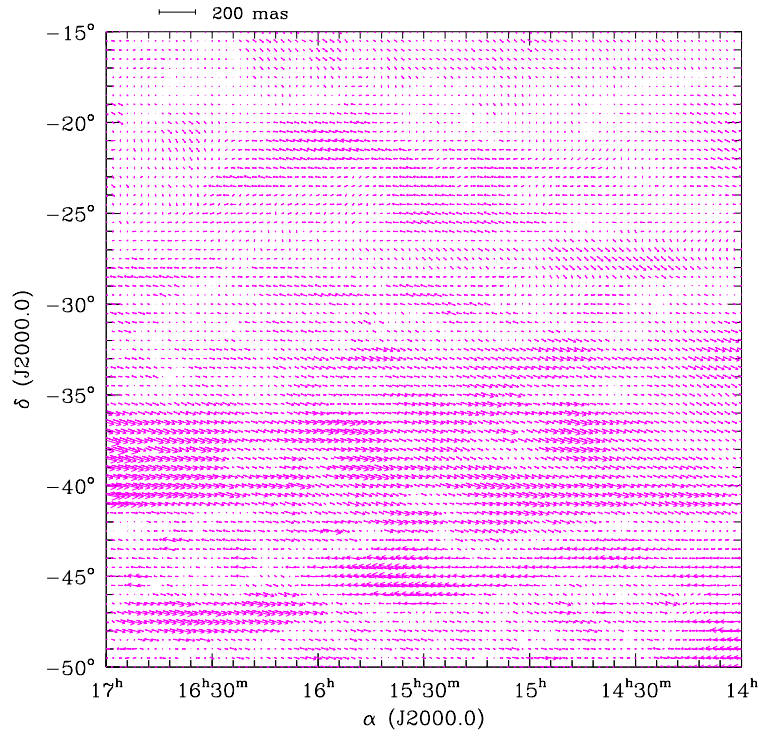


Figure 1.1: Systematic differences of the positions between PPM stars (FK5) and Hipparcos stars (ICRS) in the region of Scorpius-Centaurus. At each grid point the residuals of the 15 nearest stars common to both catalogues were averaged and are given in the sense FK5–ICRS. The largest systematic difference in the region shown here is 170 mas, the median of these differences is 22 mas.

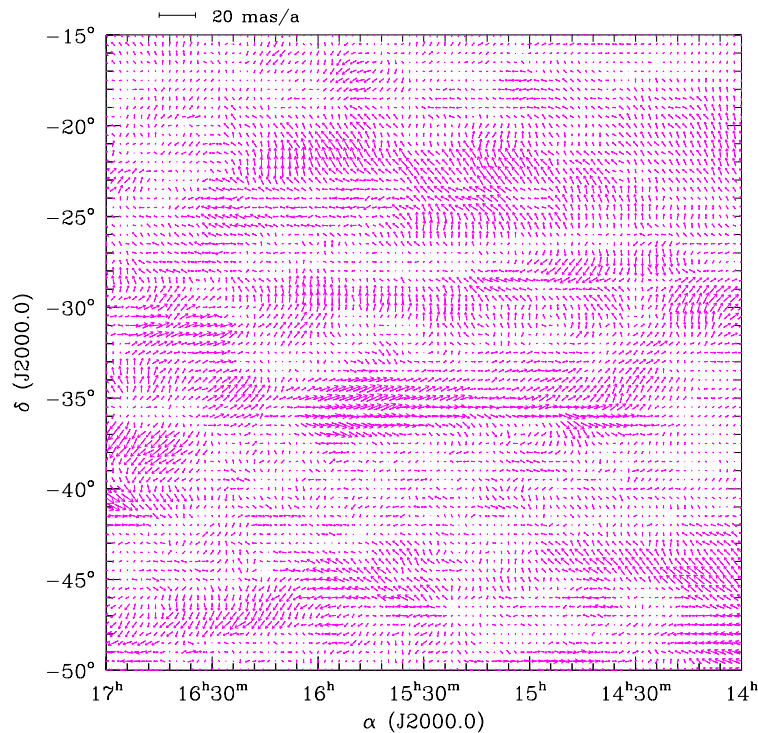


Figure 1.2: Systematic differences of the proper motions between PPM stars (FK5) and Hipparcos stars (ICRS) in the region of Scorpius-Centaurus, calculated in the same way as the positional differences shown in Fig. 1.1. The largest vector in the region shown here corresponds to 12 mas/a, the median of the systematic proper motion differences is 2.8 mas/a.

In order to be able to use data from catalogues still available only in the FK5 system (PPM and STARNET), a simple reduction of these catalogues to the ICRS system was performed in limited regions of the sky. A $1^\circ \times 1^\circ$ grid was defined and for every grid point the differences in position and proper motion of the 15 nearest stars present in Hipparcos and PPM were averaged to yield the correction at each individual grid point. These corrections were then applied to all the stars in PPM and STARNET in the regions of interest, assuming that STARNET is in the system of PPM.

Figures 1.1 and 1.2 show the grid with the derived corrections for the region of the Scorpius-Centaurus association as an example. Clearly there are some regions where rather large corrections are required, and others with virtually no corrections needed.

Since the mean sky density of Hipparcos is ≈ 3 stars per square degree taking the nearest 15 stars to every $1^\circ \times 1^\circ$ grid point means some oversampling, which guarantees a smooth variation of the corrections. A magnitude equation has not been considered for this provisional conversion between systems, because its effect is supposed to be small with respect to the errors in the source catalogues and should have no meaning for the kinematical studies described in the following.

Remarks to the tables

Abbreviations in the columns of the catalogue number are A for ACT, T for TRC and S for STARNET, followed by the GSC number given in those catalogues. An asterisk after a star name means that the star is present in more than one of the proper motion Catalogues (HIP, PPM, ACT, TRC and STARNET), and refers to the tables in the Appendix where all available proper motions are given.

The positions in all tables are valid for equinox and epoch J2000.0 and are given in the ICRS-system, as are the proper motions. Note that the mean errors of the proper motions in right ascension are multiplied by $\cos \delta$ (whereas the proper motions themselves are not). For some ACT stars no proper motion errors are quoted as they are not provided in the original catalogue for a small number of stars.

The magnitudes are quoted from the same catalogue as the positions and proper motions. With the exception of STARNET in the southern hemisphere, where B magnitudes are given in the catalogue, all other magnitudes are V magnitudes. Finally, the last column gives the distance and its uncertainty based on the Hipparcos parallax where this information is available. Note that distances are given for all the Hipparcos stars, irrespective of whether the proper motion from Hipparcos is used or not.

2 Taurus-Auriga

The results of this chapter have already been published (Frink et al. 1997), and large parts of the text have been adopted from that paper. It has extensively been updated with proper motions from the Hipparcos, ACT and TRC catalogues which have not been available when the paper was written, and proper motions from PPM and STARNET have been transformed to the Hipparcos astrometric system. The discussion has been supplemented with some additional material and newer work, leading to the conclusion that it is possible that the southern stars are still bound to the cloud.

2.1 Overview

The T-association Taurus-Auriga (Tau-Aur) is a large star forming region with several hundreds of pre-main sequence stars known. Its distance of only about 140 pc (Elias 1978, Kenyon et al. 1994) makes it an ideal object for studying the properties of the cloud resulting from ongoing star formation, e.g. its stellar content, age, distribution and motion of the stars and so on.

Before the launch of ROSAT about 150 T Tauri stars which are associated with Taurus-Auriga have been known, most of them classical T Tauri stars. The ROSAT All-Sky Survey (RASS) and some deep ROSAT pointings have revealed so far 4 new CTTS and 82 WTTS in the central region of Taurus-Auriga, between 4^h and 5^h in right ascension and $+15^\circ$ and $+34^\circ$ in declination (Wichmann et al. 1996, Strom & Strom 1994, Carkner et al. 1996). Both CTTS and WTTS show the characteristic strong Li I $\lambda 6708 \text{ \AA}$ absorption line, but in contrast to CTTS, WTTS are stronger X-ray-emitters (Neuhäuser et al. 1995b) and so easier to detect by ROSAT. WTTS however lack the strong H_α emission, Ca II emission and IR-excess of the CTTS, most of which were discovered by objective prism surveys.

In addition to these new TTS discovered in the central region of Taurus-Auriga pre-main sequence stars have also been found in a large area south of the Taurus-Auriga dark clouds (Neuhäuser et al. 1995c, Magazzù et al. 1997, Neuhäuser et al. 1997).

Proper motions of all these stars are required to kinematically investigate their membership to the association and to address the question whether it is possible that the stars outside the commonly adopted boundaries of Taurus-Auriga (based on CO surveys (Ungerechts & Thaddeus 1987)) have formed near the centre of the region or rather near their present locations. Until now proper motions have been known only for about 70 mostly classical T Tauri stars in selected areas inside the large region (Jones & Herbig 1979, Walter et al. 1987, Hartmann et al. 1991, Gomez et al. 1992).

2.2 Data

2.2.1 Proper motions of PMS stars

Proper motions of PMS stars known prior to ROSAT

34 PMS stars known prior to the ROSAT mission could be identified in at least one of the proper motion catalogues (Table 2.1 and Table A.1 in the Appendix). Of these, 15 stars had no proper motion measurement so far. Previous determinations of proper motions were performed in the surveys of Jones & Herbig (1979) (which was the most extensive one, including 80 suspected or confirmed T Tauri stars together with 241 stars possibly associated with Tau-Aur) and in the spatially more restricted surveys by Hartmann et al. (1991) and Gomez et al. (1992). These previous papers publish relative proper motions of stars on pairs of photographic plates. This is not an obstacle to local kinematics. However, a comparison

Table 2.1: STARNET proper motions for 34 stars which were known to be of PMS nature before ROSAT. In the second column references for previous measured proper motions are given: (1) Jones & Herbig 1979, (2) Walter et al. 1987, (3) Hartmann et al. 1991, (4) Gomez et al. 1992. Remarks after the name of a star refer to stars not regarded as members of the Tau-Aur association and discussed separately in Sect. 2.4.1 (^(P) Pleiades candidates, ^(h) other high proper motion stars).

object	ref.	cat. No.	RA ($\alpha_{J2000.0}$)	DEC ($\delta_{J2000.0}$)	m _V [mag]	μ_{α} [mas/a]	μ_{δ}	$\sigma_{\mu_{\alpha} \cos \delta}$ [mas/a]	$\sigma_{\mu_{\delta}}$	d [pc]
classical T Tauri stars										
V773 Tau	(1)	A 1827 1236*	4 ^h 14 ^m 12 ^s .93	+28°12'12".4	10.82	10.3	-20.7	2.57	3.84	101 ⁺³⁸ ₋₂₂
FM Tau		S 1827 1032	4 14 13.58	+28 12 48.8	13.75	1.	-40.	5.9	5.9	
CY Tau	(1)	S 1827 212	4 17 33.78	+28 20 46.8	12.98	14.	-21.	5.9	5.9	
BP Tau	(1)	HIP 20160*	4 19 15.83	+29 6 26.8	11.59	6.04	-33.13	5.43	3.94	53 ⁺¹⁷ ₋₁₁
RY Tau		HIP 20387*	4 21 57.41	+28 26 35.6	10.30	10.33	-23.05	2.62	1.89	134 ⁺⁵⁴ ₋₃₁
T Tau N	(1)	HIP 20390*	4 21 59.43	+19 32 6.4	10.01	16.39	-12.48	1.88	1.62	177 ⁺⁶⁸ ₋₃₉
DF Tau	(3)	HIP 20777*	4 27 2.80	+25 42 22.4	11.82	16.07	-26.38	6.25	4.26	39 ⁺¹³ ₋₈
DG Tau	(3)	S 1820 330	4 27 4.70	+26 6 16.6	11.59	8.	-12.	3.7	3.7	
DK Tau	(3)	S 1833 37	4 30 44.28	+26 1 24.9	12.01	13.	-17.	5.0	5.0	
GG Tau		S 1270 897	4 32 30.33	+17 31 40.4	11.85	10.	-25.	3.9	3.9	
V807 Tau		S 1829 214	4 33 6.62	+24 9 55.1	11.24	12.	-19.	3.7	3.7	
DN Tau	(1)	S 1829 26	4 35 27.37	+24 14 58.8	12.17	5.	-21.	3.6	3.6	
LkCa 15		S 1278 193	4 39 17.77	+22 21 3.7	11.65	3.	-10.	4.7	4.7	
DS Tau		S 1843 937	4 47 48.42	+29 25 12.2	11.21	-18.	-22.	4.9	4.9	
UY Aur	(1)	S 2387 982	4 51 47.35	+30 47 13.4	11.75	3.	-23.	5.1	5.1	
SU Aur	(1)	A 2387 977*	4 55 59.38	+30 34 1.5	9.50	4.6	-27.9	0.95	1.82	152 ⁺⁶³ ₋₃₄
RW Aur A	(1)	A 2389 955*	5 7 49.56	+30 24 5.1	10.37	1.4	-23.3	1.00	0.95	71 ⁺⁶⁵ ₋₂₃
weak-line T Tauri stars										
NTTS 032641+2420 ^(P)		S 1802 1190	3 ^h 29 ^m 38 ^s .38	+24°30'37".7	11.69	30.	-44.	3.4	3.4	
NTTS 034903+2431 ^(P)		S 1804 123	3 52 2.27	+24 39 47.7	11.17	30.	-49.	4.8	4.8	
SAO 76411 A ^(P)		T 1262 1647*	4 2 53.57	+22 8 11.7	8.97	49.3	-51.4	1.8	1.8	
SAO 76428		A 1262 421*	4 4 28.49	+21 56 4.5	9.78	6.0	-15.4	3.13	0.85	
V410 Tau	(1)	HIP 20097*	4 18 31.10	+28 27 16.2	10.71	6.87	-27.44	2.38	1.77	137 ⁺⁵⁴ ₋₃₀
HDE 283572	(2)	HIP 20388*	4 21 58.84	+28 18 6.5	9.11	8.54	-27.45	1.57	1.14	128 ⁺²⁶ ₋₁₈
NTTS 042417+1744	(4)	A 1269 913*	4 27 10.57	+17 50 42.6	10.34	0.2	-14.6	0.92	1.07	
UX Tau A	(4)	A 1269 225*	4 30 3.99	+18 13 49.5	10.17	8.2	-12.4			
L1551-51	(4)	S 1270 1195	4 32 9.31	+17 57 22.7	11.69	13.	-18.	4.3	4.3	
V827 Tau		S 1270 1108	4 32 14.58	+18 20 14.8	12.00	11.	-16.	4.0	4.0	
V826 Tau	(4)	S 1270 604	4 32 15.85	+18 1 38.7	11.81	12.	-21.	4.3	4.3	
V830 Tau	(3)	S 1833 843	4 33 9.99	+24 33 42.9	12.03	-12.	-31.	4.7	4.7	
NTTS 043124+1824	(4)	S 1270 232	4 34 18.03	+18 30 6.6	12.70	-6.	-7.	3.9	3.9	
NTTS 043220+1815		A 1270 1331*	4 35 14.21	+18 21 35.6	11.04	0.9	-11.0	0.99	2.89	
LkCa 14 ^(h)		S 1834 177	4 36 18.92	+25 43 1.4	11.61	-161.	95.	4.6	4.6	
LkCa 19		S 2387 637	4 55 36.96	+30 17 55.4	10.51	5.	-15.	4.2	4.2	
NTTS 045251+3016		S 2387 535	4 56 2.02	+30 21 3.8	11.37	6.	-22.	4.2	4.2	

of the individual accuracy in these previous studies and in the present one is not possible, because the number of stars in common is too small.

Proper motions of PMS stars discovered by ROSAT

ROSAT observations in a region including the centre of Tau-Aur in combination with optical follow-up spectroscopy have revealed 4 new classical and 72 new weak-line T Tauri stars (Wichmann et al. 1996). Of these, 39 stars (all WTTS) have known proper motions which are given in Table 2.2 (see also Table A.2 in the Appendix).

The classification in Wichmann et al. (1996) was based on the presence of the lithium line and weak H α emission or absorption. Martín & Magazzù (1999) obtained higher resolution spectroscopy for some of these stars and applied a slightly modified classification scheme, resulting in the classification of some PTTs among the sample (2 of the stars are in Table 2.2: RXJ 0437.5+1851, which possibly belongs to the

Table 2.2: All new ROSAT-discovered PMS stars (all WTTS) in the central region of Tau-Aur by Wichmann et al. (1996) which could be identified in at least one of the proper motion catalogues. Remarks after the name of a star refer to stars with proper motions investigated in Table 2.4.

object	cat. No.	RA ($\alpha_{J2000.0}$)	DEC ($\delta_{J2000.0}$)	m_V [mag]	μ_α [mas/a]	μ_δ	$\sigma_{\cos\delta}^{\mu_\alpha}$ [mas/a]	σ_{μ_δ}	d [pc]
HD 285281	T 1258 894*	4 ^h 0 ^m 31 ^s .07	+19° 35' 20".8	10.51	6.0	-14.0	1.6	1.6	
RXJ 0403.4+1725 ^(h)	S 1254 309	4 3 24.86	+17 24 26.2	11.47	-61.	-16.	3.6	3.3	
RXJ 0405.2+2632	S 1822 1383	4 5 12.34	+26 32 43.6	11.22	18.	-25.	4.0	4.0	
RXJ 0405.3+2009	S 1258 338	4 5 19.61	+20 9 25.2	10.20	10.	-19.	3.6	3.6	
HD 284135	A 1814 409*	4 5 40.58	+22 48 12.0	9.43	3.9	-14.9	0.87	0.86	
HD 284149	A 1258 257*	4 6 38.81	+20 18 11.2	9.59	8.0	-15.4	1.64	2.87	156 ⁺⁶² ₋₃₅
RXJ 0406.8+2541	S 1818 144	4 6 51.34	+25 41 28.4	11.30	10.	-22.	4.2	4.2	
RXJ 0407.9+1750 ^(P)	S 1254 785	4 7 54.00	+17 50 26.0	11.16	21.	-49.	3.9	3.9	
RXJ 0409.2+2901 ^(P)	A 1826 877*	4 9 9.74	+29 1 30.3	10.93	23.9	-32.0	2.65	1.89	
RXJ 0412.8+2442	S 1819 498	4 12 51.21	+24 41 44.0	11.66	9.	-17.	5.7	5.7	
HD 285579 ^(P)	S 1251 201	4 12 59.87	+16 11 47.8	10.74	11.	-44.	3.8	3.8	
RXJ 0415.4+2044	A 1263 1027*	4 15 22.92	+20 44 16.9	10.49	3.0	-13.8	3.24	4.02	
RXJ 0420.4+3123	S 2371 740	4 20 24.13	+31 23 23.6	12.18	2.	-17.	7.9	7.9	
HD 285751	S 1264 822	4 23 41.36	+15 37 55.2	10.91	12.	-10.	5.1	5.1	
BD+26 718	S 1824 592	4 24 48.18	+26 43 16.0	11.46	13.	-24.	5.0	5.0	
BD+26 718B	S 1824 183	4 24 49.09	+26 43 9.4	10.47	11.	-31.	5.0	5.0	
BD+17 724B	A 1269 271*	4 27 5.98	+18 12 37.1	9.35	2.1	-15.3	0.90	0.89	
RXJ 0430.8+2113	T 1277 574*	4 30 49.19	+21 14 10.7	10.39	30.4	-27.3	1.9	2.1	
HD 284496	A 1277 1238*	4 31 16.85	+21 50 25.3	10.85	1.2	-13.6	1.56	2.13	
RXJ 0432.7+1853	A 1274 1501*	4 32 42.43	+18 55 10.2	10.82	-2.4	-13.7	1.01	1.18	
RXJ 0433.7+1823	S 1270 230	4 33 42.01	+18 24 27.3	11.93	-13.	-8.	3.3	3.3	
RXJ 0437.5+1851 ^(P)	S 1274 1515	4 37 26.87	+18 51 25.2	10.73	18.	-53.	3.4	3.4	
HD 285957	S 1266 1195	4 38 39.02	+15 46 13.0	9.86	0.	-30.	5.2	5.2	
RXJ 0439.4+3332A ^(P)	S 2378 1232	4 39 25.47	+33 32 44.8	11.17	28.	-42.	9.2	9.2	
HD 283798	HIP 21852*	4 41 55.16	+26 58 49.4	9.60	-0.79	-20.56	1.35	1.04	115 ⁺²¹ ₋₁₅
RXJ 0444.9+2717	T 1839 643*	4 44 54.46	+27 17 45.2	9.81	15.4	-20.6	5.8	5.3	
HD 30171	A 1267 425*	4 45 51.30	+15 55 49.7	9.39	13.2	-17.5	0.95	0.94	
RXJ 0448.0+2755	S 1839 1278	4 48 0.42	+27 56 19.8	12.35	-9.	-5.	6.3	6.3	
RXJ 0450.0+2230	S 1292 639	4 50 0.18	+22 29 57.7	11.07	-1.	-17.	3.3	3.3	
RXJ 0452.8+1621	S 1280 559	4 52 50.15	+16 22 9.3	11.31	7.	-17.	4.8	4.8	
RXJ 0453.0+1920	S 1288 790	4 52 57.07	+19 19 50.1	12.07	-2.	-23.	3.9	3.9	
HD 31281	A 1284 1193*	4 55 9.62	+18 26 31.1	9.25	-3.3	-18.0	0.87	0.87	
RXJ 0455.8+1742	S 1284 522	4 55 47.65	+17 42 1.9	11.16	-6.	-22.	3.9	3.9	
HD 286179	A 1281 1215*	4 57 0.65	+15 17 53.1	10.53	-1.5	-17.1	2.29	1.04	
RXJ 0457.1+3142	A 2388 857*	4 57 6.50	+31 42 50.5	10.89	-11.2	-14.2	1.24	1.13	
RXJ 0457.2+1524	A 1281 1288*	4 57 17.66	+15 25 9.5	10.52	8.4	-17.6	1.04	3.45	
RXJ 0457.5+2014	S 1289 513	4 57 30.63	+20 14 28.6	10.89	-7.	-31.	3.6	3.6	
RXJ 0458.7+2046	S 1293 2396	4 58 39.71	+20 46 43.3	11.65	0.	-35.	5.7	5.7	
RXJ 0459.8+1430	S 697 960	4 59 46.14	+14 30 55.2	11.81	6.	-19.	5.0	5.0	

Pleiades, and RXJ 0458.7+2046). Other stars are not at all PMS stars according to Martín & Magazzù (1999), but this affects only one star in Table 2.2 (RXJ 0457.1+3142).

Additional pointed ROSAT observations led to the discovery of 8 confirmed (Strom & Strom 1994), 2 likely and 5 possible TTS (Carkner et al. 1996), but none of them could be found in STARNET or the other catalogues because they are too faint.

Recently Neuhäuser et al. (1995c, 1997) and Magazzù et al. (1997) have studied a sample of 111 stars in a region located just south of the Taurus molecular clouds. The field boundaries were chosen by these authors in such a way that the Orion field (in the lower left in Fig. 2.1) was excluded. The strip in the lower right of Fig. 2.1, which is perpendicular to the galactic plane, was included in order to search for a gradient in the space density of TTS as a function of distance from the Taurus clouds.

Proper motions of 59 stars in the sample of these authors are available, and the data are given in Table 2.3 and Table A.3 in the Appendix. Of these, 18 stars are classified as very young stars with ages $\leq 3.5 \cdot 10^7$ yrs (with lithium excess above Pleiades level), 12 as stars with ages around $\approx 10^8$ yrs (with

Table 2.3: Proper motions for stars not older than $3.5 \cdot 10^7$ yrs, $\approx 10^8$ yrs old stars and stars older than 10^8 yrs from the list of Neuhäuser et al. (1997) in a region located somewhat south of the Taurus molecular clouds. Remarks after a star's name refer again to stars discussed in Sect. 2.4.1.

object	cat. No.	RA ($\alpha_{J2000.0}$)	DEC ($\delta_{J2000.0}$)	m_V [mag]	μ_α [mas/a]	μ_δ [mas/a]	$\frac{\sigma_{\mu_\alpha}}{\cos \delta}$ [mas/a]	σ_{μ_δ} [mas/a]	d [pc]
stars not older than $3.5 \cdot 10^7$ yrs									
RXJ 0324.4+0231	S 60 489	3 ^h 24 ^m 25 ^s .26	+ 2 ^o 31' 1''0	12.83	24.	-6.	4.3	4.3	
RXJ 0338.3+1020	S 660 709	3 38 18.20	+10 20 16.5	10.97	17.	-26.	3.5	3.5	
RXJ 0344.8+0359	S 68 1471	3 44 53.17	+ 3 59 30.8	12.26	22.	-12.	4.9	4.9	
RXJ 0347.9+0616	S 71 542	3 47 56.82	+ 6 16 6.9	11.06	15.	-7.	3.5	3.5	
RXJ 0348.5+0832	A 658 922*	3 48 31.43	+ 8 31 36.7	10.99	23.1	-21.9	1.10	1.48	
RXJ 0354.1+0528	S 72 606	3 54 6.59	+ 5 27 23.5	11.63	-3.	-7.	3.9	3.9	
RXJ 0354.3+0535	A 72 921*	3 54 21.31	+ 5 35 40.8	10.29	-0.3	-6.7	1.01	0.98	
RXJ 0357.3+1258	A 665 150*	3 57 21.39	+12 58 16.7	10.93	22.8	-21.9	2.13	1.48	
BD+07 582 B ^h	PPM 147111	4 0 9.39	+ 8 18 18.7	10.80	-24.	-18.	9.3	9.3	
RXJ 0407.2+0113N	S 73 762	4 7 16.43	+ 1 13 14.3	11.14	16.	-6.	3.4	3.4	
RXJ 0422.9+0141	S 75 41	4 22 54.62	+ 1 41 31.7	12.29	-5.	-8.	4.1	4.1	
RXJ 0427.4+1039	S 672 1265	4 27 30.28	+10 38 48.8	11.33	0.	-7.	4.1	4.1	
RXJ 0427.5+0616	T 81 1414*	4 27 32.07	+ 6 15 52.0	10.65	5.3	0.8	1.6	2.0	
RXJ 0434.3+0226	S 86 318	4 34 19.51	+ 2 26 25.9	13.01	6.	-20.	4.6	4.6	
BD+08 742	T 682 674*	4 42 32.09	+ 9 6 0.8	11.07	27.9	-25.5	4.6	1.7	
RXJ 0450.0+0151	S 84 743	4 50 4.70	+ 1 50 42.7	12.15	13.	-13.	4.1	4.1	
RXJ 0511.9+1112	S 702 1689	5 12 0.30	+11 12 19.7	11.38	3.	-4.	3.6	3.6	
RXJ 0512.0+1020	S 702 2533	5 12 3.19	+10 20 6.9	11.32	2.	7.	3.6	3.6	
$\approx 10^8$ yrs old stars									
RXJ 0219.7-1026	S 5282 2210	2 ^h 19 ^m 47 ^s .39	-10 ^o 25'40''6	11.60	16.	-3.	3.7	3.7	
HD 15526 ^(h)	A 5284 686*	2 29 35.03	-12 24 8.6	9.82	43.6	-11.1	2.43	1.21	
RXJ 0329.1+0118	S 57 485	3 29 8.07	+ 1 18 5.5	10.90	4.	-9.	2.9	2.9	
RXJ 0339.6+0624	S 70 1148	3 39 40.57	+ 6 24 43.5	11.70	1.	-7.	5.5	5.5	
RXJ 0343.6+1039	A 660 825*	3 43 40.49	+10 39 13.7	10.28	-7.2	-28.3	1.10	1.32	
BD+11 533 ^h	HIP 18117*	3 52 24.76	+12 22 43.7	9.93	6.52	-16.60	1.79	1.50	153 ⁺⁵⁰ ₋₃₁
BD+07 582 ^h	PPM 147110*	4 0 9.32	+ 8 18 13.5	10.70	-12.	-39.	4.6	4.6	
RXJ 0404.4+0519	S 79 810	4 4 28.49	+ 5 18 43.2	11.18	14.	-8.	3.0	3.0	
HD 286556	S 674 504	4 9 51.54	+12 9 2.1	12.02	3.	-27.	4.2	4.2	
RXJ 0423.5+0955	S 672 1156	4 23 30.23	+ 9 54 29.6	11.64	-12.	-7.	5.3	5.3	
HD 286753	A 676 1123*	4 25 35.32	+12 9 59.4	10.66	28.7	-24.9	1.09	1.09	
RXJ 0442.9+0400	A 91 702*	4 42 54.74	+ 4 0 11.5	11.18	18.8	-18.7	1.86	1.08	
stars older than 10^8 yrs									
RXJ 0210.4-1308SW ^(h)	PPM 211168*	2 ^h 10 ^m 25 ^s .84	-13 ^o 7'56''9	9.40	57.	-27.	2.9	3.0	
RXJ 0212.3-1330 ^(h)	T 5283 876*	2 12 18.73	-13 30 42.2	10.70	163.9	-82.2	1.6	1.6	
RXJ 0218.6-1004	S 5282 68	2 18 39.56	-10 4 6.0	11.75	18.	-17.	4.4	4.4	
RXJ 0239.1-1028 ^(h)	S 5288 1027	2 39 8.77	-10 27 46.3	13.21	-8.	-94.	5.0	5.0	
RXJ 0248.3-1117	PPM 710125*	2 48 22.18	-11 17 12.4	9.80	9.	-13.	3.6	3.6	
RXJ 0309.1+0324	T 58 166*	3 9 9.89	+ 3 23 44.7	10.78	27.8	-6.6	1.7	2.6	
RXJ 0312.8-0414NW	T 4711 684*	3 12 50.23	- 4 14 5.0	10.27	1.6	-11.5	3.8	1.6	
RXJ 0317.9+0231 ^(h)	A 59 24*	3 17 59.14	+ 2 30 11.6	10.37	-19.7	-66.2	1.19	2.74	
RXJ 0330.7+0306N ^(h)	S 67 206	3 30 43.50	+ 3 5 46.9	11.18	39.	-84.	3.9	3.9	
RXJ 0336.0+0846 ^(h)	A 657 726*	3 36 0.34	+ 8 45 36.7	12.45	17.2	22.1			44 ⁺¹⁴ ₋₉
BD+12 511	T 664 694*	3 49 27.77	+12 54 43.8	9.76	-42.0	43.2	1.7	1.7	88 ⁺⁶⁵ ₋₂₆
RXJ 0402.5+0552	S 79 729	4 2 35.72	+ 5 51 36.6	10.80	36.	41.	3.3	3.3	
RXJ 0405.5+0324	S 76 713	4 5 30.25	+ 3 23 50.1	11.49	10.	-5.	4.4	4.4	
RXJ 0418.6+0143	S 74 1029	4 18 39.24	+ 1 42 9.6	12.34	-12.	-40.	4.2	4.2	
RXJ 0426.4+0957W	S 672 1133	4 26 26.79	+ 9 57 0.1	11.47	15.	17.	5.3	5.3	
BD+00 760 ^(h)	T 75 1529*	4 27 53.08	+ 0 49 25.7	9.51	59.5	-7.2	2.1	1.7	
RXJ 0429.9+0155	A 75 1*	4 29 56.90	+ 1 54 47.5	9.93	3.6	-3.4	1.07	1.04	
RXJ 0435.5+0455	A 90 936*	4 35 31.59	+ 4 55 32.2	10.19	-6.2	-0.5	1.48	1.02	
BD+05 706	T 91 830*	4 41 57.71	+ 5 36 34.2	9.70	1.4	-8.1	1.8	1.8	
RXJ 0442.3+0118	S 83 788	4 42 18.60	+ 1 17 39.9	11.79	3.	-25.	3.3	3.3	
RXJ 0442.6+1018	T 686 1246*	4 42 40.82	+10 17 45.4	8.81	25.2	-14.9	1.6	1.9	
HD 287017 ^(P)	T 687 419*	4 44 20.43	+ 9 41 3.6	9.37	52.9	-64.3	1.7	1.6	
RXJ 0445.3+0914	S 683 282	4 45 23.82	+ 9 13 48.6	11.75	3.	-5.	4.6	4.6	
RXJ 0448.0+0738 ^(P)	S 683 661	4 48 0.87	+ 7 37 56.3	11.15	20.	-57.	4.2	4.2	
RXJ 0515.3+1221	S 707 1311	5 15 20.57	+12 21 13.7	11.59	26.	-30.	4.5	4.5	
RXJ 0523.5+1005	S 704 2521	5 23 33.73	+10 4 29.1	11.23	-3.	-38.	4.4	4.4	
RXJ 0523.9+1101 ^(h)	S 704 2073	5 23 57.05	+11 0 55.8	10.83	2.	-114.	3.4	3.4	
RXJ 0528.4+1213	S 708 2137	5 28 25.71	+12 12 36.1	11.50	-3.	-2.	4.4	4.4	
RXJ 0530.9+1227	S 709 1637	5 30 57.22	+12 27 26.4	10.69	13.	-25.	5.4	5.4	

^(h) classification is doubtful (Neuhäuser et al. 1997), these stars may either be ZAMS or PMS stars

lithium, but no excess) and 29 stars as even older with ages $> 10^8$ yrs (without any lithium detected) by Neuhäuser et al. (1997). The youngest stars with spectral types F or G are just reaching the main sequence, whereas stars with spectral type K are pre-main sequence stars. Only one star is present in Hipparcos, and for 33 stars the STARNET proper motion is the only one available, since most of the stars are rather faint.

2.2.2 High proper motion stars

As mentioned already in the Introduction, large epoch differences can help to reduce the errors in the proper motions, but on the other hand make the identification of high proper motion stars more difficult and sometimes erroneous. In the sample discussed here there are some stars with very high proper motions in STARNET, which are possibly spurious and caused by misidentifications. These stars are investigated in more detail in Sect. 2.4.1 and flagged by a ^(h) in the tables.

Additionally, some stars in the tables have been flagged by a ^(P) because they have the rather high typical proper motion of the Pleiades cluster. Their relation to the Pleiades cluster is investigated in Sect. 2.4.2.

2.2.3 Distance to Taurus-Auriga

The canonical value for the distance to the dark clouds of the Taurus-Auriga SFR is 140 pc. It has been determined by Elias (1978), who averaged the distances derived with 3 different methods. Greenstein (1937) and McCuskey (1939) already derived distances of about 140 pc from plotting the observed numbers of stars in that region versus magnitude. Reddening of field stars versus distance yielded ≈ 150 pc (Gottlieb & Upson 1969), whereas the stellar luminosities of stars associated with the dark clouds argued for distances around 135 pc (Racine 1968, Elias 1978).

More recently, Kenyon et al. (1994) derived spectroscopic parallaxes and obtained a distance of 140 ± 10 pc for the northern portion of the cloud, with no indications for substantial variations in distance across the cloud. Preibisch & Smith (1997) have determined a best fit distance of 152 ± 10 pc on the basis of rotational properties of 25 WTTS.

Finally, the Hipparcos parallaxes confirm the above results which are all in good agreement with each other. Wichmann et al. (1998b) averaged the parallaxes of the TTS in the Taurus region which were included intentionally in the Hipparcos Input Catalogue, i.e. mostly classical TTS since the ROSAT detected population of weak-line TTS was not yet known at that time. They derived a weighted mean parallax of 7.06 ± 0.71 mas from 4 stars, corresponding to a distance of 142 ± 14 pc, which is in perfect agreement with the other distance determinations.

Taking into account all the other stars now known to be related to the SFR and present in the Hipparcos Catalogue ‘by accident’, the weighted mean parallax of altogether 9 stars would be 7.73 ± 1.49 mas, corresponding to a distance of 129_{-21}^{+31} pc. BP Tau and DF Tau have been excluded from that solution since their Hipparcos parallaxes clearly would place them foreground to the clouds, although Wichmann et al. (1998b) show that the parallax of BP Tau can be explained in the framework of statistical fluctuations and is consistent with a mean distance of 140 pc. Furthermore the sample is biased towards brighter stars, i. e. nearer and/or earlier type stars, so a slightly lower value than the distance to the whole cloud complex is expected for these stars.

2.3 Kinematics

2.3.1 Velocity dispersion

Positions and proper motions of the stars from Tables 2.1–2.3 are shown in Figs. 2.1 and 2.2. Stars with proper motions clearly off the Taurus mean motion are excluded from the discussion in this section; they are discussed separately in Sect. 2.4.1. Clustering of the remaining 82 young stars around the overall

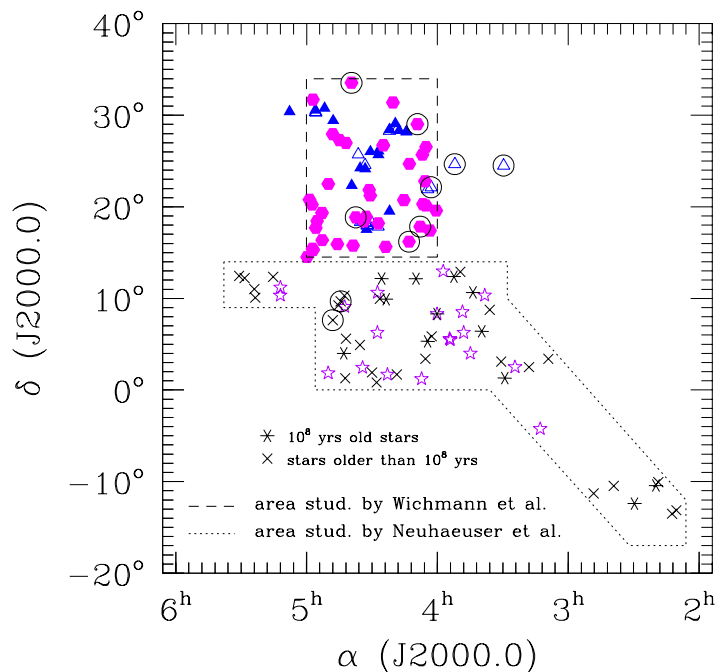


Figure 2.1: Positions of the stars in Tables 2.1–2.3. Stars of Table 2.1 (TTS known prior to ROSAT) are marked with triangles (CTTS filled, WTTS open), stars of Table 2.2 (WTTTS studied by Wichmann et al. 1996) with filled hexagons and the youngest stars of Table 2.3 (stars studied by Neuhäuser et al. 1995c, 1997 and Magazzù et al. 1997) with open stars. 10^8 yrs old stars and stars older than 10^8 yrs of Table 2.3 are marked with centered stars and crosses, respectively. A circle around a symbol indicates possible Pleiades members, see Sect. 2.4.2. The regions studied by those authors are indicated, too.

mean values $(\mu_\alpha \cos \delta, \mu_\delta) \approx (5.5, -17.7)$ mas/a is visible in the proper motion diagram, with a relatively large scatter around the mean motion. Also, there is a slight difference in motion between the stars in the central region (Tables 2.1 and 2.2) with a mean proper motion of $(4.5, -19.7)$ mas/a and those from the southern region (upper part of Table 2.3) with a mean of $(8.7, -11.2)$ mas/a. The difference in μ_δ is significant with a confidence level larger than 99.9% in a t -test for distributions with different dispersions.

First the velocity dispersion inferred from the scatter in proper motions is discussed. At a distance of 140 pc the scatter in proper motions corresponds to a velocity dispersion in one coordinate of 5.8 km/s for the whole complex. Splitting the sample into stars in the central and the southern region yields a velocity dispersion in the central part of Tau-Aur of 4.9 km/s, while the stars in the southern region exhibit a velocity dispersion of 7.4 km/s.

The mean error of the proper motions is ≈ 3.5 mas/a, corresponding to 2.3 km/s at a distance of 140 pc. Subtracting this from the observed scatter we get an intrinsic scatter of 4.3 km/s for the stars in the central part and 7.0 km/s for the stars in the southern region. These values appear very large compared to previous investigations. Jones & Herbig (1979) derive an overall intrinsic velocity dispersion of 3.2 km/s and 2.2 km/s in their x - and y -direction (x essentially parallel to right ascension, y parallel to declination), respectively, but the region investigated by Jones & Herbig (1979) is smaller than our ‘central region’ which is roughly the same as in Wichmann et al. (1996).

There is a significant difference in the determination of proper motions by Jones & Herbig (1979) and proper motions from all-sky catalogues. The region in Jones & Herbig (1979) is separated into subregions each corresponding to plate pairs. Proper motions are determined differentially from these plate pairs. This minimizes the effect of projection of the space motions over large areas of the sky, which is inherent in the proper motions on absolute systems like the ICRS.

The mean proper motion of $\mu_x = 6.4$ mas/a and $\mu_y = -22.0$ mas/a given by Jones & Herbig (1979) is comparable to our mean motion, indicating that the difference of the two astrometric systems is small. A thorough conversion of the proper motions between the Jones-Herbig system of relative proper motions

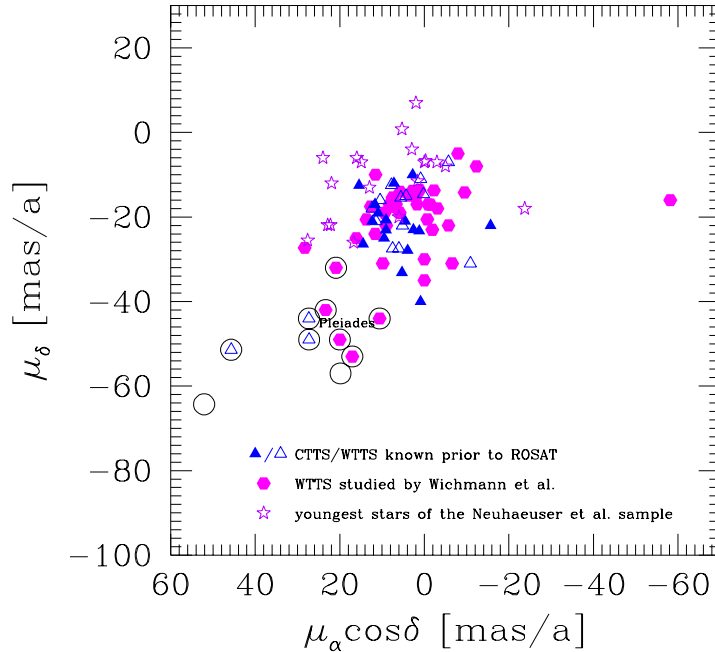


Figure 2.2: Proper motions of all the stars in the centre (Tables 2.1 and 2.2) and of the youngest stars in the south (upper part of Table 2.3). The coding of the different stars is the same as in Fig. 2.1. Note that the proper motion of LkCa 14 is too large to be shown in this diagram (it maybe wrong anyway, see Sect. 2.4.1). The stars located in the south have on average less negative proper motions in declination as compared to the stars in the central region. This is just the opposite of what would be observed if they were ejected from the densest parts of the clouds.

and the ICRS proper motion system is not possible because only few stars are in common.

Jones & Herbig (1979) subdivided the complex into smaller subregions, as they had a fainter limiting magnitude and a larger number of stars. Within these subgroups they determined the intrinsic velocity dispersion in the following way. From the measured scatter of the proper motions they subtracted the scatter expected from the accuracy of their measurements. However, these two quantities are almost equal. So, they derived an upper limit of 1–2 km/s in most of their subgroups.

The size of the sample investigated here does not allow for a further subdivision. The velocity dispersion of the complex can be studied only as a whole. A velocity dispersion of ≈ 5 km/s would disintegrate the Tau-Aur complex in a time of the order 10^7 years, but typically smaller than the ages of the PMS stars. A large part of the measured velocity dispersion can be attributed to the ad hoc assumption that all stars are situated at a distance of 140 pc, as will be discussed in the next section.

2.3.2 Space velocities

As the stars of our sample populate a large region on the sky the influence on proper motions caused by projection effects has to be taken into account. It is necessary to consider the total space velocities for a discussion of the velocity dispersion. In the literature (see Table 1 in Neuhaeuser et al. 1995b for references) radial velocity measurements for 28 stars from Table 2.1 can be found as well as for 29 stars from Table 2.2 (Wichmann et al. 1999b).

The space velocities of these 57 stars calculated under the assumption of a fixed distance of 140 pc are shown in Fig. 2.3 (upper panel). The histograms for the total sample of stars are shown in grey, and the contribution of the stars from Table 2.1 is overplotted in black. The corresponding velocity dispersions are $\sigma_U = 2.7$ km/s, $\sigma_V = 4.6$ km/s and $\sigma_W = 4.0$ km/s. The low dispersion in U is caused mainly by the distance-independent radial velocities. The large dispersion in V and W cannot be explained by the mean errors of the proper motions, and it is suggested that this is (at least partly) due to the lack of

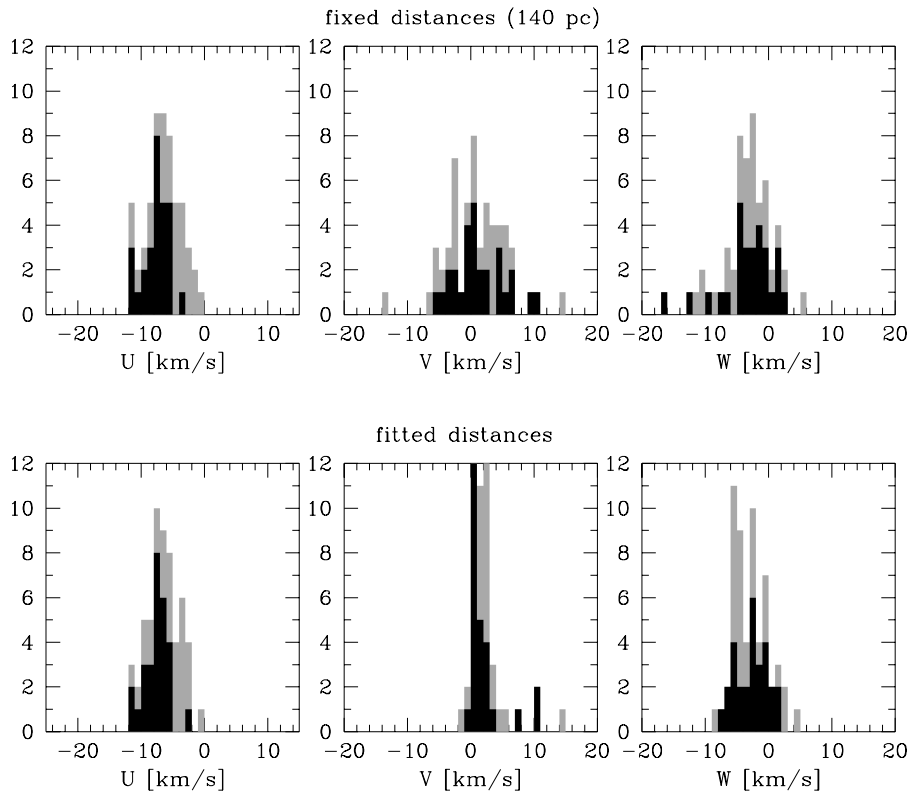


Figure 2.3: Space velocities for 28 TTS of Table 2.1 (shown in black) and 29 TTS of Table 2.2 (shown in grey together with the stars of Table 2.1) with radial velocities available. In the upper panel space velocities are calculated assuming fixed distances of 140 pc for all stars, in the lower panel distances are adjusted so that the resulting space velocity for every star is as close as possible to the mean space velocity of the upper panel. U points in the direction of the galactic centre, V in the direction of galactic rotation and W towards the north galactic pole. The highest peaks in the V velocities based on fitted distances are due to 22 (left peak) and 12 stars(right peak), respectively.

knowledge of the true distances.

This hypothesis was tested by varying the distance of each star in order to minimize the difference between the corresponding space velocity and the mean space velocity of the complex at a fixed distance of 140 pc. By this, the dispersion in the velocity components is significantly reduced to 2.6 km/s, 2.8 km/s and 2.7 km/s (Fig. 2.3; lower panel). The resulting velocity dispersion is now almost equal in all three components, an indication for the correctness of the hypothesis. A velocity dispersion of about 2.7 km/s in one component is very close to the formal mean error of the proper motions. This sets an upper limit to the intrinsic velocity dispersion. This upper limit must be small compared to 2.7 km/s in order to have no influence on the measured velocity dispersion. This result is consistent with the result of Jones & Herbig (1979) for the smaller subgroups within their sample.

The distances calculated in the manner described above are shown in Fig. 2.4. The mean of these distances is 136 pc, close to 140 pc but this is partly an effect of the fitting procedure. The dispersion of the distances is 42 pc which is comparable to the extent of the association in the tangential plane of at least 20° or 49 pc at a distance of 140 pc.

It is impossible to solve for the mean motion of the cluster and the distances of the stars simultaneously. Minimizing the velocity dispersion always favours lower distances and a lower mean cluster motion, so all these values would tend to zero. Minimizing only the relative dispersion, normalized to the absolute value of the space velocity, yielded a velocity dispersion which was much lower than expected from the mean errors of the proper motions and in turn an unbelievably high dispersion in the resulting distances.

These kinematically determined individual distances of the stars are not to be taken too literally; for this the method is too coarse. However, the method yields a general tendency for the distribution of the

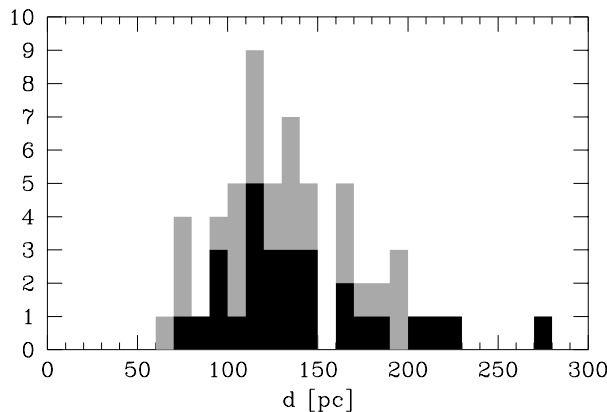


Figure 2.4: Distance histogram for the stars shown in Fig. 2.3. Distances are calculated requiring that the resulting space velocities are close to the mean. The mean of the distances is 136 pc with a dispersion of 42 pc.

radial distances of the TTS in Taurus-Auriga, and shows that a large fraction of the observed dispersion in the proper motions could be attributed to a spread in distances.

2.3.3 Search for high velocity escapers

Sterzik & Durisen (1995) proposed that the large halo of WTTS found around several star forming regions maybe made up of so-called run-away T Tauri stars or RATTs, produced numerously during the decay of young few-body systems and ejected with escape velocities larger than 3 km/s according to their simulations.

In the sample of 18 very young stars located south of the Taurus molecular clouds with known proper motions, there is no likely candidate which could have been ejected from the central part of the association. It should be kept in mind, however, that dynamically ejection mechanisms favour low-mass escapers. These stars are absent in this magnitude-limited subsample; about half of the PMS stars in Neuhäuser et al. (1997) are too faint even for the STARNET catalogue.

In order to be able to estimate the frequency of RATTs from a statistically more expressive sample, a special search for such RATTs has been undertaken by Neuhäuser et al. (1999). The kinematical selection of candidate RATTs stars has been performed in the framework of this thesis, and therefore it will be described shortly in the following.

There are about 200 more PMS candidates in the ROSAT databases in the region south of Taurus which have not yet been observed spectroscopically because the observations are rather time-consuming. Instead, the optical counterparts of these X-ray sources have been identified in the Hipparcos, PPM and STARNET catalogues (ACT and TRC and even Hipparcos have not yet been available when the proposal was written, but later on some Hipparcos stars have been added to the sample). In addition, Luytens NLTT Catalogue (Luyten 1979) of stars with proper motions larger than 200 mas/a has been used as an additional source of proper motions, since such high proper motion stars could easily have been missed in STARNET with its large epoch difference.

A region extending from 2^h to 5^h in right ascension and from -15° to $+15^\circ$ in declination has been searched for such kinematical and X-ray RATTs candidates in the magnitude interval 7–16 mag. All stars with relative proper motions larger than 10 mas/a as referred to the mean proper motion of the stars in central Taurus (corresponding to a relative velocity of 6.6 km/s at a distance of 140 pc) and with the angle between their observed and their expected (if they were really RATTs ejected from central Taurus) relative proper motion vectors not exceeding 45° have been chosen as preliminary RATTs candidates. Stars present in the Catalogue of Nearby Stars (CNS3, Gliese & Jahreiß 1991) have been removed from the sample; the proper motion of these stars are supposed to be high just because they are near and not because they have a large space velocity as a result of an ejection mechanism. Known halo stars or other

stars not qualifying for the interpretation as RATTs have also been removed from the final list as far as they could be figured out in the literature.

The first sample selected in the way just described comprised 33 stars, and only for 5 of them the lithium line could be detected, but none with a sufficient equivalent width to be classified as PMS star.

For the second sample the same selection criteria as above were imposed, but now the proper motions should fit to the interpretation that the stars escaped from the Pleiades cluster. Since the mean proper motion of the Pleiades cluster is already rather negative in declination, there were not so many stars with even larger negative proper motions in declination. Additionally, there were some stars which fitted into both samples according to the kinematical criteria, and those were removed from this second sample. This resulted in a total of 17 stars which probably could have been ejected from the Pleiades, and indeed 3 of them show a strong lithium line, i.e. may really be very young, and another 4 show at least a low lithium strength.

For the third sample only the very best kinematical RATTs candidates have been chosen, irrespective of whether they have been detected in X-rays or not. The relative proper motion was constrained to be larger than 100 mas/a, and the angle between the observed and expected proper motion directions was allowed to be 5° at most. Even with these strong criteria there were about 75 candidates, but only 8 of them could be observed, and none of them had detectable lithium.

The conclusion clearly is that the RATTs mechanism can not contribute significantly to the observed widely distributed population of WTTS found with ROSAT south of Taurus.

2.3.4 Relation of the southern stars to Taurus-Auriga

Different scenarios for the origin of the youngest stars in the southern region and their possible relation to the Taurus molecular clouds are discussed:

(a) First it is assumed that the young stars in the southern region belong to the Taurus-Auriga complex and share the same mean space motion. Because of their different proper motions the southern stars cannot fulfill the requirement of the same space motion if they are at a distance of 140 pc. Varying their distances as described above (with a solution in the distance interval between 0 and 300 pc for only 14 out of 18 stars), it turns out that they would be located at smaller distances than the stars in the central area with a median distance of 90 pc. This however leads to a conflict in the HR diagram (Fig. 2.5): Nearly all the stars in the south would lie below the main sequence for 90 pc which is in contradiction to their zero-age main sequence or even pre-main sequence nature. The velocity dispersions calculated with these distances are $\sigma_U = 5.3$ km/s, $\sigma_V = 2.5$ km/s and $\sigma_W = 3.3$ km/s. The dispersions in V and W are close to the values derived for the stars in the central region, but the dispersion in U (which is more or less independent of the distances) is higher than expected for members of a common star forming region.

(b) If the stars were more distant than 140 pc the HR diagram would constrain them to be really very young pre-main sequence stars. At the same time they would show a velocity dispersion higher than expected for a group of very young stars, and likewise very high X-ray luminosities. In the tangential plane the two complexes would pass more or less closely depending on the distance difference.

(c) If the stars are located at comparable distances to the Taurus-Auriga association of about 140 pc, this would make their location in the HR diagram comparable to the Taurus member stars. Kinematically they would not be related to the Taurus clouds, but the two complexes would rather approach each other with a relative velocity of ≈ 6.3 km/s and were adjacent to each other now only by chance. It might be possible that the Taurus clouds originated in a high-velocity cloud impact, so that the Taurus clouds oscillate around the galactic plane. During the last passage through the plane, the stars were separated (combing-out) from the Taurus clouds, and now move ahead and already begin to fall back to the plane. Alternatively, all the young stars south of Taurus may just be Gould's belt members with typical ages of $3-5 \cdot 10^7$ yrs; see Neuhäuser et al. (1997) for a discussion.

Another possibility is that the southern stars are still bound to the cloud. One could imagine that they disperse slowly away from the central cloud after their birth, but begin to fall back in the direction of the cloud (which coincides with the direction to the galactic plane) after a certain time. Given the observation that the southern stars have a relative velocity of 6.3 km/s at a mean separation of 20° or

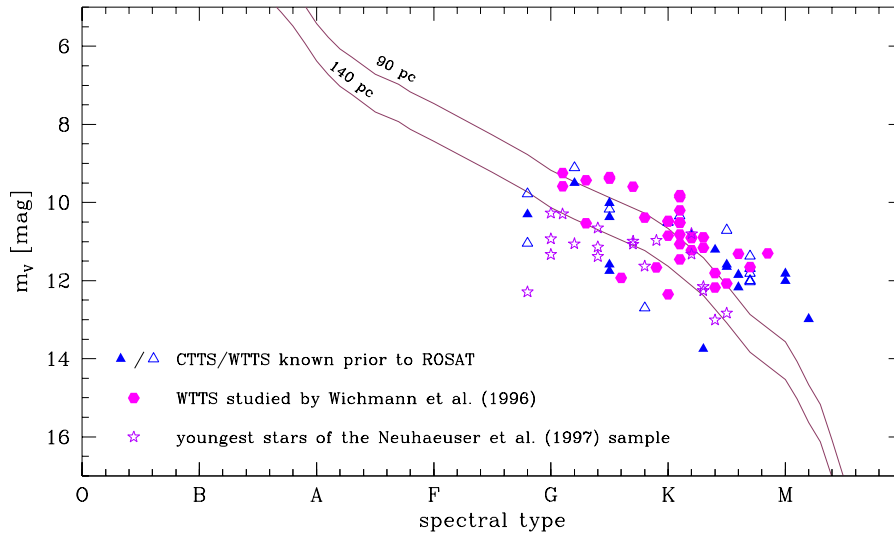


Figure 2.5: Hertzsprung Russell diagram for the stars of Tables 2.1 and 2.2 and the youngest stars of Table 2.3 without the high proper motion stars discussed separately in section 2.4.1. Apparent V -magnitudes were taken from the proper motion source catalogues (typical errors up to 0.3 mag in GSC) without corrections for extinction. Spectral types were taken from SIMBAD for stars of Table 2.1, from Wichmann et al. (1996) for stars of Table 2.2 and from Magazzù et al. (1997) for the stars of Table 2.3. The ZAMS is calculated for a distance of 140 pc and 90 pc, respectively. Some pre-ROSAT CTTS and WTTS appear below the ZAMS because no correction for absorption was applied.

50 pc from the central cloud, which is assumed to be spherical with a radius of 20 pc, this requires a total cloud mass of more than $1.4 \cdot 10^5 M_{\odot}$ for the stars to be bound. In this calculation the K_z -force acting perpendicular to the galactic plane has been taken into account; for an isolated system more than $2.3 \cdot 10^5 M_{\odot}$ for the mass of the central cloud would be needed to keep the stars bound.

The CO-survey of Ungerechts & Thaddeus (1987) in the regions of Perseus, Auriga and Taurus yields a total mass of the Taurus clouds of $3.5 \cdot 10^4 M_{\odot}$, and for each of the IC 348 and NGC 1499 clouds a mass of $5 \cdot 10^4 M_{\odot}$. Altogether the region spanning 750 square degrees contains a total cloud mass of $2 \cdot 10^5 M_{\odot}$, but this value is a little bit uncertain due to uncertainties in the distances to the clouds.

Assuming a total cloud mass of $2 \cdot 10^5 M_{\odot}$, which is clearly at the higher end, the escape velocity at the edge of the cloud, 20 pc away from the centre, would be around 9–10 km/s in the z -direction, slightly larger than the observed velocity dispersion. Stars with a relative velocity of 6–7 km/s at a distance of 50 pc from the centre of the cloud in the tangential plane (which is just below the escape velocity of 7.0 km/s in the z -direction) travel out to 80 pc and return back to 50 pc in a time span of $\approx 4 \cdot 10^7$ yrs, comparable to the ages of the stars.

As a result of the absence of the repelling K_z -force, the escape velocities in the direction of the galactic plane are supposed to be smaller, around 6–7 km/s at a distance of 20 pc from the cloud centre. Similarly, the tidal radius in the plane is only 40 pc, half of its value in the z -direction.

Neither of the above scenarios is completely convincing. Maybe the stars in the southern area do not have a common origin and are not located at approximately similar distances. Briceno et al. (1997) suggest that the population discovered by ROSAT south of the Taurus clouds is not made up of pre-main sequence but rather main sequence stars for which no common kinematic behaviour is expected. However, the Hipparcos parallaxes for some of the stars clearly confirm their pre-main sequences nature (Neuhäuser & Brandner 1998).

The kinematical findings from this section indicate most probably that the PMS stars in the southern extension move towards the central Taurus-Auriga region. This implies a larger separation of the two complexes in the past. Nevertheless this is in accordance with a common star formation process if the total cloud mass in the region is at least $2 \cdot 10^5 M_{\odot}$.

Table 2.4: Stars with conspicuous proper motions in the Tau-Aur region. The last column indicates the result of the proper motion check via POSS I or other proper motion catalogues, respectively: a \checkmark -sign indicates that the proper motion could be confirmed by comparison with POSS I, a ?-sign indicates a doubtful proper motion because the check with POSS I was not conclusive, and a * -sign indicates that the proper motions are similar in several catalogues.

object	Tab.	cat. No.	μ_α [mas/a]	μ_δ	
Pleiades candidates					
NTTS 032641+2420	2.1	S 1802 1190	30.	-44.	\checkmark
NTTS 034903+2431	2.1	S 1804 123	30.	-49.	\checkmark ⁽¹⁾
SAO 76411 A ⁽²⁾	2.1	T 1262 1647	49.3	-51.4	*
RXJ 0407.9+1750	2.2	S 1254 785	21.	-49.	\checkmark
RXJ 0409.2+2901	2.2	A 1826 877	23.9	-32.	*
HD 285579	2.2	S 1251 201	11.	-44.	\checkmark
RXJ 0437.5+1851	2.2	S 1274 1515	18.	-53.	\checkmark
RXJ 0439.4+3332A	2.2	S 2378 1232	28.	-42.	\checkmark
HD 287017	2.3	T 687 419	52.9	-64.3	*
RXJ 0448.0+0738	2.3	S 683 661	20.	-57.	?
other high proper motion stars					
RXJ 0210.4-1308SW	2.3	PPM 211168	57.	-27.	*
RXJ 0212.3-1330	2.3	T 5283 876	163.9	-82.2	*
HD 15526	2.3	A 5284 686	43.6	-11.1	*
RXJ 0239.1-1028	2.3	S 5288 1027	-8.	-94.	\checkmark
RXJ 0317.9+0231	2.3	A 59 24	-19.7	-66.2	*
RXJ 0330.7+0306N	2.3	S 67 206	39.	-84.	?
RXJ 0336.0+0846	2.3	A 657 726	17.2	22.1	*
RXJ 0403.4+1725	2.2	S 1254 309	-61.	-16.	?
BD +00 760	2.3	T 75 1529	59.5	-7.2	*
LkCa 14	2.1	S 1834 177	-161.	95.	?
RXJ 0523.9+1101	2.3	S 704 2073	2.	-114.	?

⁽¹⁾ checked by comparison with Schilbach et al. (1995)

⁽²⁾ classified as non-member by van Leeuwen et al. (1986)

2.4 High proper motion stars

2.4.1 Verification of high proper motions

Prior to the physical interpretation of the large proper motions of a number of stars, these proper motions have to be carefully investigated. As mentioned, STARNET proper motions are derived from AC and GSC. For a certain number of stars in STARNET misidentifications of their positions on the AC and/or GSC plates can occur because of the large (≈ 80 years) epoch difference. It was decided to cross-check large proper motions either by comparison with the proper motion given in another catalogue, if available, or by testing the star's position on the plates of a third epoch. This is by no means an easy task, because accurate astrometric data in this magnitude range are rare.

Table 2.4 summarizes the stars with large proper motions from Tables 2.1, 2.2 and 2.3. The sample can be split into stars with proper motions close to the mean proper motion of the Pleiades cluster ($\mu_\alpha \approx 16$ mas/a, $\mu_\delta \approx -44$ mas/a) and those with proper motions randomly far off the mean motion of Tau-Aur. The proper motions of 16 stars in Table 2.4 could be confirmed by comparison with their positions on the digitized POSS I plates (indicated by a \checkmark) or by independent proper motion measurements (indicated by a *). The digitized POSS I is well suited to check the erroneously large proper motions because in this case there should be a large, easily detectable offset from the expected position. This turned out to be the case for the 5 remaining stars; their proper motions seem to be erroneous in STARNET.

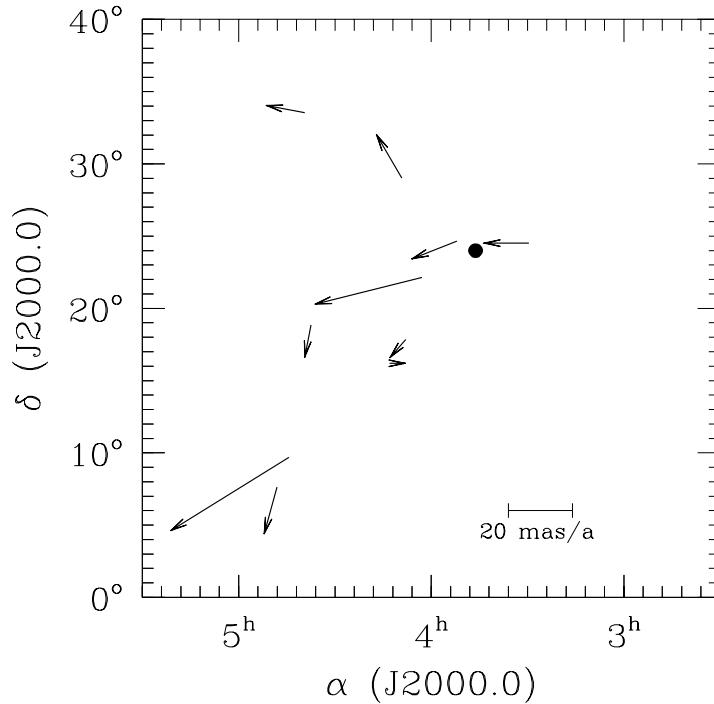


Figure 2.6: Positions of the possible Pleiades members and escapers and directions of their proper motions relative to the cluster mean ($\mu_\alpha = 16 \text{ mas/a}$, $\mu_\delta = -44 \text{ mas/a}$). The filled circle indicates the centre of the Pleiades cluster at about $\alpha = 3^{\text{h}}$, $\delta = 24^\circ$. The scale for the length of the arrows is indicated in the lower right corner of the plot.

2.4.2 Pleiades membership

In the proper motion plot (Fig. 2.2) we find a secondary crowding of stars with proper motions similar to that of the Pleiades. Indeed the star NTTS 034903+2431 is found to match both photometric and proper motion membership criteria of the Pleiades cluster by Schilbach et al. (1995, their star No. 36000) and classified as highly probable Pleiades member. SAO 76411 A, on the other hand, corresponds to the star Pels 178, which was included in the photometric investigation of the Pleiades cluster by van Leeuwen et al. (1986) and classified as non-member.

Figure 2.6 shows the distribution on the sky of the stars regarded as candidate Pleiades member stars (upper part of Table 2.4). The position of the centre of the Pleiades cluster is indicated by a filled circle. The arrows show the proper motions of the stars from Table 2.4 relative to the mean motion of the known Pleiades member stars. Two stars close to the centre of the Pleiades have small motions relative to the Pleiades cluster; one of them is the star classified as highly probable proper motion member by Schilbach et al. (1995). Three stars about 10° away from the Pleiades centre show no relative motion and should be checked further photometrically for membership. Finally, the stars SAO 76411 A, RXJ 0409.2+2901, RXJ 0439.4+3332A, HD 287017 and RXJ 0448.0+0738 could have been ejected from the Pleiades a few million years ago. This is consistent with the findings of Kroupa (1995), who expects from the result of numerical N-body simulations of star clusters that during the lifetime of a cluster a certain fraction of stars can be ejected with velocities up to 100 km/s due to close encounters between binary systems. The ejection rate is estimated to be higher in the earlier phases of cluster evolution.

2.5 Summary

Proper motions of altogether 73 stars in the central region of Taurus-Auriga have been presented. Among the sample there are 17 CTTS and 17 WTTS known to belong to the Tau-Aur SFR before ROSAT, as well as 39 stars of the sample of Wichmann et al. (1996) found by optical follow-up spectroscopy of promising

ROSAT WTTS candidates. Proper motions of 63 of these stars are consistent with membership to the association. They show a velocity dispersion small compared to 2.7 km/s after correction for a possible spread in distances, a limit which is given by the accuracy of the proper motions. This is consistent with the derivation of an upper limit for the velocity dispersion in subgroups of the Taurus-Auriga complex of about 1–2 km/s by Jones & Herbig (1979).

Additionally, proper motions for 59 stars detected recently south of the Tau-Aur clouds (Neuhäuser et al. 1995c, Magazzù et al. 1997, Neuhäuser et al. 1997) could be identified in the proper motions catalogues. A comparison of the space velocities reveals that the stars in the central region of Tau-Aur are kinematically different from the PMS stars detected south of the association. However, no young stars were found in the sample that appear to be ejected from the Taurus-Auriga association. The distances of the southern stars are rather uncertain, but if it is assumed that they are located at the same distances as the central clouds (140 pc), both complexes would approach each other with a net velocity of about 6.3 km/s.

This can also be explained within the framework of a common origin for the stars in the centre and in the south if the southern stars are still bound to the cloud, which implies a rather high cloud mass of $\approx 2 \cdot 10^5 M_{\odot}$. It would be interesting to observe similar fields west or east of the Taurus clouds to see whether stars with similar properties to those observed south of Taurus can also be found *in* the galactic plane or only perpendicular to it. From the theoretical side of view simulations could be carried out to see whether the interplay of the cloud potential, the K_z -force and the velocities of the stars can really reproduce the observed constellation, and what type of initial conditions are needed.

Among the high proper motion stars in the sample 9 new Pleiades candidates or runaways were found, and 1 additional was known before. They are located up to $\approx 20^\circ$ away from the centre of the Pleiades cluster, and their directions of motion are consistent with them being ejected from the cluster a few million years ago.

3 Chamaeleon

The results of this chapter have already been published (Frink et al. 1998), and large parts of the text have been adopted from that paper. It has been updated with proper motions from the ACT Catalogue which has not been available when the paper was written, and the discussion takes some new references into account.

3.1 Overview

The Chamaeleon cloud complex, located in the southern hemisphere, was first discussed as a separate system of dark clouds by Hoffmeister (1962). He identified 26 RW Auriga type variable stars in this region, some of which also showed H_{α} emission.

Objective prism surveys conducted in the following decades increased the number of emission-line stars suspected to be associated with the Chamaeleon dark clouds. First results were reported by Henize (1963). The surveys conducted in 1962 and 1970 revealed 32 emission-line stars (Henize & Mendoza 1973), which were all confirmed in the extensive survey by Schwartz (1977) in the southern hemisphere and, particularly, in the Chamaeleon region. Altogether he found 45 stars in the Cha I cloud and 19 in the Cha II cloud. In another objective prism survey Hartigan (1993) found 21 new H_{α} emission-line objects in Cha I and 5 in Cha II.

Gregorio-Hetem et al. (1992) and Torres et al. (1995) used far-infrared IRAS colours to preselect T Tauri star candidates over the whole sky and found, among others, 8 bona-fide plus 1 probable TTS in or around the Chamaeleon region.

Parallel to the objective prism surveys X-ray surveys have expanded the membership lists since the late eighties. X-ray observations with the Einstein Observatory revealed 22 X-ray sources, of which 6 or 7 were associated with new probable cloud members (Feigelson & Kriss 1989). By means of high dispersion optical spectroscopy, Walter (1992) confirmed the pre-main sequence (PMS) nature for 5 of these sources as well as for 2 new candidates.

The ROSAT All-Sky Survey (RASS) has revealed 179 X-ray sources in total, of which 77 have been classified as WTTS (Alcalá et al. 1995). They are located not only near the known cloud structures, but also up to $\approx 10^{\circ}$ away from any known cloud material. For about 70 of them high resolution spectroscopy is now available, and more than 50% of the sources turn out to be in fact very young weak-line T Tauri stars (Covino et al. 1997). Some additional sources were found from ROSAT pointed observations in the Cha I cloud (Feigelson et al. 1993).

Altogether, the membership list compiled by Lawson et al. (1996) contains 117 bona-fide or probable T Tauri stars in the inner region of the association, apart from the wider distributed population investigated by Covino et al. (1997).

The discovery of many weak-line T Tauri stars up to about 50 pc away from the known molecular cloud cores of several nearby star forming regions (e.g. Chamaeleon: Alcalá et al. 1995; Orion: Alcalá et al. 1996; Lupus: Krautter et al. 1997, Wichmann et al. 1997b; Taurus-Auriga: Neuhäuser et al. 1997, Magazzú et al. 1997) has raised the question about their origin. Before, with the exception of TW Hya (Ruciński & Krautter 1983), pre-main sequence stars had only been found near the densest parts of molecular clouds, and it was assumed that all stars originate from these cloud cores. While Wichmann et al. (1997b) found that the mean age of WTTS far from the clouds was higher than for WTTS projected onto the dark clouds in Lupus, Alcalá et al. (1997) found some of the youngest WTTS far from the molecular clouds in Chamaeleon. In order to travel 30 pc in $5 \cdot 10^6$ yrs (a typical T Tauri age in the Cha I cloud) a relative velocity of about 6 km/s would be required, much more than the value of 1–2 km/s considered typical for the intrinsic velocity dispersion by Jones & Herbig (1979) or the value

of 0.9 ± 0.3 km/s derived by Dubath et al. (1996) using the radial velocities of 10 stars associated with the Cha I cloud.

Several scenarios have been put forward to account for the widely spread population of WTTS, including models where star formation takes place in the cloud cores and the stars are ejected out of these clouds subsequently (Sterzik & Durisen 1995) as well as models where star formation takes place in small cloudlets which disappear after the formation process (Feigelson 1996).

The kinematic signature of these processes should still be visible: while in the first scenario the velocity vectors of the stars should point away from the dense cores from where they were ejected, the second scenario may have produced small numbers of comoving WTTS with rather high relative velocities between different groups.

Triggered star formation by means of supernova explosions or the impacts of high velocity clouds (HVC) with the galactic plane have been proposed to explain the positions of some SFR with respect to the galactic plane (Tenorio-Tagle et al. 1987, Lépine & Duvert 1994). Nevertheless, in Chamaeleon there is no evidence of any OB association which could have triggered star formation. Lépine & Duvert (1994) however successfully modeled the observed geometry of the clouds with respect to the galactic plane with a rather simple model of a high velocity cloud impact, which also may have given rise to the observed widely spread PMS stars.

Proper motions can help to provide proofs for any of the above scenarios. A crucial point in the kinematical analysis however are the individual distances of the stars. Hipparcos parallaxes are available only for a very small fraction of the sample. The two bright late B-type stars HD 97300 and HD 90480 known to be associated with the Cha I cloud (Whittet et al. 1997) are located at distances of 188 pc and 175 pc, respectively. T Cha seems to be located closer (66 pc) than the other T Tauri stars associated to Cha I and Cha II, although the Hipparcos parallax has a very large error. Sz 6 is located at 143 pc, and the Hipparcos results for Sz 19 and CV Cha are uncertain. For stars not measured by Hipparcos a mean value of 170 pc is adopted unless stated otherwise, taking the Hipparcos results (Wichmann et al. 1998b) as well as determinations based on various other methods (see Schwartz 1991 for a review) into account. Note that this value is also in good agreement with the recent distance estimate of 160 ± 15 pc to the Cha I cloud by Whittet et al. (1997) derived on the basis of reddening distributions. We make no distinction between the distance to the Cha I and the Cha II clouds, because indications for a larger distance to Cha II are rather uncertain (Schwartz 1991, Brandner & Zinnecker 1997, Whittet et al. 1997).

3.2 Data

3.2.1 The samples

In Table 3.1 all the stars which were known or suspected to be connected to the Chamaeleon association before the ROSAT mission are listed, along with their proper motions. Altogether these are 14 stars: the 2 well-known late B type stars HD 97048 and HD 97300, with entries from Hipparcos, and 6 classical and 6 weak-line T Tauri stars. T Cha was included, although it maybe located foreground to the Chamaeleon clouds as indicated by its Hipparcos parallax (Wichmann et al. 1998b). Only one of these stars (BF Cha) is associated with the Cha II cloud, whereas the other stars are located close to Cha I. There is a third cloud in the Chamaeleon region termed Cha III which apparently also shows star formation activity (Pfau et al. 1996), but the sources are on average 2 mag fainter than in the other two clouds and none could be identified in STARNET.

As in other nearby star forming regions, optical follow-up observations of X-ray sources discovered by ROSAT led to the identification of 77 probable new pre-main sequence stars in the Chamaeleon region (Alcalá et al. 1995, 1997). These new T Tauri stars are not only located close to the clouds like most of the T Tauri stars known before, but also up to $\approx 10^\circ$ away from any known site of star formation.

Precise determinations of the lithium line (6708 \AA) strength by means of high resolution spectroscopy and comparison with the typical lithium equivalent width of young main sequence stars (like the Pleiades) of the same spectral type confirmed the pre-main sequence nature for more than half of these stars (Covino et al. 1997). We could identify 31 stars of the total sample in at least one of the proper motion catalogues

Table 3.1: Stars which could be identified at least in one proper motion catalogue and which were known to be associated with the Cha I or the Cha II cloud before the ROSAT mission. Additional designations for the stars are given in the last column.

object	cat. No.	RA ($\alpha_{J2000.0}$)	DEC ($\delta_{J2000.0}$)	m _V [mag]	μ_{α} [mas/a]	μ_{δ} [mas/a]	$\frac{\sigma_{\mu_{\alpha}}}{\cos \delta}$ [mas/a]	$\sigma_{\mu_{\delta}}$ [mas/a]	d [pc]	other designations
early-type stars										
HD 97048	HIP 54413*	11 ^h 8 ^m 3 ^s .32	-77° 39' 17".5	8.44	-92.19	1.70	0.82	0.78	175 ⁺²⁷ ₋₂₀	CHXR 29, Sz 25
HD 97300	HIP 54557*	11 9 50.02	-76 36 47.7	9.03	-94.07	-1.04	1.03	0.89	188 ⁺⁴³ ₋₃₀	CHXR 42
classical T Tauri stars										
Sz 6	HIP 53691*	10 ^h 59 ^m 6 ^s .97	-77° 1' 40".3	11.22	-97.03	1.64	2.07	1.76	143 ⁺⁵³ ₋₃₀	CHXR 6
CS Cha	S 9414 574	11 2 24.79	-77 33 35.4	12.47	-160.	16.	6.7	6.7		CHXR 10, Sz 9
Sz 19	HIP 54365*	11 7 20.72	-77 38 7.3	10.97	-113.29	3.27	3.07	2.91	210 ⁺³⁰³ ₋₇₈	CHXR 23
VW Cha	S 9414 754	11 8 1.25	-77 42 28.6	13.36	-218.	8.	7.7	7.7		CHXR 31, Sz 24
CV Cha ^(b)	T 9410 60*	11 12 27.71	-76 44 22.2	10.97	-100.3	2.5	2.1	2.9		CHXR 51, Sz 42
BF Cha	S 9417 708	13 5 20.57	-77 39 1.6	13.19	-98.	1.	4.5	4.5		Sz 54
weak-line T Tauri stars										
CHXR 8	T 9414 444*	11 ^h 0 ^m 14 ^s .51	-77° 14' 38".0	11.15	-96.5	6.1	2.0	3.5		
CHXR 11	S 9414 642	11 3 11.45	-77 21 3.7	12.41	-166.	20.	7.4	7.4		
CHXR 32	S 9414 640	11 8 14.79	-77 33 52.1	12.69	-260.	34.	7.7	7.7		Glass I
Sz 41	S 9410 300	11 12 26.10	-76 37 3.7	11.39	230.	44.	7.7	7.7		CHXR 50
CHXR 56	S 9414 209	11 12 42.50	-77 22 25.9	10.90	-195.	-30.	7.1	7.1		HM Anon
T Cha	HIP 58285*	11 57 13.53	-79 21 31.6	11.86	-214.50	-9.87	5.08	3.79	66 ⁺¹⁹ ₋₁₂	RXJ 1157.2-7921

^(b) CV Cha is a double system (CCDM 11125-7644) with 2 entries in Hipparcos (HIP 54738 and HIP 54744) and an orbital solution qualified as poor. Its parallax is rather uncertain (3.14 ± 7.39 mas).

(Table 3.2).

Unfortunately, of the 31 stars newly discovered with ROSAT for which we can find proper motions only 8 are confirmed low-mass PMS stars, whereas in the whole sample of Covino et al. (1997) the fraction of bona-fide PMS to non-PMS stars is about twice as high (40 out of 81). This is a consequence of the fact that most of the confirmed low-mass PMS stars in the Covino et al. (1997) sample having spectral types later than G5 are normally fainter than about $V \approx 11.5$ mag and hence are not included in the Hipparcos, PPM, ACT/TRC and/or STARNET catalogues, while the other objects classified as ZAMS stars or with dubious PMS nature by Covino et al. (1997) have on average earlier spectral types and hence are sufficiently bright to be present in the aforementioned catalogues.

Similarly, only sources detected with the ROSAT All-Sky Survey and none of the sources detected only in ROSAT PSPC pointed observations could be identified in any of the proper motion catalogues. This means that there is no artificial spatial clustering in the present sample due to possibly locally varying sensitivities present within the region indicated in Fig. 3.2.

3.2.2 Discordant proper motions

Most of the proper motion determinations agree very well (Tables A.4 and A.5 in the Appendix). However, for some of the stars there are significant differences, and these are listed in Table 3.3.

The most probable reason for differences in the proper motions are non-resolved binary or multiple systems: in general it is not clear whether the photocentre or the brighter component was observed, and sometimes this may be different for the positions of the first and second epoch, especially for variable stars. This may lead to spurious proper motions in the ACT and STARNET catalogues.

Orbital motion further complicates the determination of the mean proper motion for the whole system. The largest effect is expected for the Hipparcos proper motions, since 3 years of data collection covers only a short fraction of the orbits of long period binaries. Thus the instantaneous motion of the photocentre

Table 3.2: Stars with proper motions from the ROSAT sample investigated by Alcalá et al. (1995, 1997) and Covino et al. (1997). The classification in T Tauri stars and ZAMS and other stars is based on the lithium criterium as applied by C97. Note however that some of the stars classified as ZAMS stars or stars of unknown nature fall well above the main sequence when placing them in the HR diagram with the help of the Hipparcos parallax (Neuhäuser & Brandner 1998).

object	cat. No.	RA ($\alpha_{J2000.0}$)	DEC ($\delta_{J2000.0}$)	m_V [mag]	μ_α [mas/a]	μ_δ	$\frac{\sigma_{\mu_\alpha}}{\cos \delta}$ [mas/a]	σ_{μ_δ}	d [pc]
T Tauri stars									
RXJ 0837.0-7856	T 9402 921*	8 ^h 36 ^m 56 ^s .23	-78°56'45".7	10.68	-153.9	27.6	2.1	1.6	
RXJ 0850.1-7554	T 9395 2139*	8 50 5.44	-75 54 38.2	10.60	-76.0	32.7	1.7	2.0	
RXJ 0951.9-7901	A 9404 195*	9 51 50.68	-79 1 37.8	10.23	-149.4	39.5	0.98	2.67	
RXJ 1150.4-7704	S 9415 1685	11 50 28.23	-77 4 38.4	13.09	-223.	-16.	4.5	4.5	
RXJ 1158.5-7754a	HIP 58400*	11 58 28.15	-77 54 29.6	10.61	-197.82	-0.83	1.36	1.15	86 ⁺¹¹ ₋₉
RXJ 1159.7-7601	HIP 58490*	11 59 42.27	-76 1 26.1	11.09	-165.21	-4.74	1.73	1.48	92 ⁺¹⁷ ₋₁₃
RXJ 1201.7-7859	A 9420 1420*	12 1 39.13	-78 59 16.9	8.65	-213.2	-5.5	0.84	0.84	
RXJ 1239.4-7502	T 9412 59*	12 39 21.26	-75 2 39.2	10.40	-177.9	-13.6	2.8	2.7	
ZAMS and other stars									
RXJ 0849.2-7735	T 9399 1491*	8 ^h 49 ^m 11 ^s .10	-77°35'58".6	9.00	-46.1	19.7	2.9	2.1	
RXJ 0853.1-8244	S 9506 1465	8 53 5.26	-82 44 0.4	12.34	-2.	-21.	3.7	3.7	
RXJ 0917.2-7744	T 9399 2104*	9 17 10.37	-77 44 2.0	10.68	-174.2	11.2	2.3	1.7	
RXJ 0919.4-7738N	HIP 45734*	9 19 24.67	-77 38 36.4	8.03	-501.70	70.40	1.31	1.15	73 ⁺⁷ ₋₆
RXJ 0928.5-7815	A 9400 1990*	9 28 15.02	-78 15 22.4	8.64	-118.5	17.7	1.00	2.41	
RXJ 0936.3-7820	HIP 47135*	9 36 17.82	-78 20 41.6	8.65	-360.66	49.76	0.70	0.64	63 ⁺³ ₋₃
RXJ 0952.7-7933	T 9404 1702*	9 53 13.74	-79 33 28.5	9.67	-76.7	4.7	1.6	2.4	
RXJ 1009.6-8105	T 9409 1040*	10 9 58.31	-81 4 11.4	9.68	104.4	-24.4	1.6	2.1	
RXJ 1039.5-7538S	HIP 52172*	10 39 31.73	-75 37 56.3	9.38	13.26	16.75	1.64	1.40	128 ⁺²⁹ ₋₂₀
RXJ 1120.3-7828	S 9415 2314	11 20 19.68	-78 28 21.0	11.46	46.	73.	3.7	3.7	
RXJ 1125.8-8456	T 9511 1593*	11 25 17.77	-84 57 16.4	7.70	-511.7	10.9	1.8	2.1	83 ⁺⁴ ₋₄
RXJ 1140.3-8321	S 9507 2466	11 40 16.52	-83 21 0.3	12.26	-366.	28.	3.9	3.9	
RXJ 1203.7-8129	S 9424 988	12 3 24.66	-81 29 55.3	12.15	-98.	-10.	3.7	3.7	
RXJ 1207.9-7555	T 9412 2105*	12 7 51.16	-75 55 16.1	10.24	-636.0	-6.7	1.6	2.9	
RXJ 1209.8-7344	S 9239 1321	12 9 42.79	-73 44 41.5	12.87	-51.	-5.	3.6	3.6	
RXJ 1217.4-8035	T 9420 439*	12 17 26.92	-80 35 6.8	8.63	-24.5	-8.4	2.1	3.2	
RXJ 1220.6-7539	A 9412 1370*	12 20 34.37	-75 39 28.7	10.51	-472.0	3.5	1.52	2.85	
RXJ 1223.5-7740	A 9416 555*	12 23 29.04	-77 40 51.4	8.31	-306.6	12.2	0.84	0.88	
RXJ 1225.3-7857	A 9420 742*	12 25 13.42	-78 57 34.8	10.76	-123.4	-23.1	4.20	1.03	
RXJ 1233.5-7523	A 9412 190*	12 33 29.78	-75 23 11.3	9.55	-383.2	16.0	0.84	0.84	66 ⁺⁵ ₋₄
RXJ 1307.3-7602	A 9413 2147*	13 7 22.92	-76 2 36.2	10.71	-57.6	7.4	0.88	2.01	
RXJ 1325.7-7955	S 9434 97	13 25 41.79	-79 55 16.2	12.07	-50.	0.	5.0	5.0	
RXJ 1349.2-7549E	A 9426 682*	13 49 12.92	-75 49 47.5	9.67	-267.3	-31.2	1.97	1.19	

seen by Hipparcos does not reflect the mean motion of the centre of mass for these kind of systems (Lindgren et al. 1997, Wielen 1997).

Two stars of Table 3.3 are present in the Double and Multiple Systems Annex of the Hipparcos Catalogue, where the observational effects of duplicity have been taken into account. Sz 19 is perhaps an astrometric binary with a short period which could not be resolved by Hipparcos. Indeed Schwartz (1977) notes a close companion to Sz 19 in the south, confirmed by Reipurth & Zinnecker (1993) and Ghez et al. (1997), and the secondary is variable with magnitude differences of at least 2.5 mag (Brandner 1992). For RXJ 1125.8-8456 a non-linear model of the motion including acceleration terms was fitted to the Hipparcos observations, which has no meaning outside the mission interval. Although this is formally a single-star solution, we may deal with an unresolved system with a period in the range 10–100 years (Lindgren et al. 1997).

Similar effects may be responsible for the inconsistencies in the proper motions of the other two stars from Table 3.3: RXJ0837.0-7856 was not observed by Hipparcos, but is flagged as dubious astrometric reference star in the Tycho catalogue, as is RXJ 1159.7-7601. The latter star is additionally flagged as 'perhaps non-single' in the ACT catalogue.

Table 3.3: Stars with discordant proper motions in one or more catalogues. As usual, all proper motions have been transformed to the astrometric reference system defined by Hipparcos, so no systematic differences should be present.

[mas/a]	μ_α	μ_δ	$\frac{\sigma_{\mu_\alpha}}{\cos \delta}$	σ_{μ_δ}
Sz 19				
HIP	-113.29	3.27	3.07	2.91
ACT	-120.8	8.3	3.14	2.17
TRC	-108.8	10.9	1.6	6.1
STARNET	-106.	45.	4.4	4.5
RXJ 1159.7-7601				
HIP	-165.21	-4.74	1.73	1.48
ACT	-199.5	-7.5	8.73	2.93
TRC	-188.8	-8.2	2.9	1.9
STARNET	-224.	-20.	3.8	3.8

[mas/a]	μ_α	μ_δ	$\frac{\sigma_{\mu_\alpha}}{\cos \delta}$	σ_{μ_δ}
RXJ 0837.0-7856				
ACT	-147.3	26.2	1.49	1.83
TRC	-153.9	27.6	2.1	1.6
STARNET	-321.	59.	3.7	3.7
RXJ 1125.8-8456				
HIP	-545.22	12.13	0.65	0.55
PPM	-482.	12.	2.1	2.4
ACT	-555.5	12.2	0.87	1.35
TRC	-511.7	10.9	1.8	2.1
STARNET	-388.	9.	3.2	3.2

Another source of errors in the ACT and STARNET catalogues may be wrong identifications of stars, favoured by large epoch differences and large proper motions. For TRC this problem has been circumvented by setting an upper limit on the maximal allowed differences of positions at different epochs. This prevents misidentifications, but on the other side stars with really high proper motions ($\gtrsim 180$ mas/a) will not be present in the catalogue due to this selection process.

All these effects may explain the large differences between proper motions in different catalogues, although in most of the cases the actual error source is difficult to find out.

3.3 Kinematics

3.3.1 Proper motions

Positions and proper motions of the stars in Tables 3.1 and 3.2 are plotted in Fig. 3.1. The two open star symbols denote the early type stars HD 97048 and HD 97300, the filled triangles classical TTS and the open triangles weak-line TTS known before the ROSAT mission. The filled circles represent confirmed low-mass PMS stars, while the open ones are objects classified as ZAMS stars or with dubious PMS nature by Covino et al. (1997). One immediately notes that there is a trend for proper motion vectors pointing to the west, with some scatter especially for the ZAMS stars, as expected from their probably higher velocity dispersion. For a more detailed analysis, the data were also plotted in galactic coordinates (Figs. 3.2 and 3.3), which are better suited for a rectangular illustration due to the position of the Chamaeleon association near to the southern equatorial pole. The motion of the stars is partly due to the reflex motion of the Sun, which is about $(\mu_l \cos b, \mu_b) \approx (-17, -6)$ mas/a at the position of the Chamaeleon association and a distance of 170 pc. Note however that this value strongly depends on the adopted distance (for half the distance the value would be twice as high), whereas the variations caused by different positions on the sky are rather low within the studied area.

Bona-fide PMS stars

From Fig. 3.3 we infer at least 2 or 3 different areas in the proper motion diagram where confirmed PMS stars tend to cluster (Table 3.4). It turns out that these subgroups are not only apparent in the proper motion diagram, but likewise they correspond to different regions in the position diagram, which independently confirms the subdivisions. The first subgroup consists of the 2 early type stars and 3 CTTS (Sz 6, Sz 19 and CV Cha), all located in the cloud core of Cha I. In the second subgroup there are 5 new PMS stars (RXJ 0837.0-7856, RXJ 1158.5-7754a, RXJ 1159.7-7601, RXJ 1201.7-7859 and RXJ 1239.4-7502), which all have very similar proper motions and, with the exception of RXJ 0837.0-

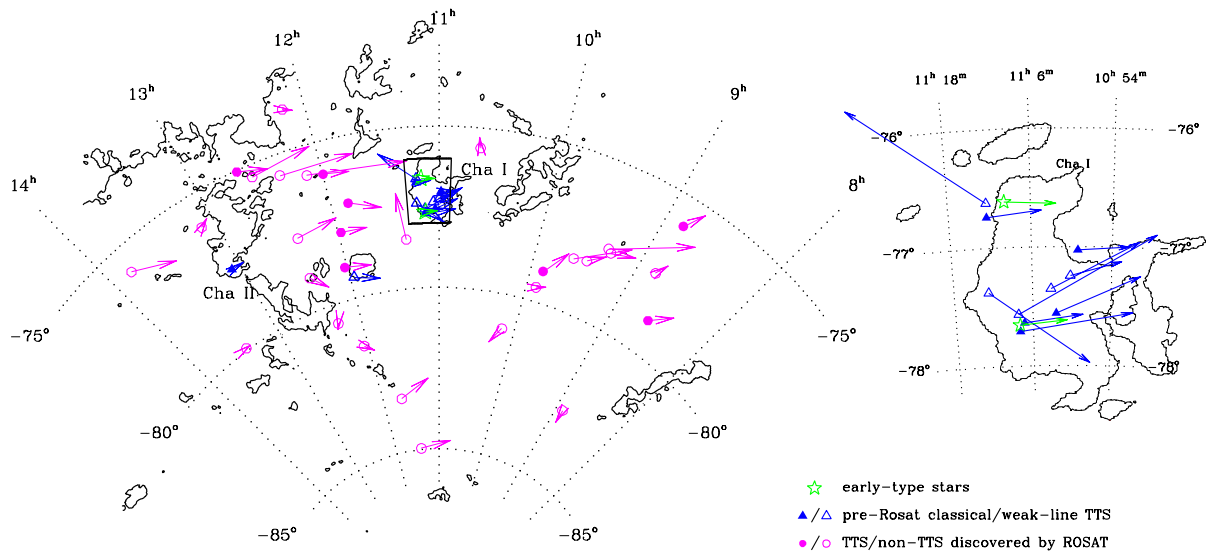


Figure 3.1: Positions and proper motions of the stars in Tables 3.1 and 3.2. Contours are from the IRAS $100\ \mu\text{m}$ survey. The marked region around Cha I is shown on an enlarged scale, too. Most of the new ROSAT discovered stars are either located between these two clouds or west of Cha I. 1° corresponds to $50\ \text{mas/a}$; the largest arrow in the figure (RXJ 1207.9-7555 between Cha I and Cha II) corresponds to $156\ \text{mas/a}$.

7856¹, are all located between the Cha I and Cha II clouds. Besides these ROSAT detected PMS stars one CTTS (VW Cha) and one WTTS (T Cha) also match the requirements of subgroup 2. Note that T Cha is also located between Cha I and Cha II, whereas the position of VW Cha is close to the core of the Cha I cloud.

The proper motions of subgroups 1 and 2 point into the same direction, but the absolute values are about twice as high for the second group. This finding is consistent with a scenario where the mean distance for the second subgroup is about half of the mean distance for the first subgroup. Then, both groups would have consistent space velocities. Indeed this picture is confirmed by the Hipparcos parallaxes: with the assumption for the mean distance of Cha I of $170\ \text{pc}$ (the distances for 4 stars in subgroup 1 are $175\ \text{pc}$ (HD 97048), $188\ \text{pc}$ (HD 97300), $143\ \text{pc}$ (Sz 6) and $210\ \text{pc}$ (Sz 19)) a mean distance of about $90\ \text{pc}$ for stars in subgroup 2 would be expected. The parallaxes as observed by Hipparcos for 3 stars in subgroup 2 correspond to distances of $86\ \text{pc}$ (RXJ 1158.5-7754a), $92\ \text{pc}$ (RXJ 1159.7-7601) and $66\ \text{pc}$ (T Cha), which gives very strong support to the above interpretation.

Very recently, Terranegra et al. (1999) have derived proper motions for faint stars in the Chamaeleon region using ESO Schmidt plates, and their results confirm the existence of subgroup 2. Indeed, they found some new stars possibly belonging to this kinematical group, extending the list of candidate members to altogether 17 stars now. They added the 4 ROSAT sources and confirmed PMS stars RXJ 1150.4-7704 (which was rejected on the basis of the STARNET proper motion before), RXJ 1204.6-7731, RXJ 1219.7-7403, RXJ 1220.4-7407, 3 stars of the low-resolution spectroscopy study of Alcalá et al. (1995), namely RXJ 1150.9-7411, RXJ 1156.0-7700 (HIP 58180) and RXJ 1202.8-7718, as well as another Herbig Ae/Be star, HD 104237 (HIP 58520).

The existence of subgroup 3 is not so obvious as for the other 2 subgroups. The 3 stars which were grouped together are CS Cha, CHXR 11 and RXJ 0850.1-7554. Nevertheless, assuming its existence 4 more stars with higher (BF Cha and CHXR 8) or lower distances (RXJ 0951.9-7901 and CHXR 32) could be attributed to it.

Only 2 WTTS and 1 new PMS (Sz 41, CHXR 56 and RXJ 1150.4-7704) are left from the sample of the bona-fide PMS stars (Table 3.1 and upper part of Table 3.2) which do not fit in any of the above subgroups because of quite different proper motions. Sz 41 is at least a double system: besides a faint companion another star nearly as bright as the primary is located $11''4$ away from Sz 41 (Brandner 1992;

¹Note from Table 3.3 that RXJ 0837.0-7856 has a different proper motion in STARNET which would make it a good candidate for a run-away TTS (RATTS), possibly ejected some 10^6 years ago.

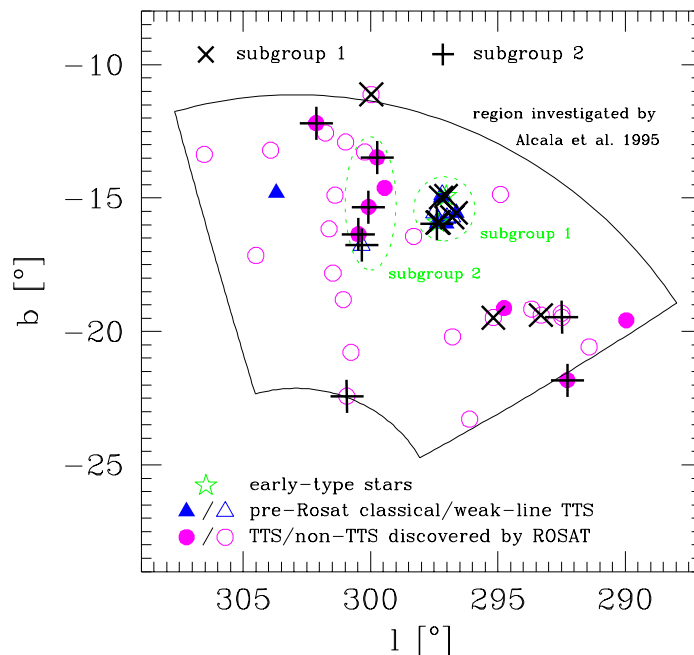


Figure 3.2: Positions of the stars in Tables 3.1 and 3.2 in galactic coordinates. The subgroups 1 and 2 defined in Section 3.3.1 are indicated by the overplotted symbols 'x' and '+'. Stars with dubious PMS nature according to Covino et al. (1997) and others which could be attributed to one of the subgroups on the basis of their proper motions are also coded. For illustration the approximate positions of subgroups 1 & 2 on the sky and the region investigated by Alcalá et al. (1995) are indicated, too, whereas for subgroup 3 there is no pronounced clustering in the position diagram.

Reipurth & Zinnecker 1993). RXJ 1150.4-7704 is flagged as a possible spectroscopic binary by Covino et al. (1997). Thus it is possible that the proper motions of these stars are not representing their space motions.

The velocity dispersions in the subgroups are of the same order of magnitude as the errors of the proper motions, and so the intrinsic velocity dispersions must be much smaller (at a distance of 170 pc 1 mas/a corresponds to 0.8 km/s). To some extent this was expected, because only stars with similar proper motions were grouped together. On the other hand such low values for the intrinsic velocity dispersion agree with other determinations. Jones & Herbig (1979) derived a value of 1–2 km/s in one coordinate for the intrinsic velocity dispersions of subgroups in Taurus-Auriga and considered this as typical for associations. Dubath et al. (1996) calculated a value of 0.9 ± 0.3 km/s based on the radial velocities of 10 stars in Cha I.

ZAMS stars and others

The stars of Table 3.2 classified as stars with dubious PMS nature or as ZAMS stars by Covino et al. (1997) clearly show a very large range in proper motions, which independently confirms the conclusions from applying the lithium criterion by Covino et al. (1997). This criterion is very conservative, as it rejects stars with lithium abundances similar to the Pleiades as weak-line TTS, although it may very well be the case that some truly pre-main sequence stars exhibit such low lithium strengths. Note that all the stars with Hipparcos parallaxes in Table 3.2 fall well above the main sequence when comparing their positions in the HR diagram with various PMS evolutionary tracks (Neuhäuser & Brandner 1998).

There are a few other stars in Table 3.2 which - rated from their proper motions - probably fall into this category of unrecognized weak-line T Tauri stars. Judging from the proper motions alone one could assign RXJ 0928.5-7815, RXJ 0952.7-7933 and RXJ 1209.8-7344 to subgroup 1, RXJ 0917.2-7744 and RXJ 1125.8-8456 (its Hipparcos parallax corresponding to 83 pc also fits this interpretation) to subgroup 2, and RXJ 0849.2-7735 and RXJ 1223.5-7740 to subgroup 3. One must however bear in mind

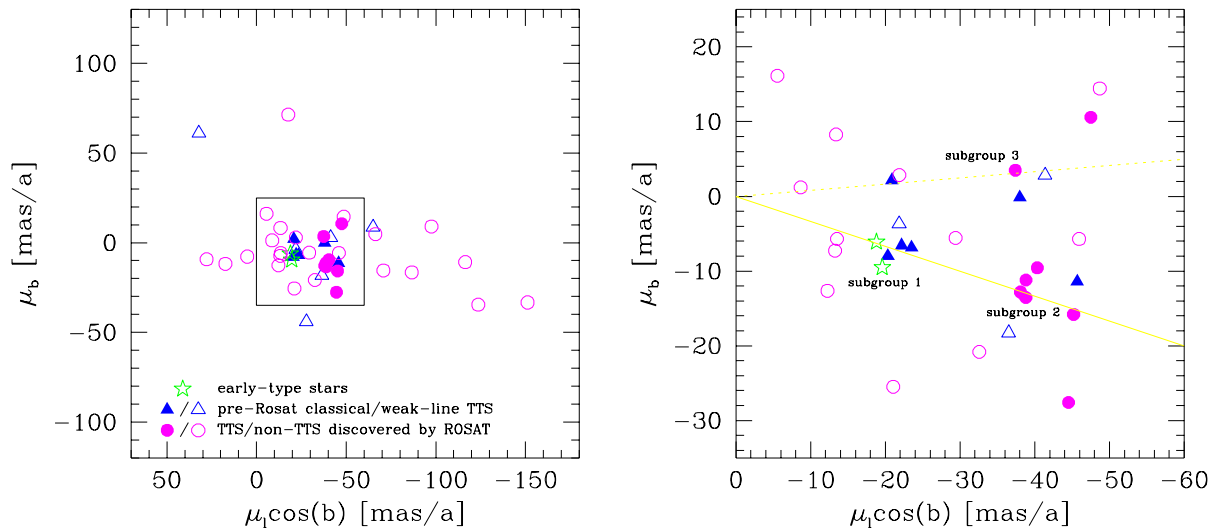


Figure 3.3: Proper motion diagram in galactic coordinates for all the stars in Tables 3.1 and 3.2. The right panel is an enlarged reproduction of the central marked region of the left panel. The different subgroups are introduced in Section 3.3.1, and the lines correspond to motions for varying distances.

Table 3.4: Subgroups derived from the proper motion diagram (Fig. 3.3) with their mean proper motions and dispersions. The number of stars in each subgroup is given in the last column.

sub-group	$\mu_l \cos b$ [mas/a]	μ_b [mas/a]	# of stars
1	-21.0 ± 1.8	-6.8 ± 2.0	6
2	-40.5 ± 3.6	-13.2 ± 3.0	7
3	-38.9 ± 2.1	2.1 ± 1.9	3

that the reflex motion of the sun is very similar to the typical proper motion of Chamaeleon member stars, making it difficult to distinguish between members and field stars on the basis of the proper motions alone.

3.3.2 Space velocities

Space velocities have been calculated for all stars in subgroups 1 and 2 and the Hipparcos stars with radial velocities available in the literature (HD 97048 from Finkenzeller & Jankovics (1984), 4 CTTS from Dubath et al. (1996), and T Cha and stars in Table 3.2 from Covino et al. (1997)). For stars not observed by Hipparcos a distance of 170 pc for subgroup 1 and 90 pc for subgroup 2 was adopted.

The space velocities have been corrected for the effect of differential galactic rotation, assuming the IAU standard values of 8.5 kpc for the distance to the galactic centre and 220 km/s for the velocity of the Local Standard of Rest. The value of this correction depends on the galactic azimuthal angle and therefore in general also on the distances of the stars. The mean corrections in the U -velocities for stars in subgroup 1 and 2 are 3.8 km/s and 2.0 km/s, respectively (the corrections in the V -velocities are practically zero). Additionally, the motion of the Sun ($(U, V, W) = (9, 12, 7)$ km/s, Delhaye 1965) has been added to the space velocities, although it does not change the relative velocities between the groups which are of interest here.

The coincidence of the mean values for the three space velocity components of Hipparcos PMS stars and the combined sample of subgroups 1 & 2 is artificial to some extent (see Table 3.5) as the 6 Hipparcos stars form a subset of subgroups 1 & 2. The mean values for subgroup 1 and 2 are also in quite good agreement.

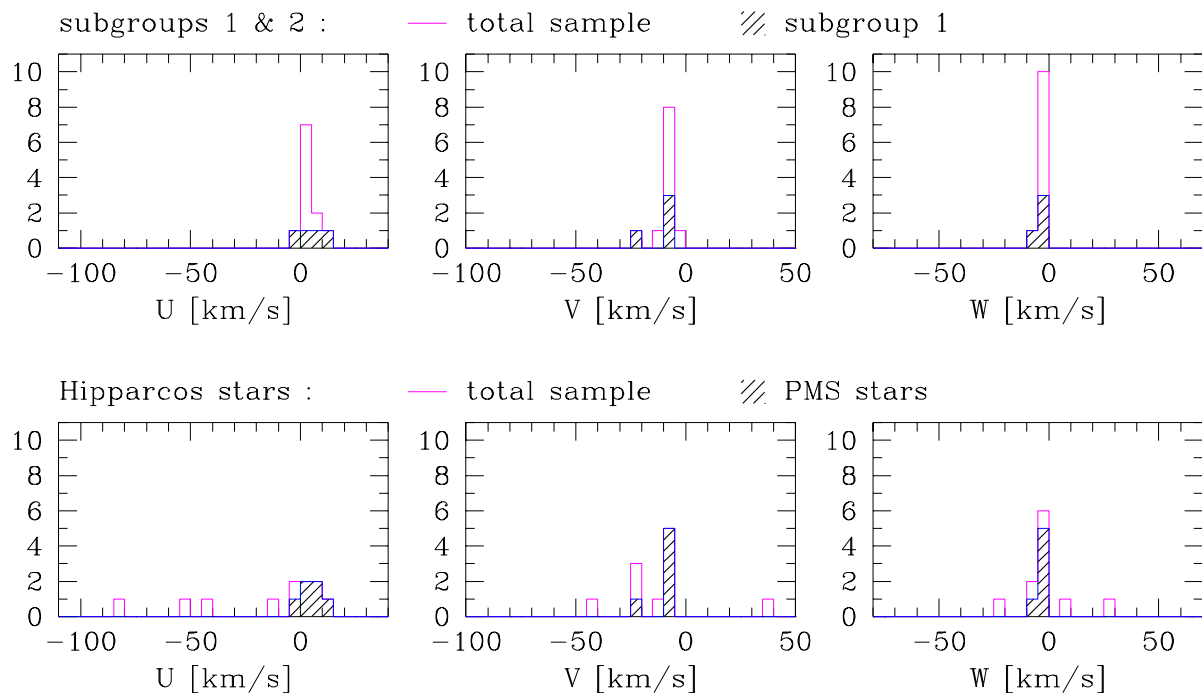


Figure 3.4: Space velocity histograms shown separately for stars in subgroups 1 and 2 (upper panels) and for Hipparcos stars (lower panels). In the upper diagrams the contribution of subgroup 1 is hatched, and no significant differences between the two subgroups are visible. In the lower diagrams the contribution of the PMS stars is hatched. We assumed the same distances as in Table 3.5 and corrected the velocities for the effects of differential galactic rotation and the motion of the Sun.

The interpretation of different proper motions in terms of different distances is further confirmed when taking the additional information on the radial velocities and projection effects due to different positions in space into account.

Comparing the Hipparcos PMS stars with ZAMS stars and stars of dubious PMS nature in Fig. 3.4, one again notes the clear peak in the distribution of the PMS stars and the large scatter of the presumably older stars.

3.4 Discussion

3.4.1 Structure of the Chamaeleon clouds

The IRAS 100μ map of the Chamaeleon region shows several filamentary clouds which extend over an area of more than 100 square degrees. It is an open question whether the individual structures termed Cha I, Cha II and Cha III are really physically related to each other. There is another cloud, DC 300.2-16.9 (Hartley et al. 1986), located between Cha I and Cha II roughly at the position of T Cha.

The Hipparcos parallax of T Cha implies a relatively small distance of 66 pc. Note however that the large parallax error for this star puts an upper limit of 85 pc while the lower limit is 54 pc. The latter would place T Cha practically on the main sequence, which is absolutely inconsistent with the pronounced PMS characteristics of this star (Alcalá et al. 1993). Even the mean distance of 66 pc would give an extremely old age of some 40 Myr for this star. Since T Cha is definitely a T Tauri star the upper limit of 85 pc should be closer to the true distance of T Cha.

On the other hand, an upper limit of 180 pc has been established for the distance to the cloud DC 300.2-16.9 (Boulanger et al. 1998), to which T Cha seems to be associated. Thus, it may well be that this cloud is also located closer than the Cha I cloud, maybe also at about 90 pc from the Sun. The Hipparcos parallaxes of the other stars in subgroup 2 as well as the analysis of the proper motions in

Table 3.5: Mean space velocities and dispersions separately for stars of subgroups 1 & 2 and Hipparcos PMS stars as well as for the total samples, as shown in Fig. 3.4. U -velocities are positive in the direction of the galactic centre. The velocities have been corrected for the effects of differential galactic rotation and the reflex motion of the Sun. For the calculation of the space velocities we used either the Hipparcos parallaxes or, where not available, a distance of 170 pc for stars in subgroup 1 and 90 pc for stars in subgroup 2.

	#	$\langle U \rangle$ [km/s]	σ_U	$\langle V \rangle$ [km s ⁻¹]	σ_V	$\langle W \rangle$ [km/s]	σ_W
subgroup 1	4	4.8	6.5	-10.8	8.2	-3.5	2.6
subgroup 2	7	2.8	3.0	-7.8	3.2	-2.5	1.5
subgroups 1 & 2	11	3.5	4.4	-8.9	5.4	-2.9	2.0
Hipparcos PMS	6	5.2	5.5	-9.6	6.7	-3.1	2.5
all Hipparcos stars	11	-14.9	30.6	-10.7	18.5	-1.1	11.9

Section 3.3.1 support this scenario of stars and even some cloud material at distances of about 90 pc, as well as the additional proper motions of fainter stars by Terranegra et al. (1999).

The question now is how can a SFR be such large in volume? Models for the formation scenario of the Chamaeleon cloud complex which possibly could explain the existence of PMS stars far off the observed molecular clouds are discussed in the next section.

Alternatively, it is also possible that the observed cloud material belongs to distinct structures as considered by Whittet et al. (1997). In this case the stars in subgroups 1 & 2 would have the same space velocities although they are not associated with the same cloud material. However, it is not unusual that young stars exhibit rather low velocities relative to the field stars in the same region (cf. the Taurus SFR or the Scorpius-Centaurus OB association).

Moreover, placing the stars of subgroup 2 at a mean distance of 90 pc rises their mean ages by about a factor of 6 to 18 Myr as compared to a mean age of 3 Myr for a mean distance of 170 pc. This could easily be explained if they belong to another structure than the stars of subgroup 1.

There are too few stars in the Chamaeleon region with distance information available to decide whether a population of PMS stars with distances intermediate between the two subgroups at around 130 pc exists. In principle, the majority of dispersed T Tauri stars detected with the flux-limited RASS are expected to be located between 90 pc and 150 pc, and the optical, IR and deep X-ray pointed observations have been sufficiently sensitive to detect PMS stars at more than 150 pc. However, most of these stars were too faint to be included in the Hipparcos Input Catalogue.

3.4.2 Implications for the formation scenario of the Chamaeleon cloud complex

The discovery of large populations of WTTS distributed over regions of 10–20 degrees or even more in extent centered around active cloud cores has raised questions about the scenario of their formation. Several scenarios have been suggested to account for the existence of very young stars far away from the known sites of star formation.

Sterzik & Durisen (1995) proposed that the WTTS halo observed around star formation regions might be due to high velocity ($\gtrsim 3$ km/s) escapers (run-away TTS or RATTs) produced by dynamical interactions in small stellar systems. This would imply that the velocity vectors of the stars point away from the dense molecular cloud cores from where they were ejected.

There are no indications for such an overall correlation between positions and proper motions. Only for some 2 or 3 stars in the sample the ejection scenario may be invoked, namely Sz 41, CHXR 56, and perhaps RXJ 0837.0-7856, if their proper motions are not spurious due to binarity. On the contrary, if it

is assumed that subgroup 2 is at the same distance as subgroup 1 (ignoring the Hipparcos parallaxes for the moment), the stars of subgroup 2 would move with higher space velocities in the direction of lower right ascension than the stars of subgroup 1 while being located at higher right ascension (cf. Fig. 3.1). This means that they would approach the Cha I molecular cloud. Given the direction of motion, it cannot be excluded that some stars may have been ejected from the Cha II cloud. However, the fact that these stars seem to form a co-moving group is inconsistent with the prediction of any ejection model, in which the motion would be completely random, so that the ejection scenario can be excluded as the dominant process for producing the dispersed population of WTTS in Chamaeleon.

Lépine & Duvert (1994) tried to explain the displacement with respect to the galactic plane of several near-by star forming regions including Chamaeleon by infall of high velocity clouds (HVC) on the galactic plane. There is no detailed prediction for the kinematics of the stars in the HVC impact scenario, except for the fact that, subsequent to the impact, clouds and stars will oscillate around the galactic plane and tend to separate from each other (combing-out). Given the fact that at least the stars in subgroups 1 & 2 display practically no net motion perpendicular to the galactic plane after correcting their proper motions for the solar reflex motion, one might speculate that they are just reversing their direction of motion, although the offset of the Chamaeleon association from the galactic plane is not very large. Nevertheless, these indications are far from being conclusive and depend strongly on the adopted distances.

Feigelson (1996) proposed that low mass stars may form in dispersed cloudlets in a turbulent environment. Also, it has long been suspected that Bok globules are the sites of isolated star formation. Recent studies (Launhardt & Henning 1997, Yun et al. 1997) have shown that such globules can be associated with embedded IR and IRAS point sources in which very young low mass stars are found. It is however not clear if these globules are related to Feigelson's cloudlets.

In order to explain the observed distribution of WTTS Feigelson (1996) considers models with a velocity dispersion of the order of 1 km/s (due to internal thermal motions in the gas of the parent cloud), with thermal velocity dispersal in combination with dynamical ejection, and with star formation in small cloudlets distributed over a larger region. Comparing the predictions of his models with the properties of the observed WTTS population, he found that the first two dispersal models encounter serious problems. In particular, the thermal dispersal model can explain the number of WTTS found far from the active clouds, but not their low ages. In order to overcome this difficulty within the framework of the current model one would have to assume an unplausibly high velocity dispersion even at the time of their formation. An improved dispersal model, where a certain fraction of the dispersing stars is made up of high velocity escapers, cannot account for the observations either, unless the ejection rate significantly increased recently. The model can indeed explain the existence of some very young stars far from their sites of origin, but simultaneously it produces a population of older ejected stars, which would lead to an unplausibly high star formation efficiency.

As already pointed out above, the proper motion data of the stars discussed in the previous sections are inconsistent with any dispersal model either, as the velocity vectors are not oriented away from any single point.

In the most promising model investigated by Feigelson star formation takes place in long-lived active cloud cores as well as in a number of small short-lived cloudlets distributed over a rather large region. These cloudlets are believed to possess high velocities relative to their parental giant molecular clouds because of its turbulent structure. After producing some stars with very low internal velocity dispersion the cloudlets disappear, leaving behind streams of T Tauri stars with high relative velocities between each other.

As proper motions are available only for a very small fraction of all the young stars in the Chamaeleon region (probably for less than 10% according to the estimate by Feigelson of several hundred stars yet to be discovered), it is difficult to verify the predictions of the model quantitatively. If we ignore the stars in subgroups 1 & 2 for the moment, which we assume to have formed in the dense cloud cores, we are left with not more than 33 stars which possibly originated in small cloudlets. Feigelson estimates the number of cloudlets to be of the order of 50, so that not more than one or two stars of the same cloudlet can be expected in the present sample. Although the model cannot be confirmed decisively, from the proper motion diagram (Fig. 3.3) one could select good candidate stars which possibly were formed in cloudlets. New proper motions determined by Relke & Pfau (1999) seem to give strong support to Feigelson's cloudlet model, too.

Another limiting factor in this kinematical study is the lack of precise distances for the majority of the stars. For a more detailed comparison with the model of Feigelson one needs to correct the proper motions of the wider distributed TTS and not only of the stars in the two subgroups for galactic rotation and the reflex of the solar motion, which requires knowledge of the individual distances. Similarly, comparisons with the ejection scenario are also hampered by the lack of precise distances, as the relative velocities can change sign when putting the stars at higher or lower distances.

3.5 Summary

Proper motions from the Hipparcos, PPM, ACT/TRC and STARNET catalogues for altogether 45 stars in the Chamaeleon region have been analysed, 22 of which are bona-fide pre-main sequence stars and 23 are of dubious PMS nature or ZAMS stars. On the basis of the distribution of the proper motions the presence of several subgroups in the data is suggested, which roughly coincide with similar groups on the sky. Given the kinematical distances which are independently confirmed by the Hipparcos parallaxes, the two subgroups might belong to distinct structures of the Chamaeleon clouds.

There is no indication in these data for a slow dispersal of stars out of the active cloud cores, and so the model proposed by Sterzik & Durisen (1995) cannot account for the large distribution of WTTS observed far from any known cloud material. However, the observed motions are more or less consistent with the high velocity cloud impact model of Lépine & Duvert (1994) if the stars are currently at their turning point. The most promising model at the moment is the cloudlet model proposed by Feigelson (1996), where star formation takes place far off the active cloud cores and which produces small groups of TTS with low internal velocity dispersions, but high relative velocities between groups.

Larger proper motion catalogues produced hopefully by future space missions like DIVA or GAIA will help to settle the question of the formation scenario of this large population of weak-line T Tauri stars in the Chamaeleon region.

4 Lupus

4.1 Overview

The first T Tauri stars in Lupus have been discovered by Joy (1945) and Henize (1954). Objective prism surveys conducted by The (1962) and Schwartz (1977) revealed the existence of numerous additional H_α emission stars, and so the term T association seemed to be justified.

The molecular clouds in the Lupus region consist of four subgroups, termed Lupus 1, 2, 3 and 4. Recently, Tachihara et al. (1996) observed a region spanning 25.4 square degrees for CO emission and discovered a new cloud east of Lupus 3 which they termed Lupus 5. Large-scale systematic CO observations in the Lupus region covering 170 square degrees have been carried out by Murphy et al. (1986), and the total cloud mass has been estimated to be about $3 \cdot 10^4 M_\odot$.

Most of the classical T Tauri stars were found in the Lupus 3 subgroup. Besides these TTS two very bright A-type stars (the Herbig Ae/Be star HR 5999 and HR 6000) are also located in Lupus 3, which form a common proper motion pair (Bessel & Eggen 1972).

Like in other nearby SFR, optical follow-up observations of promising TTS candidates from the ROSAT All-Sky Survey as well as from additional pointed observations enlarged the membership list of Lupus enormously. Krautter et al. (1997) identified altogether 136 new T Tauri stars in a region of 230 square degrees, and in contrast to the classical TTS these stars did not concentrate in the centres of the dark clouds.

Wichmann et al. (1997a) found the ages of the so-called off-cloud WTTS to be higher than those of the on-cloud WTTS or CTTS. A second difference between WTTS and CTTS shows up in their mass distributions. Whereas among the CTTS population in Lupus low-mass stars ($< 0.5 M_\odot$) are more frequent than in other nearby SFR (Appenzeller et al. 1983, Krautter & Kelemen 1987, Strom et al. 1987, Krautter 1991), the relative amount of higher mass stars increases for the ROSAT discovered WTTS population. This might indicate that SF in Lupus is controlled by magnetic forces (Krautter 1991) or might reflect the fact that the Lupus SFR is older than the Taurus or Chamaeleon region (Hughes et al. 1994, Wichmann et al. 1997a).

Wichmann et al. (1997b) investigated whether it is possible that the WTTS discovered by ROSAT are related to the Gould's Belt system (see Pöppel 1997 for a recent review). Their study area consisted of a narrow strip perpendicular to Gould's Belt, and indeed they found a clustering of those stars exactly towards Gould's Belt midplane.

In contrast to other regions, the majority of the stars classified as possible TTS in medium resolution studies was confirmed to be very young in a recent high resolution spectroscopy study by Wichmann et al. (1999a).

For a review of distance estimates to the Lupus clouds and stars see Krautter (1991). He concludes that the distance is most probable between 130pc and 170pc, and suggests to use a mean distance of 150pc. Several other distance estimates have become available since then. While Hughes et al. (1993) derived a distance of 140 ± 20 pc using spectroscopic parallaxes, averaging the Hipparcos parallaxes of 5 stars yields a distance of 190 ± 27 pc (Wichmann et al. 1998b), which is at the higher end of the considered distance range.

Investigating the rotational properties of a number of ROSAT discovered WTTS by means of a statistical approach, Wichmann et al. (1999a) conclude that the mean distance to the Lupus SFR should be in the range 135–165pc. Note that these latter distance estimates would make the Lupus clouds at least as distant as the Scorpius Centaurus OB association, whose mean distance ranges from 118 ± 2 pc for Lower Centaurus Crux over 140 ± 2 pc for Upper Centaurus Lupus to 145 ± 2 pc for Upper Scorpius, as determined by de Zeeuw et al. (1999) from Hipparcos parallaxes of hundreds of member stars.

Table 4.1: Proper motions for stars have been known to be associated to the Lupus SFR before the ROSAT mission. Altogether these are two bright A stars and 4 classical and 4 weak-line T Tauri stars. F403 has been identified as a WTTS by Hughes et al. (1993).

object	cat. No.	RA ($\alpha_{J2000.0}$)	DEC ($\delta_{J2000.0}$)	m_V [mag]	μ_α [mas/a]	μ_δ [mas/a]	$\frac{\sigma_{\mu_\alpha}}{\cos \delta}$ [mas/a]	σ_{μ_δ} [mas/a]	d [pc]	other des.
early-type stars										
HR 5999	HIP 79080*	16 ^h 8 ^m 34 ^s .28	-39° 6′ 18″.3	7.01	-12.32	-24.25	0.85	0.72	208 ⁺⁴⁶ ₋₃₂	
HR 6000	HIP 79081*	16 8 34.57	-39 5 34.3	6.62	-8.31	-22.46	0.80	0.67	241 ⁺⁶⁰ ₋₄₀	
classical T Tauri stars										
Sz 75	S 7340 177	15 ^h 49 ^m 12 ^s .08	-35° 39′ 4″.9	13.20	-20.	-18.	7.2	7.2		GQ Lup
Sz 77	S 7340 239	15 51 46.99	-35 56 44.3	13.58	2.	-31.	7.3	7.3		
Sz 83	HIP 78094*	15 56 42.31	-37 49 15.5	11.45	-13.58	-23.16	3.80	2.14	230 ⁺¹⁰⁵² ₋₁₀₃	RU Lup
Sz 88	S 7851 459	16 7 0.64	-39 2 20.2	13.91	-8.	-37.	7.0	7.0		HO Lup
weak-line T Tauri stars										
Sz 68 ^(b)	HIP 77157*	15 ^h 45 ^m 12 ^s .87	-34° 17′ 30″.6	10.50	-16.79	-20.20	2.17	1.61	159 ⁺⁷⁷ ₋₃₉	HT Lup
Sz 82	S 7838 962*	15 56 9.20	-37 56 6.2	12.65	-6.	-23.	6.8	6.8		IM Lup
RY Lup	HIP 78317*	15 59 28.39	-40 21 51.3	11.19	-12.28	-22.12	3.13	2.04	108 ⁺⁴⁸ ₋₂₅	
F 403	S 7859 1039	16 0 44.48	-41 55 30.8	12.76	-28.	-22.	4.5	4.5		

^(b) also detected in X-rays: RXJ 1545.2-3417

Murphy et al. (1986) noted that the Lupus clouds seem to be projected onto a gap between the US and UCL subgroups of the Sco-Cen association, but from the above distance discussion it seems unlikely that the Lupus clouds are foreground to Sco-Cen, as speculated by them to explain the lack of OB stars in this gap.

However, it will be interesting to find out whether any kind of relation between Sco-Cen and Lupus could be established in the future, and how different circumstances possibly favour or prevent the formation of massive early-type stars in a SFR.

4.2 Data

4.2.1 Pre-main sequence stars known before ROSAT

Krautter (1991) compiled a list of TTS in the Lupus SFR known at that time. It comprised altogether 60 stars, of which 7 (4 CTTS and 3 WTTS) could be identified in the Hipparcos, PPM, ACT, TRC and/or STARNET proper motion catalogues (Table 4.1 and Table 4.2 in the Appendix). Unfortunately most of the stars in the sample from Krautter (1991) have magnitudes fainter than 12–13 mag, which is just too faint to find a larger number of them in the STARNET catalogue. One additional WTTS (F403) is listed that was found by Hughes et al. (1993) only by chance - it was included in their field star sample to determine the distance of the Lupus dark clouds by means of an extinction versus distance plot.

The two bright A-type stars HR 5999 (a Herbig Ae/Be star) and HR 6000 have also been included in Table 4.1 with their Hipparcos proper motions. Note that HR 6000 probably is a binary with a TTS as faint companion (van den Ancker et al. 1996). Tycho also confirmed the duplicity.

4.2.2 Pre-main sequence stars discovered with ROSAT

As already mentioned in the introduction, quite a number of PMS stars have been discovered with the help of ROSAT and optical follow-up observations in the Lupus region. Of the 136 stars identified by Krautter et al. (1997) 66 could be found in at least one of the proper motion catalogues, and they are

Table 4.2: ROSAT discovered WTTS in the central part of the Lupus region (Krautter et al. 1997) and in a narrow strip perpendicular to Gould's Belt (Wichmann et al. 1997b). 5 stars have been marked that turned out to be older than PMS, either ZAMS or unrelated field stars, in a recent high resolution spectroscopy study (Wichmann et al. 1999a).

object	cat. No.	RA ($\alpha_{J2000.0}$)	DEC ($\delta_{J2000.0}$)	m _V [mag]	μ_{α} [mas/a]	μ_{δ} [mas/a]	$\sigma_{\mu_{\alpha}}^{\cos \delta}$ [mas/a]	$\sigma_{\mu_{\delta}}$ [mas/a]	d [pc]	other des.
stars from Krautter et al. (1997)										
RXJ 1505.9-4311	S 7833 587	15 ^h 5 ^m 56 ^s .85	-43° 12' 3'' 0	13.65	-35.	-22.	4.8	4.8		
RXJ 1507.2-3505	T 7319 749*	15 7 14.81	-35 4 59.6	10.80	-42.6	-30.8	1.6	1.8		
RXJ 1507.4-4601	S 8293 2359	15 7 27.46	-46 1 6.3	11.71	-49.	-9.	3.7	3.7		
RXJ 1507.6-4603	S 8293 2003	15 7 37.75	-46 3 14.5	12.15	-26.	-10.	4.0	4.0		
RXJ 1507.9-4515 [‡]	T 8293 642*	15 7 54.50	-45 15 21.2	10.77	36.5	-0.3	3.3	2.3		
RXJ 1508.0-3337	S 7315 1685	15 8 5.09	-33 37 55.7	13.09	-34.	-30.	6.1	6.1		
RXJ 1508.6-4423	T 7833 2400*	15 8 37.74	-44 23 16.9	10.85	-25.2	-7.7	1.8	1.6		
RXJ 1508.7-4400	T 7833 2559*	15 8 38.50	-44 0 52.1	10.51	-31.4	-20.0	2.2	3.1		HD 133938
RXJ 1508.8-3715	S 7323 133	15 8 53.80	-37 15 46.9	12.64	-20.	-27.	5.5	5.5		
RXJ 1511.0-3251	S 7316 564	15 11 4.59	-32 51 29.7	12.41	-2.	-15.	6.9	6.9		
RXJ 1514.2-4103 [‡]	HIP 74565*	15 14 7.54	-41 3 36.2	10.44	-26.22	-31.35	2.19	1.59	195 ⁺¹⁰² ₋₄₉	HD 134974
RXJ 1514.7-3445	A 7320 427*	15 14 39.58	-34 45 41.3	9.23	-21.1	-21.5	3.61	1.30		HD 135127
RXJ 1515.7-3331	S 7316 888	15 15 45.36	-33 31 59.7	11.61	-31.	-30.	5.5	5.5		
RXJ 1515.8-4418	S 7834 1690	15 15 52.70	-44 18 17.6	12.96	-31.	-28.	5.3	5.3		
RXJ 1516.6-4406	S 7834 696	15 16 36.76	-44 7 20.6	12.18	-5.	-26.	4.3	4.3		
RXJ 1518.4-3738	A 7822 158*	15 18 26.93	-37 38 2.2	11.26	-22.8	-29.4	2.50	1.22		
RXJ 1518.8-4050	A 7826 2975*	15 18 52.83	-40 50 52.9	10.96	-21.6	-22.7	3.37	3.16		
RXJ 1519.2-4056	S 7826 2835	15 19 16.00	-40 56 7.9	12.15	-32.	-35.	4.6	4.6		
RXJ 1522.2-3959	S 7839 870	15 22 11.66	-39 59 50.4	12.46	-19.	-15.	5.3	5.3		
RXJ 1523.4-4055	S 7839 1905	15 23 25.57	-40 55 47.2	12.21	-31.	-35.	4.9	4.9		
RXJ 1524.0-3209	S 7317 295	15 24 3.06	-32 9 50.8	13.17	-21.	-29.	6.7	6.7		
RXJ 1524.5-3652	S 7325 465	15 24 32.35	-36 52 2.6	12.44	-28.	-22.	5.6	5.6		
RXJ 1525.0-3604	A 7325 212*	15 25 3.60	-36 4 45.6	11.03	-17.1	-28.8	2.50	1.28		
RXJ 1525.3-3845 [‡]	T 7835 2569*	15 25 17.01	-38 45 25.9	9.15	-43.1	-30.7	2.3	1.6		HD 137059
RXJ 1525.5-3613	S 7325 8	15 25 33.20	-36 13 47.0	12.73	-9.	-24.	5.6	5.6		
RXJ 1526.0-4501	T 8295 1530*	15 25 59.65	-45 1 15.7	11.13	-19.2	-21.4	1.9	1.9		
RXJ 1529.6-3546	A 7326 928*	15 29 38.58	-35 46 51.4	10.62	-27.4	-27.0	4.94	2.04		
RXJ 1529.7-3628	S 7326 638	15 29 47.30	-36 28 37.8	12.91	-18.	-29.	7.2	7.2		
RXJ 1529.8-4522	S 8295 528	15 29 48.91	-45 22 45.8	12.91	-9.	-25.	4.8	4.8		
RXJ 1531.3-3329	A 7318 593*	15 31 21.93	-33 29 39.5	10.76	-26.4	-30.7	1.80	1.41		
RXJ 1534.1-3916 [‡]	A 7836 1509*	15 34 7.35	-39 16 17.4	10.62	-35.1	-28.5	1.75	2.76		
RXJ 1534.6-4002	S 7840 1008	15 34 38.16	-40 2 27.9	11.87	-36.	-33.	5.5	5.5		
RXJ 1538.0-3807	S 7836 597	15 38 2.64	-38 7 22.8	12.94	-26.	-19.	5.6	5.6		
RXJ 1538.6-3916	S 7836 1589	15 38 38.26	-39 16 55.3	11.59	-28.	-31.	4.5	4.5		
RXJ 1538.7-4411	PPM 761327*	15 38 43.06	-44 11 47.2	10.70	-33.	-26.	3.9	3.9		
RXJ 1539.7-3450	S 7335 747	15 39 46.35	-34 51 2.5	12.90	-35.	-18.	7.0	7.0		
RXJ 1540.0-4634	S 8296 1835	15 40 2.46	-46 34 18.6	12.23	-33.	-17.	5.2	5.2		
RXJ 1544.0-3311	A 7331 782*	15 44 3.77	-33 11 11.2	10.77	-25.5	-25.7	1.19	1.13		
RXJ 1544.8-3811	S 7837 494	15 44 47.13	-38 11 41.0	12.21	-24.	-30.	5.8	5.8		
RXJ 1545.9-4222	T 7845 1174*	15 45 52.25	-42 22 16.4	10.69	-23.3	-25.8	1.7	1.9		
RXJ 1546.6-3618	S 7340 723	15 46 41.19	-36 18 47.9	12.03	-20.	-32.	5.0	5.0		
RXJ 1547.6-4018	S 7841 1001	15 47 41.75	-40 18 27.0	11.18	-25.	-30.	4.5	4.5		
RXJ 1548.6-4335	S 7849 3155	15 48 42.03	-43 35 20.9	11.56	-31.	-18.	4.1	4.1		
RXJ 1549.7-3925	HIP 77524*	15 49 44.97	-39 25 9.1	10.65	-31.66	-25.17	1.99	1.79	151 ⁺⁶² ₋₃₄	HD 141277
RXJ 1549.9-3629	S 7340 1137	15 49 59.20	-36 29 57.4	12.34	-20.	-22.	5.2	5.2		
RXJ 1555.4-3338	S 7333 713	15 55 26.20	-33 38 23.6	13.66	-24.	-35.	7.6	7.6		
RXJ 1559.8-3628	S 7341 574*	15 59 49.45	-36 28 28.6	11.74	-31.	-43.	6.0	6.0	73 ⁺²² ₋₁₄	CD -36 10569
RXJ 1601.1-3320	A 7333 719*	16 1 8.97	-33 20 14.2	10.90	-13.2	-20.4	2.85	2.24		
RXJ 1601.8-4026	S 7855 709	16 1 49.45	-40 26 18.9	13.48	-20.	-16.	5.5	5.5		
RXJ 1601.9-3613	S 7341 534	16 1 59.14	-36 12 56.6	12.74	-12.	-37.	5.5	5.5		
RXJ 1603.8-4355	HIP 78684*	16 3 45.37	-43 55 49.2	9.76	-19.62	-25.52	2.43	1.93	143 ⁺⁷⁵ ₋₃₇	HD 143677
RXJ 1603.8-3938	T 7855 1106*	16 3 52.48	-39 39 1.2	11.20	-24.4	-30.6	5.8	2.3		
RXJ 1604.5-3207	A 7334 429*	16 4 30.56	-32 7 28.8	10.99	-21.1	-25.5	3.45	2.83		
RXJ 1605.0-3857 [‡]	HIP 78774*	16 4 57.07	-38 57 15.7	9.24	-34.13	-46.60	1.40	1.26	161 ⁺⁵³ ₋₃₂	HD 143978
RXJ 1605.7-3905	A 7851 1*	16 5 45.00	-39 6 6.6	10.65	-23.9	-31.6	1.29	1.04		

[‡] age probably around 10⁸ yrs

[‡] probably older than 10⁸ yrs

Table 4.2: continued.

object	cat. No.	RA ($\alpha_{J2000.0}$)	DEC ($\delta_{J2000.0}$)	m _V [mag]	μ_{α} [mas/a]	μ_{δ} [mas/a]	$\frac{\sigma_{\mu_{\alpha}}}{\cos \delta}$ [mas/a]	$\sigma_{\mu_{\delta}}$ [mas/a]	other des.
RXJ 1606.3-4447	S 7863 547	16 ^h 6 ^m 23 ^s 34	-44° 47' 35'' 6	12.84	-28.	-28.	4.7	4.7	
RXJ 1608.3-3843	S 7851 1078	16 8 18.27	-38 44 5.1	12.97	-14.	-30.	7.4	7.4	
RXJ 1608.9-3905	T 7851 426*	16 8 54.27	-39 6 5.9	11.07	-12.8	-28.9	1.6	1.6	
RXJ 1610.0-4016	S 7856 51	16 10 4.81	-40 16 12.5	11.85	-18.	-33.	6.4	6.4	
RXJ 1612.0-3840	S 7852 143	16 12 1.45	-38 40 27.7	12.76	-2.	-27.	5.5	5.5	
RXJ 1613.1-3804	S 7852 415	16 13 12.70	-38 3 51.1	13.14	-13.	-20.	5.1	5.1	
RXJ 1615.9-3241	S 7347 36	16 15 56.98	-32 41 25.2	12.86	-20.	-43.	6.6	6.6	
RXJ 1621.2-4030	PPM 321619*	16 21 12.19	-40 30 20.6	10.70	-12.	-27.	2.9	2.9	HD 147048
RXJ 1623.5-4030	T 7857 514*	16 23 29.55	-39 58 0.8	10.73	-15.1	-28.6	1.9	1.8	HD 147402
HD 147454	A 7352 572*	16 23 32.30	-34 39 49.9	9.26	-24.9	-24.9	1.44	1.89	
SAO 207620	A 7352 908*	16 23 37.64	-34 40 21.8	9.51	-19.1	-31.1	3.49	1.71	
stars from Wichmann et al. (1997b)									
RXJ 1410.8-2355	S 6730 365	14 ^h 10 ^m 49 ^s 71	-23° 55' 28'' 8	11.67	-13.	-31.	6.0	6.0	
RXJ 1412.2-1630	A 6138 383*	14 12 14.04	-16 29 53.4	10.97	-7.0	-6.9	1.11	3.75	
RXJ 1419.3-2322	A 6731 58*	14 19 21.15	-23 22 13.5	9.07	43.6	-30.7	1.15	2.86	
RXJ 1428.0-2927	S 6744 1827	14 28 1.89	-29 26 30.1	13.77	-19.	-9.	10.1	10.1	
RXJ 1447.3-3503	S 7305 2424	14 47 23.44	-35 3 13.6	12.43	-26.	-42.	5.1	5.1	
RXJ 1448.2-4103	S 7823 2490	14 48 13.19	-41 2 59.0	11.85	-31.	-25.	4.4	4.4	
RXJ 1450.4-3507	T 7305 380*	14 50 25.82	-35 6 48.7	10.81	-17.0	-19.1	4.5	1.6	
RXJ 1450.5-3459	S 7305 1254	14 50 35.08	-34 59 5.8	12.86	-15.	-27.	7.1	7.1	
RXJ 1452.4-3740	S 7820 310	14 52 26.22	-37 40 8.7	12.45	-18.	-16.	6.9	6.9	
RXJ 1454.2-3955	S 7824 2095	14 54 11.24	-39 55 23.8	12.33	-26.	-29.	5.2	5.2	
RXJ 1457.3-3613	T 7310 2431*	14 57 19.63	-36 12 27.4	10.25	-29.0	-24.6	1.6	2.6	
RXJ 1458.6-3541	A 7310 503*	14 58 37.70	-35 40 30.5	10.95	-25.8	-26.0	1.18	1.14	
RXJ 1459.3-4013	A 7824 1291*	14 59 22.76	-40 13 12.1	9.79	-34.4	-26.5	3.59	1.11	
RXJ 1500.6-4309	S 7833 141	15 0 37.69	-43 8 33.6	12.56	-22.	-20.	4.8	4.8	
RXJ 1500.8-4331	A 7833 2037*	15 0 51.89	-43 31 21.1	10.96	-28.4	-19.3	2.19	1.02	
RXJ 1501.2-4121	A 7829 504*	15 1 11.55	-41 20 40.6	10.16	-20.6	-16.3	1.68	3.74	
RXJ 1502.4-3405	S 7319 685	15 2 26.03	-34 5 13.4	13.35	-16.	-26.	5.8	5.8	
RXJ 1505.4-3857	S 7821 2107	15 5 25.87	-38 57 1.3	12.55	-36.	-3.	6.0	6.0	
RXJ 1509.3-4420	T 7833 1240*	15 9 17.71	-44 20 9.8	10.24	-1.4	-1.8	1.7	2.5	
RXJ 1512.8-4508	A 8294 2230*	15 12 50.18	-45 8 4.5	10.46	-31.4	-21.3	2.50	1.26	
RXJ 1518.0-4445	S 7834 108	15 18 1.25	-44 44 26.8	12.33	-34.	-20.	4.3	4.9	
RXJ 1519.6-4760	T 8298 1675*	15 19 37.02	-47 59 34.2	10.32	-49.5	-39.2	1.6	3.2	
RXJ 1550.1-4746	S 8313 1145	15 50 12.00	-47 46 10.3	11.31	-10.	-5.	4.4	4.4	

listed in Table 4.2 and Table A.7 in the Appendix. Note that in a recent high resolution spectroscopy study by Wichmann et al. (1999a) it turned out that 4 of the stars are more likely ZAMS than PMS stars, and one star showing only a very weak lithium abundance probably is even older.

As can be seen from that study the fraction of ZAMS or even older stars in the sample discovered with ROSAT is rather small in the Lupus region as compared to other nearby star forming regions like e.g. Taurus or Chamaeleon, so that only very few of the 30 stars in the sample in Table 4.2 that have not yet been observed with high resolution are not expected to be PMS stars.

The second part of Table 4.2 contains stars from the sample of Wichmann et al. (1997b) that could be identified in the proper motion catalogues. These are 23 stars out of a total of 34 stars that were newly identified by Wichmann et al. (1997b) in a strip perpendicular to Gould's Belt.

Thus there are altogether 99 stars with known proper motions from the lists of Krautter et al. (1991), Krautter et al. (1997) and Wichmann et al. (1997b) to be analyzed in the next sections.

4.3 Proper motions

The positions of the stars in Tables 4.1 and 4.2 are shown in Fig. 4.1. The regions investigated by Krautter et al. (1997) and Wichmann et al. (1997b) are indicated, as well as the galactic plane and the

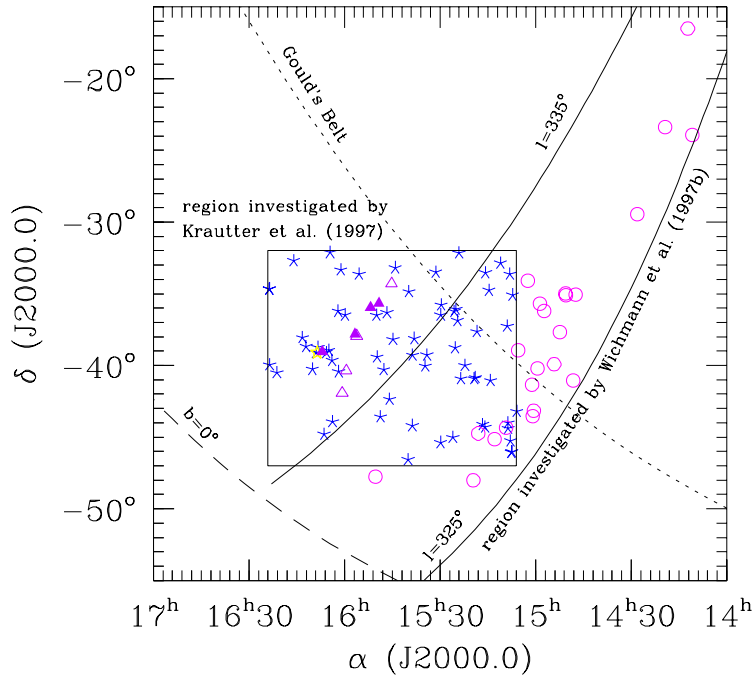


Figure 4.1: Position diagram for all the stars of Tables 4.1 and 4.2. For the meaning of the symbols, see Fig. 4.2. The positions of the classical T Tauri stars correspond to the Lupus 1, 2 and 3 clouds. The regions investigated by Krautter et al. (1997) and Wichmann et al. (1997b) are indicated, as well as the galactic plane and the approximate position of Gould's Belt.

approximate position of Gould's Belt. The T Tauri stars known before ROSAT (indicated by triangles) cluster at the positions of the Lupus 1, 2 and 3 clouds, respectively (cf. with the map of Murphy et al. 1996), whereas the WTTS identified by Krautter et al. (1997) (indicated by asterisks) are distributed over the whole field of search. The WTTS identified by Wichmann et al. (1997b) in a strip perpendicular to Gould's Belt (indicated by open circles) however cluster exactly at Gould's Belt midplane.

The corresponding proper motion diagram is shown in Fig. 4.2. Discarding some outliers, among which there are many stars located rather far away from the Lupus clouds from the sample of Wichmann et al. (1997b), the overall dispersion seen in the proper motions is still very high. The two early-type stars as well as one CTTS (Sz 75) and two WTTS (Sz 82 and RY Lup) have similar proper motions with a mean of $(\mu_\alpha \cos \delta, \mu_\delta) \approx (-9.4, -22.1)$ mas/a, possibly reflecting the mean proper motion typical for younger stars still associated with the Lupus clouds. Two classical T Tauri stars have proper motions quite different from the mean, which is difficult explain. Maybe the STARNET proper motion should not be taken too literally, since the mean errors of about 7 mas/a in one proper motion component are rather large.

The dispersion of about 8.0 mas/a (corresponding to 5.7 km/s at a distance of 150 pc) among the stars in the sample (discarding only the two extreme outliers RXJ 1419.3-2322 and RXJ 1507.9-4515) is rather large. However, it is comparable to the observed dispersion in the Taurus-Auriga association if the southern stars are included, though this is still larger than expected for stars of a common origin. Subtracting the contribution from the mean errors of the proper motions of 4.0 mas/a, the inferred intrinsic scatter is 6.9 mas/a or 4.9 km/s at a distance of 150 pc in the Lupus region. Jones & Herbig (1979) considered a value of 1–2 km/s which they derived for subgroups in Taurus-Auriga as typical. The larger velocity dispersion found here may have various reasons:

(i) In contrast to the determination of the velocity dispersion by Jones & Herbig (1979), who used relative proper motions, the velocity dispersion calculated from the absolute proper motions in Tables 4.1 and 4.2 will include projection effects, and considering larger regions instead of subgroups will increase this effect. However, all attempts to establish a meaningful subgrouping in the Lupus region by searching for correlations between positions and proper motions have failed, and so only the whole sample can be considered.

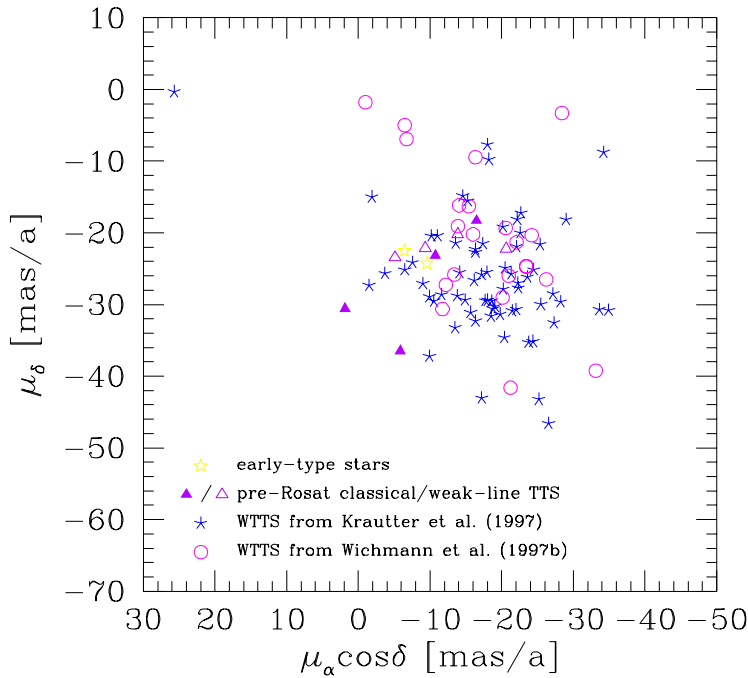


Figure 4.2: Proper motion diagram for stars of Table 4.1 and 4.2. No clear clustering is visible. The two early-type stars as well as one CTTS and two WTTs have very similar proper motions, possibly indicating the typical motion of young stars associated with the Lupus clouds. Even if some outliers are discarded, the remaining dispersion is still rather large. The WTTs in the upper left with a quite different proper motion from the mean is RXJ 1507.9-4515, which is believed to be older than 10^8 yrs and not kinematically related to the Lupus clouds. Note that the proper motion of RXJ 1419.3-2322 is too large to be shown in this diagram and is therefore omitted.

(ii) As strongly indicated by the results of Wichmann et al. (1997b), a large fraction of the WTTs might be related to the Gould’s Belt structure. There is an age difference between on-cloud and off-cloud WTTs, and if this inhomogeneous population of stars formed at different epochs this could easily explain a larger velocity dispersion, especially since Gould’s Belt is known to expand. Unfortunately, there is no detailed prediction for the velocity field of Gould’s Belt member stars in a certain direction on the sky (see e.g. Lindblad & Westin 1985, Blaauw 1991), so that members could not be disentangled from other young stars in the same region on purely kinematical grounds.

(iii) A third reason for an increased velocity dispersion may be the presence of various subgroups with similar motions and possibly slightly different distances. Note that the radial velocity measurements of Dubath et al. (1996) revealed the existence of a separate high velocity subgroup in the south-west part of the Lupus 3 cloud. Dubath et al. (1996) identified 3 CTTS as members of that group, but none of them has a proper motion available. The possibility that the rather large velocity dispersion is caused by a spread in distances is investigated in the next section.

4.4 Space velocities

In order to compare the motions of the stars in the sample without projection effects inherent in the proper motions, space velocities have been calculated for all the stars of Tables 4.1 and 4.2 with radial velocities available. Radial velocities for Sz 68 and Sz 83 have been taken from the catalogues of Barbier-Brossat (1989) and Wilson (1953), respectively, and Sz 82 was included in the sample by Wichmann et al. (1999a). Additionally, radial velocities for 37 stars of the list of Krautter et al. (1997) with known proper motions have been taken from Wichmann et al. (1999a).

The corresponding space velocities calculated with the assumption of a mean distance of 150 pc are shown in Fig. 4.3 (upper panels), corrected for the effects of galactic rotation and the motion of the

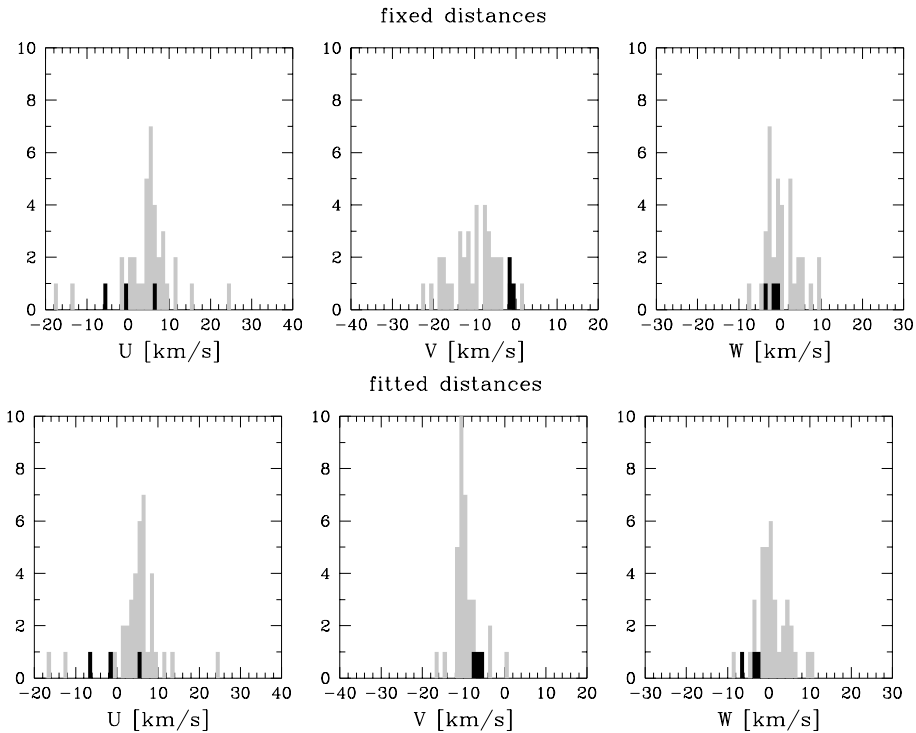


Figure 4.3: Space velocities calculated for Sz 68, Sz 82 and Sz 83 (black) as well as for 36 WTTS from the upper part of Table 4.2 with radial velocities available. U is the velocity in the direction of the centre of the galaxy, V in direction of galactic rotation and W perpendicular to the galactic plane in the direction of the northern galactic pole. In the upper panels a mean distance of 150 pc was assumed in the calculation of the velocities, whereas the velocities in the lower panel were calculated with the fitted distances of Fig. 4.4 (the peak in the V velocities in the lower panel corresponds to 13 stars). The overall dispersion is clearly reduced when fitted distances are used, especially for the V velocities.

Sun. Hipparcos parallaxes have not been used since they are available only for a very small number of stars in the sample and are not very accurate. The older star RXJ 1507.9-4515 is not included in the figure because its proper motion is far off the mean and the star is not related to Lupus kinematically. The observed dispersion in the space velocities is again rather large; $\sigma_U = 6.9$ km/s, $\sigma_V = 5.6$ km/s and $\sigma_W = 3.9$ km/s for the 36 WTTS shown in grey.

With the aim to test the hypothesis that part of this dispersion could be caused by different distances of the stars the same procedure as for the stars in the Taurus region was carried out. The distances of the stars were fitted under the requirement that the resulting space velocity was as close as possible to the mean space velocity calculated with a fixed distance of 150 pc in all 3 velocity components simultaneously.

The space velocities calculated with these fitted distances are shown in the lower panels of Fig. 4.3, and the corresponding distances in Fig. 4.4. The velocity dispersion could be clearly reduced to $\sigma_U = 6.4$ km/s, $\sigma_V = 2.9$ km/s and $\sigma_W = 3.9$ km/s with the largest effect for the V -velocities.

As can be seen from Fig. 4.4 the mean of the distances calculated in this way is close to 150 pc, which is a constraint in this method. The dispersion of the distances (36 pc) however is not fixed, but rather reflects the minimum value up to which the velocity dispersion could be reduced by rigorously adjusting the distance of each star. The velocity dispersion derived in this way will be smaller than its true value, whereas the dispersion in the distances is too large. This is just the opposite relation between true and derived dispersions as compared to the case of fixed distances.

However, what one can expect from this exercise is merely a tendency for the distances of individual stars to be lower or higher than the overall mean value, assuming that the star has the same space velocity and is a kinematical member of the group of stars under consideration.

The three pre-ROSAT TTS shown in black in Fig. 4.3 and Fig. 4.4 probably have larger distances

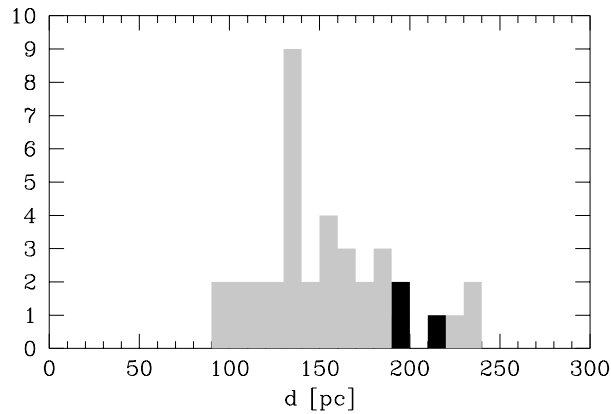


Figure 4.4: Distances calculated with the constraint that the resulting space velocity is as close as possible to the mean value of the space velocities calculated with a fixed distance of 150 pc. Thus the mean of the fitted distances is constrained to be close to 150 pc, but the method can reveal a trend for individual stars to higher or lower values than the mean distance.

than the mean: their V -velocities calculated with fixed distances are smaller than the mean when fitted distances are used. These fitted distances are around 200 pc for these three stars, in good agreement with the Hipparcos parallaxes available for two of them.

Similarly, although radial velocities for the two early-type stars are not available, they might also be located at larger distances than the majority of the WTTS, as indicated by their relatively small proper motions. Again the Hipparcos parallaxes confirm this tendency.

4.5 Summary

Proper motions of altogether 99 stars in the Lupus SFR have been presented and investigated. The sample comprises two early-type stars known to be associated to the Lupus clouds as well as 4 CTTS and 4 WTTS known in that region before the ROSAT mission. In addition, 66 stars from the investigation of Krautter et al. (1997) and 23 stars from the sample of Wichmann et al. (1997b) have been included. As indicated also by their positions and higher ages as compared to the on-cloud stars, a large fraction of the stars in the sample of Wichmann et al. (1997b) might be related to Gould's Belt.

The observed velocity dispersion of the young stars in a large region encompassing the Lupus clouds is rather large, around 5.7 km/s or 4.9 km/s if corrected for the errors of the proper motions at a distance of 150 pc.

However, it has been shown that part of this velocity dispersion can be explained in terms of different distances. In particular, the two early-type stars as well as 3 more pre-ROSAT TTS might probably be located at slightly larger distances (around 200 pc) than previously thought, in accordance with the Hipparcos parallaxes available for some of them.

5 Scorpius-Centaurus

5.1 Overview

Kinematical studies in the Scorpius-Centaurus OB association and especially in its youngest subgroup Upper Scorpius have a rather long tradition. Soon after it became clear that there was a clustering of bright stars in the Scorpius-Centaurus region and that most of these stars shared more or less the same space motion, Kapteyn (1914) investigated whether this motion was systematic enough to derive individual parallaxes for the member stars, leading to the first convergent point determination in this region.

Most kinematical studies conducted in the following confirmed the existence of the so-called *Southern Stream* (e.g. Rasmuson 1921, Plaskett & Pearce 1934), although Smart (1939) doubted the existence of a moving group: he identified the streaming velocity with the solar motion and the convergent point with the solar antapex. Blaauw (1946) did really pioneering work investigating the kinematics of this association more systematically than previous works, including the definition of subgroups, the derivation of velocity dispersions and the investigation of expansion.

Bertiau (1951) determined the convergent point of a sample of 77 B-type stars in the Upper Scorpius region using proper motions in the N30 system with the aim of deriving absolute magnitudes as accurate as possible. He fitted two different models to the relative motions of member stars and found that they are more likely due to an overall expansion than caused by differential galactic rotation.

Based on the same proper motions Petrie (1961) determined the convergent point with the help of new radial velocities, and he noted, similar to Smart, that the convergent point was very close to the solar antapex and the peculiar motions therefore very small. According to his view, the moving cluster model was not strictly applicable to Upper Scorpius.

Later on Jones (1971) repeated the convergent point determination using FK4 proper motions. He extracted a list of 47 firm member stars, and his convergent point was very close to that calculated by Bertiau. However, the kinematical parallaxes were about 20% smaller due to systematic differences between the N30 and the FK4 proper motion systems, and so the calibration of the luminosities was uncertain.

Kinematic studies of the Scorpius-Centaurus association have encountered a new stimulation by the planned Hipparcos mission in the eighties. At Leiden the **Specter** Consortium formed, aiming at complementing the kinematical Hipparcos data with extensive ground-based photometric data to greatly improve the stellar census of nearby OB associations (de Geus et al. 1989, de Geus et al. 1990).

A second stimulation for studies in the Upper Scorpius region was imposed by the Einstein and ROSAT X-ray satellites, with which quite a number of TTS have been detected in this classical OB association (Walter et al. 1994, Kunkel et al. 1999, Preibisch et al. 1998a). Extrapolating the observed numbers of early-type stars in the Scorpius-Centaurus association by means of a Miller Scalo IMF, the total number of low-mass stars expected in this region is of the order of two thousand, of which only 1% has been discovered yet (Martín 1998).

Thus Upper Scorpius is an ideal region to study the interplay between high- and low-mass stars, since most other nearby SFR contain low-mass stars only. Additionally, the favourable conditions in this region allow for the determination of individual kinematical distances via the convergent point method, which is of interest especially for the low-mass stars because the majority of them was too faint for inclusion in the Hipparcos Catalogue. Independent age determinations obtained from the comparison of their positions in the HRD with theoretical isochrones could possibly confirm the very low age estimated grossly from the lithium line widths as a function of spectral type.

Table 5.1: All the 8 stars from Walter et al. (1994) for which proper motion information is available. The 3 stars with RXJ numbers have been discovered independently by Kunkel et al. (1999) as PMS stars.

object	cat. No.	RA ($\alpha_{J2000.0}$)	DEC ($\delta_{J2000.0}$)	m_V [mag]	μ_α [mas/a]	μ_δ	$\frac{\sigma_{\mu_\alpha}}{\cos \delta}$ [mas/a]	σ_{μ_δ}	d [pc]
NTTS 155203-2338 ¹	A 6779 1372*	15 ^h 54 ^m 59 ^s .87	-23 ^o 47'18''2	9.03	-34.1	-39.4	2.20	1.58	90 ⁺¹² ₋₁₀
NTTS 155220-2313	HIP 77960*	15 55 17.59	-23 22 3.7	8.46	-17.89	-26.46	1.31	0.98	
NTTS 155828-2232 ²	S 6779 174	16 1 25.67	-22 40 40.4	12.02	-5.	-20.	5.7	5.7	
NTTS 160153-1922 ³	S 6208 1239	16 4 47.73	-19 30 22.6	12.27	-14.	-10.	6.3	6.3	
NTTS 160814-1857	S 6209 968	16 11 8.87	-19 4 46.9	12.48	-26.	-26.	7.5	7.5	
NTTS 160905-1859	S 6209 1039	16 11 59.25	-19 6 51.8	12.04	-22.	0.	5.7	5.7	
NTTS 160946-1851	T 6209 1316*	16 12 40.51	-18 59 28.1	11.01	-12.4	-22.2	4.7	2.3	
NTTS 161431-2256	T 6793 501*	16 17 31.39	-23 3 36.0	10.25	-12.8	-17.1	2.3	5.6	

¹ RXJ 1554.9-2347

² RXJ 1601.4-2240

³ RXJ 1604.7-1930

The current scenario for SF in the Scorpius-Centaurus OB association is as follows (Preibisch et al. 1998b): 15 Myr ago star formation started in Upper Centaurus Lupus. The shock wave of a supernova triggered star formation in Upper Scorpius (5–6 Myr ago), but strong winds of O stars halted star formation only short time later. 1 Myr ago another supernova in Upper Scorpius might have triggered star formation in ρ Ophiuchi, which is located just east of Upper Scorpius and shows signs of ongoing star formation. ROSAT data give support to supernova events in the Scorpius-Centaurus association.

5.2 Data

5.2.1 Early-type stars

Quite recently, de Zeeuw et al. (1999) investigated the stellar census of several nearby OB associations, including Scorpius-Centaurus (Sco-Cen), on the basis of proper motions and parallaxes given in the Hipparcos Catalogue. Altogether they list 521 members of Sco-Cen, the majority of which are early-type members (up to spectral type F). Nevertheless some late-type members are included, but their number is small and it is not sure whether they really belong to the association or are rather field stars selected only because the kinematics of member and field stars is very similar.

Given the fact that the vast majority of early-type Upper Scorpius member stars should be included in the Hipparcos Catalogue (a main sequence star of 9th magnitude at a distance of 145 pc has spectral type F), no effort has been made to search for additional kinematical members of Upper Scorpius in the more comprehensive proper motion catalogues. Furthermore, the problem of the inclusion of field stars becomes more severe for less accurate proper motions and lack of parallax information for these stars (Frink & Röser 1996). The sample of early-type members used in this study is therefore identical to that of de Zeeuw et al. (1999), consisting of 120 members in the region of Upper Scorpius and 221 members in the region of Upper Centaurus Lupus.

5.2.2 Late-type stars

Late-type member stars in the Scorpius-Centaurus association have been discovered only very recently by means of their X-ray emission. A small sample of 28 Einstein sources was investigated by Walter et al. (1994). Of these, 8 stars could be identified at least in one proper motion catalogue, and the data are given in Table 5.1 (see Table A.8 for all identifications).

Kunkel et al. (1999) conducted follow-up observations of promising PMS candidate stars selected from the ROSAT All-Sky Survey in the region of the Upper Scorpius association (US-A) as well as in a region located between Upper Scorpius and Upper Centaurus Lupus (termed US-B, see Fig. 5.1). Judging from the lithium line widths as a function of spectral type, they found 59 very young PMS stars, 33 stars of intermediate age and 7 active ZAMS stars in their sample. Of these, 27 PMS stars, 12 intermediate age

Table 5.2: 39 stars of the investigation of Kunkel et al. (1999) for which proper motions are available. 27 stars are younger than the Pleiades as judged from their lithium line widths and can therefore be regarded as WTTS, whereas 12 stars have lithium line widths which make their ages comparable to those of the Pleiades of approximately 10^8 years.

object	cat. No.	RA ($\alpha_{J2000.0}$)	DEC ($\delta_{J2000.0}$)	m _V [mag]	μ_{α} [mas/a]	μ_{δ} [mas/a]	$\frac{\sigma_{\mu_{\alpha}}}{\cos \delta}$ [mas/a]	$\sigma_{\mu_{\delta}}$ [mas/a]	d [pc]
stars younger than $\approx 3.5 \cdot 10^7$ years									
RXJ 1524.2-3030	T 7313 421*	15 ^h 24 ^m 11 ^s .48	-30°30'58"/3	11.01	-28.6	-25.7	1.9	2.6	
RXJ 1530.4-3218	HIP 75924*	15 30 26.24	-32 18 12.9	8.52	-33.48	-31.72	2.82	2.77	92 ⁺³⁸ ₋₂₁
RXJ 1530.8-3021	S 7314 985	15 30 47.92	-30 22 5.5	12.22	-24.	-30.	5.9	5.9	
RXJ 1531.3-3329	A 7318 593*	15 31 21.93	-33 29 39.5	10.76	-26.4	-30.7	1.80	1.41	
RXJ 1537.0-3136	PPM 294055*	15 37 2.11	-31 36 40.0	9.60	-31.	-32.	2.9	2.7	
RXJ 1537.8-3045	S 7327 689	15 37 51.31	-30 45 16.0	12.22	-30.	-27.	5.4	5.4	
RXJ 1539.4-2958	HIP 76675*	15 39 25.32	-34 46 47.7	8.85	2.17	39.88	1.45	1.18	73 ⁺⁷ ₋₅
RXJ 1544.0-3311	A 7331 782*	15 44 3.77	-33 11 11.2	10.77	-25.5	-25.7	1.19	1.13	
RXJ 1545.2-3417	HIP 77157*	15 45 12.87	-34 17 30.6	10.50	-16.79	-20.20	2.17	1.61	159 ⁺⁷⁷ ₋₃₉
RXJ 1545.8-3020	HIP 77199*	15 45 47.60	-30 20 55.8	9.48	-78.97	-99.66	1.13	0.93	41 ⁺² ₋₂
RXJ 1548.0-2908	A 6790 1227*	15 48 2.91	-29 8 37.0	10.73	-28.5	-23.3	1.17	3.85	
RXJ 1549.0-3102	A 7328 1706*	15 49 2.72	-31 2 53.8	10.97	-22.5	-23.0	1.21	2.07	
RXJ 1549.3-2600	A 6782 878*	15 49 21.00	-26 0 6.4	11.02	-16.5	-28.3	1.31	2.61	
RXJ 1551.9-2621	A 6786 1545*	15 51 54.39	-26 22 5.5	9.57	-24.5	-39.0	1.05	2.11	
RXJ 1552.5-2633	S 6786 632	15 52 31.24	-26 33 53.4	13.11	-20.	-49.	6.4	6.4	
RXJ 1555.4-3338	S 7333 713	15 55 26.20	-33 38 23.6	13.66	-24.	-35.	7.6	7.6	
RXJ 1555.8-2512	A 6783 2045*	15 55 48.81	-25 12 24.0	10.42	-27.3	-17.1	2.20	1.07	
RXJ 1558.2-2328	T 6779 780*	15 58 12.70	-23 28 36.5	10.38	-16.9	-20.1	1.6	2.8	
RXJ 1600.0-2509	T 6783 1747*	16 0 0.78	-25 9 42.4	10.62	-16.6	-24.2	2.3	1.9	
RXJ 1600.2-2417	S 6779 1587	16 0 14.71	-24 18 19.2	13.21	-0.	2.	6.6	6.6	
RXJ 1600.6-2159	S 6212 1183	16 0 40.56	-22 0 31.7	12.15	-15.	-12.	6.3	6.3	
RXJ 1601.9-2008	A 6208 1543*	16 1 58.23	-20 8 12.0	10.49	-5.4	-23.3	4.32	1.52	
RXJ 1602.8-2401B	S 6780 836	16 2 52.43	-24 2 22.3	12.13	-11.	1.	5.8	5.8	
RXJ 1602.9-2022	S 6208 1010	16 2 53.94	-20 22 47.8	13.49	-19.	-18.	7.6	7.6	
RXJ 1603.6-2245	T 6780 56*	16 3 35.49	-22 45 56.1	11.08	-26.7	-27.4	1.7	4.4	
RXJ 1603.9-2031B	S 6208 1022	16 3 57.67	-20 31 5.6	13.49	-5.	-27.	7.6	7.6	
RXJ 1604.3-2130	S 6212 830	16 4 21.63	-21 30 28.7	13.30	-15.	-23.	8.3	8.3	
$\approx 10^8$ years old stars									
RXJ 1528.0-2600	S 6767 844	15 ^h 28 ^m 3 ^s .21	-26°0'3"/0	12.34	-23.	-3.	5.3	5.3	
RXJ 1528.7-3117	HIP 75769*	15 28 44.04	-31 17 38.0	8.71	27.99	40.14	2.75	3.12	87 ⁺²⁵ ₋₁₆
RXJ 1529.4-2850	HIP 75836*	15 29 26.88	-28 50 52.3	8.77	-57.80	-54.02	1.37	1.26	90 ⁺¹⁴ ₋₁₁
RXJ 1535.2-2828	HIP 76304*	15 35 13.64	-28 28 27.8	8.20	14.33	-75.24	1.01	0.86	80 ⁺⁷ ₋₇
RXJ 1538.2-3229	A 7331 52*	15 38 16.15	-32 29 23.5	10.69	-41.3	-24.3	3.20	2.90	
RXJ 1543.4-2925	S 6789 1021	15 43 29.17	-29 25 35.3	12.21	3.	0.	6.7	6.7	
RXJ 1545.6-3208	S 7332 823	15 45 35.27	-32 8 49.6	12.51	-13.	-11.	5.2	5.2	
RXJ 1546.1-2804	T 6786 811*	15 46 10.75	-28 4 23.4	9.26	-70.4	-23.3	4.7	2.6	
RXJ 1550.9-2534	T 6782 178*	15 50 56.42	-25 34 19.0	9.71	-14.0	-19.9	1.6	2.7	
RXJ 1558.1-2405	S 6779 1232	15 58 8.13	-24 5 52.9	13.11	-21.	-20.	5.1	5.1	
RXJ 1601.3-2652	HIP 78483*	16 1 18.42	-26 52 21.5	9.49	-12.72	-21.50	1.50	1.31	150 ⁺⁴⁸ ₋₂₉
RXJ 1602.8-2401A	S 6780 835	16 2 51.25	-24 1 57.0	13.25	-7.	-12.	8.4	8.4	

stars and none of the older stars have proper motion information available, and the data are given in Table 5.2 and Table A.9 in the Appendix.

Similarly, Preibisch et al. (1998a) used the multiobject spectrograph FLAIR at the UK Schmidt telescope to search for further PMS stars among the ROSAT database in an extended field in the Upper Scorpius region (see Fig. 5.1). Altogether they found 39 PMS stars, 12 stars of intermediate age and 27 unrelated field stars, of which 23 PMS stars, 9 stars of intermediate age and 13 older stars could be identified in proper motion catalogues (Table 5.3 and Table A.10 in the Appendix). Additionally, Preibisch et al. (1998a) observed a sample of candidate members which was selected purely from kinematical data, but no PMS stars could be identified among this sample. Thus they concluded that the PMS population found by means of ROSAT must be rather complete, with a conservative completeness limit of 75% in the magnitude interval $11.5 \text{ mag} \leq B \leq 13.5 \text{ mag}$.

At fainter magnitudes (14–17 mag), Sciortino et al. (1998) identified PMS stars from Einstein and

Table 5.3: 45 Stars with proper motions from the list of Preibisch et al. (1998a). 23 stars are supposed to be PMS stars judging from their lithium line widths, 9 stars have lithium abundances comparable to that of the Pleiades and are of intermediate age and 13 stars are even older, presumably unrelated field stars.

object	cat. No.		RA ($\alpha_{J2000.0}$)	DEC ($\delta_{J2000.0}$)	m_V [mag]	μ_α [mas/a]	μ_δ	$\frac{\sigma_{\mu_\alpha}}{\cos \delta}$ [mas/a]	σ_{μ_δ}	
stars younger than $\approx 3.5 \cdot 10^7$ years										
GSC 6770	655	S 6770 655	15 ^h 19 ^m 52 ^s .92	-28° 2'26".4	12.85	-47.	-40.	6.8	6.8	
GSC 6764	1305	S 6764 1305	15 35 57.82	-23 24 5.1	13.14	-8.	-31.	8.1	8.1	
GSC 6785	476	S 6785 476	15 41 6.76	-26 56 26.5	12.63	-32.	-31.	5.1	5.1	
GSC 6195	768	S 6195 768	15 57 2.29	-19 50 42.0	12.66	-29.	-26.	6.2	6.2	
GSC 6191	552	S 6191 552	15 58 47.71	-17 57 59.6	12.87	-20.	-15.	5.7	5.7	
GSC 6191	19	S 6191 19	15 59 2.08	-18 44 14.5	13.02	2.	-33.	7.6	7.6	
GSC 6204	812	S 6204 812	16 3 2.68	-18 6 5.1	12.80	-15.	-21.	5.7	5.7	
GSC 6784	1219	S 6784 1219	16 5 50.51	-25 33 13.8	11.67	-56.	-35.	4.6	4.6	
GSC 6784	39	A 6784 39*	16 8 43.41	-26 2 16.8	10.34	-14.0	-25.5	1.05	1.04	
GSC 6213	194	S 6213 194	16 9 41.00	-22 17 59.7	13.75	-3.	-26.	7.8	7.8	
GSC 6784	997	S 6784 997	16 10 19.12	-25 2 30.8	12.95	-30.	-38.	5.7	5.7	
GSC 6793	797	S 6793 797	16 13 2.70	-22 57 44.6	12.62	-20.	-30.	8.0	8.0	
GSC 6213	306	T 6213 306*	16 13 18.58	-22 12 49.0	10.58	-15.6	-23.2	2.6	2.7	
GSC 6793	569	S 6793 569	16 13 29.27	-23 11 7.7	12.48	-20.	-36.	6.1	6.1	
GSC 6793	994	S 6793 994	16 14 2.11	-23 1 2.1	12.19	-14.	-22.	6.1	6.1	
GSC 6793	819	S 6793 819*	16 14 11.07	-23 5 36.2	11.46	-13.	-23.	5.5	5.5	
GSC 6801	186	S 6801 186	16 14 59.18	-27 50 23.2	11.84	-13.	-30.	5.5	5.5	
GSC 6793	1406	T 6793 1406*	16 16 17.94	-23 39 47.5	10.82	-10.2	-23.0	1.6	1.9	
GSC 6214	2384	S 6214 2384	16 19 33.94	-22 28 29.5	12.03	-25.	-27.	5.8	5.8	
GSC 6214	210	S 6214 210	16 21 54.66	-20 43 8.9	13.14	-24.	-24.	7.8	7.8	
GSC 6798	35	S 6798 35	16 23 32.35	-25 23 48.5	12.13	-13.	-15.	5.7	5.7	
GSC 6794	156	T 6794 156*	16 24 51.37	-22 39 32.7	9.90	-17.9	-33.9	2.1	2.0	
GSC 6794	337	S 6794 337	16 27 39.56	-22 45 23.6	12.30	-15.	-33.	6.7	6.7	
$\approx 10^8$ years old stars										
GSC 6762	602	T 6762 602*	15 ^h 19 ^m 50 ^s .28	-23°13'57".8	10.86	-14.4	-17.7	1.8	2.8	
GSC 6771	1281	S 6771 1281	15 22 16.25	-26 52 25.4	12.99	-16.	-19.	6.9	6.9	
GSC 6189	101	S 6189 101	15 37 49.17	-18 40 45.5	12.33	-15.	-22.	5.5	5.5	
GSC 6781	1046	T 6781 1046*	15 42 49.91	-25 36 40.6	10.74	-17.3	-28.7	1.6	2.5	
GSC 6191	274	A 6191 274*	15 58 20.56	-18 37 25.1	10.30	-15.2	-22.1	5.38	2.34	
GSC 6209	1215	S 6209 1215	16 8 34.38	-19 11 56.3	12.49	0.	-24.	7.4	7.4	
GSC 6797	599	T 6797 599*	16 15 32.15	-25 30 31.1	10.70	-14.0	-24.0	1.9	1.6	
GSC 6210	676	PPM 265457*	16 21 59.95	-20 15 0.5	10.00	-14.	-19.	3.5	3.4	
GSC 6802	206	S 6802 206	16 22 13.17	-26 55 24.6	12.52	15.	-15.	6.6	6.6	
stars older than $\approx 10^8$ years										
GSC 6762	1092	T 6762 1092*	15 ^h 17 ^m 11 ^s .67	-24°17'42".6	11.06	8.1	-2.3	2.2	1.6	
GSC 6771	369	T 6771 369*	15 25 17.25	-27 29 31.0	10.64	-49.7	-32.7	5.3	3.6	
GSC 6768	1212	PPM 732235*	15 34 22.92	-25 14 39.1	9.90	-24.	-13.	4.3	3.8	
GSC 6193	553	S 6193 553	15 37 29.95	-20 2 47.2	12.14	-127.	-12.	5.6	5.6	
GSC 6198	166	T 6198 166*	15 51 1.04	-21 55 53.7	10.62	14.5	-53.0	1.6	3.4	
GSC 6195	157	S 6195 157	15 55 6.69	-19 46 31.5	12.82	1.	-4.	7.7	7.7	
GSC 6779	113	S 6779 113	15 55 38.92	-23 12 51.3	12.86	-9.	1.	6.2	6.2	
GSC 6199	1511	S 6199 1511	15 56 14.89	-21 0 40.7	12.73	-11.	-36.	7.9	7.9	
GSC 6212	1330	S 6212 1330	16 6 33.17	-22 8 52.2	12.00	-61.	-73.	5.7	5.7	
GSC 6784	874	S 6784 874	16 8 43.47	-24 50 18.5	12.07	19.	13.	5.7	5.7	
GSC 6788	326	S 6788 326	16 10 5.75	-26 26 7.2	13.16	-2.	-14.	6.8	6.8	
GSC 6793	562	S 6793 562	16 14 27.05	-23 9 40.9	12.36	-6.	-5.	6.1	6.1	
GSC 6214	2006	A 6214 2006*	16 18 4.79	-22 24 39.5	10.67	-1.1	-23.3	1.58	1.25	

ROSAT data using a detection algorithm based on wavelet transforms. Since half of their sources had been missed by conventional analysis techniques, they concluded that the stellar census based on X-ray surveys is more severely incomplete than previously thought. Follow-up observations in order to unambiguously prove the PMS nature of these sources are still under way, but given the faint magnitudes it is very unlikely that proper motions for these stars are available.

Thus we are left for the moment with a sample of 92 stars (including the field stars for comparison) from the lists of Walter et al. (1994), Kunkel et al. (1999) and Preibisch et al. (1998) to be investigated

kinematically in the following sections.

5.3 Positions and proper motions

Positions and proper motions of the stars in Tables 5.1, 5.2 and 5.3 are shown in Fig. 5.1, together with the kinematic members of Upper Scorpius and Upper Centaurus Lupus which fall in the plotted region (118 in US and 85 in UCL). The assignment of kinematical members of the Sco-Cen association to its different subgroups was done by de Zeeuw et al. (1999) according to the positions of the stars. The division between US and UCL was made at $l = 343^\circ$ and $b = 10^\circ$, indirectly visible in Fig. 5.1 through the different plotting symbols for both subgroups (light grey dots with additional underlaid crosses for UCL members only). The stars from Walter et al. (1994) (open star symbols) are all located in the centre of US, as are the stars found in US-A by Kunkel et al. (1999). The stars in US-B are closer to UCL than to US (the stars with declinations smaller than 28° have been marked with additional crosses, too). The region investigated by Preibisch et al. (1998a) comprises the environment of US without extending to UCL, and the young stars clearly concentrate in the centre of US.

Fig. 5.1 shows the proper motions of all the stars. The right diagram is a reproduction of the marked area in the left diagram on an enlarged scale. Clearly clustering is visible at the typical proper motion of the Sco-Cen association. The elongated shape of the central peak corresponds to the shape of the association and is mainly due to projection effects. Some of the outlying stars might have been ejected from the association. Good candidates are GSC 6770 655, RXJ 1529.4-2850A and RXJ 1545.8-3020 from US and RXJ 1528.7-3117 and RXJ 1602.8-2401B from UCL, all located in the region between US and UCL and moving away from the centres of the subgroups with relatively large velocities. The US member stars have a mean proper motion of $(\mu_\alpha \cos \delta, \mu_\delta) \approx (-11, -23)$ mas/a, whereas that of the UCL member stars is somewhat more negative in right ascension, $(\mu_\alpha \cos \delta, \mu_\delta) \approx (-20, -24)$ mas/a.

As expected, many of the younger late-type stars show similar proper motions as the early-type members. Their scatter is somewhat larger than that of the early-type members, but this can be attributed to their larger extent in space and to the accuracy of the proper motions: STARNET proper motions, which are the only ones available for many of the fainter stars, are on average about 5 times less accurate than Hipparcos proper motions.

Interestingly, many of the stars, especially those in US-B and marked again by additional crosses, kinematically belong to the UCL subgroup rather than to US, as indicated also by their positions.

The dispersion of the early-type members is around 3.5 mas/a for US and 5 mas/a for UCL, but part of it is caused by projection effects. The space velocities should show a smaller dispersion, but precise radial velocities are not available for many of the stars. Furthermore, the distances are not accurate enough to resolve the internal velocity dispersion. de Zeeuw et al. (1999) derived a value of 3 km/s (corresponding to 4.5 mas/a at 145 pc) for the velocity dispersion in one coordinate by comparison with Monte Carlo simulations.

5.4 Derivation of kinematical distances

5.4.1 Method

The member stars in the 3 kinematical subgroups of the Scorpius Centaurus association (Upper Scorpius, Upper Centaurus Lupus and Lower Centaurus Crux) are supposed to move through space with nearly identical velocities, reflecting the fact that they have a common origin. Assuming this model of parallel space motions, the proper motions can be used to derive individual distances to the stars if the mean space velocity of the cluster is known.

This method for deriving kinematical distances produces the best results for clusters which are near to the Sun and have a large extent on the sky. Additionally, large proper motions facilitate kinematical member selection and reduce the uncertainty in the directions of motions of individual stars. The proper motion vectors of stars with parallel space motions seem to converge to a single point as seen on the

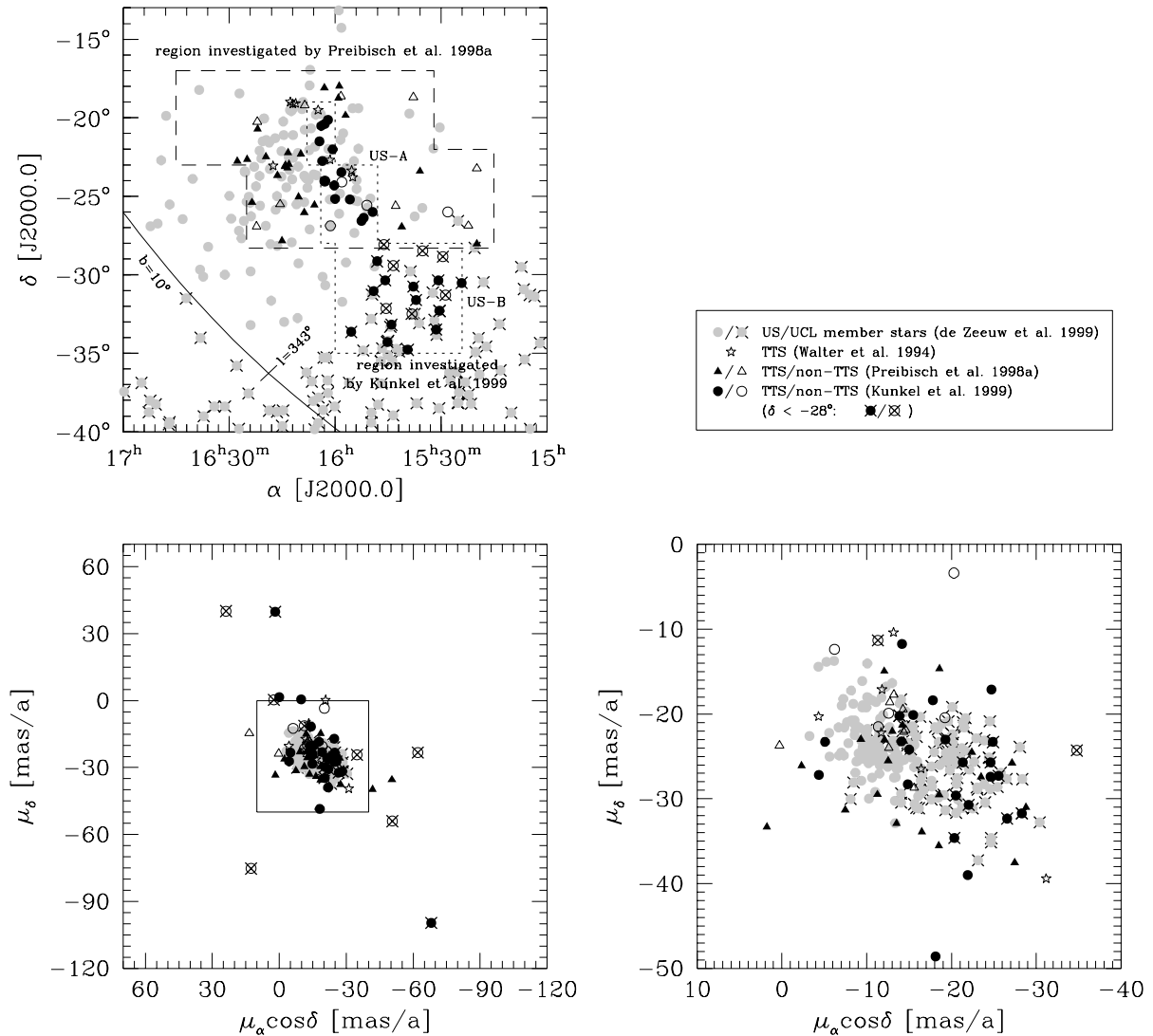


Figure 5.1: Positions and proper motions of the stars from Tables 5.1–5.3. The upper left figure shows the positions of the early-type member stars from de Zeeuw et al. (1999) in the plot region (light grey dots, additional underlaid crosses for UCL members). The regions investigated by Preibisch et al. (1998a) (long-dashed) and Kunkel et al. (1999) (short-dashed) are indicated, too, as well as the stars with known proper motions from these investigations. Filled symbols correspond to the youngest stars in these samples as deduced from the lithium line widths. The 8 stars with known proper motions from Walter et al. (1994) are marked by open star symbols. One can clearly see that the US-B region entirely falls into the UCL area rather than into the US area. Stars in US-B, that means all stars south of $\delta = -28^\circ$, have therefore been marked by additional crosses, too. The solid line corresponds to a constant galactic height of $b = 10^\circ$, used by de Zeeuw et al. (1999) to make the division between the US and UCL regions (at $l = 343^\circ$). The lower panels show the proper motions of these stars, the right one on a larger scale than the left one (the limits of the detail are indicated by the box). Stars supposed to belong to the US and UCL subgroups, respectively, populate not only different regions in the position diagram, but also separate in the proper motion diagram.

sphere, the so-called convergent point (CP). The precision of the derived kinematical distances depends mainly on the accuracy of the calculated CP. Usually the error in the position of the CP is largest in the direction of the great circle connecting the cluster and the CP, whereas its error perpendicular to this direction is small. A large extent of the cluster can effectively improve the precision of the CP position on the great circle since the intersecting lines form larger angles to each other.

The favourite cluster for application of the CP method are the Hyades (for recent investigations, see Schwan 1990, 1991 and Perryman et al. 1998). The procedure is as follows: one starts with a small

sample of secure well-known members of the cluster and calculates their CP. With this preliminary CP one searches for additional members selecting from a variety of possible criteria (Schwan 1990, 1991):

(i) The most important membership criterion is the angle between the proper motion vector of a particular star and the CP. It should be less than about $10^\circ - 15^\circ$, otherwise the difference in the directions of motion between the star and the cluster mean is too large to regard the star as a member.

(ii) A second condition for membership is the significance of the direction of the proper motion. For high absolute and reasonable accurate proper motions this is not critical, and a reasonable choice which does not exclude too many stars is a maximum value of 30° for the error of the position angle between the direction of the star's proper motion and the CP.

(iii) Closely related to the limits on the absolute values of the residual position angle and its error is the condition that the positional angle is not much larger than its error.

(iv) The derived kinematical distance should be in a reasonable interval expected for that particular cluster. This is a condition on the absolute value of the proper motion, whereas the first 3 criteria only concerned the direction of the proper motion.

(v) A very effective criterion in separating members from non-members is an upper limit on the allowed differences between the distances computed from the proper motion components in right ascension and declination separately. The difference should not be much larger than the error expected for the combined kinematical distance.

(vi) If the radial velocity of the stars is known it could be compared to the expected value calculated from the star's position and the mean space velocity of the cluster. Both radial velocities should be consistent within their respective errors.

Application of the above criteria leads to a revised membership list for the cluster, and a new CP can be determined. This new CP in turn yields a new membership list and so on, until both membership list and CP do not change any more in a new iteration.

de Zeeuw et al. (1999) used a slightly different approach to select members from the Hipparcos Catalogue. They modified the classical convergent point method sketched above (de Bruijne 1999), taking the full covariance matrix given in the Hipparcos Catalogue into account. Additionally, they applied the so-called Spaghetti method (Hoogerwerf & Aguilar 1999) which uses the trigonometric parallax from Hipparcos in addition to the positions and proper motions. In order to be selected as a member with the Spaghetti method a star's 3-dim integral of the probability distribution in velocity space has to be larger than a certain threshold. In practice it is identical to selecting member stars only in a certain distance interval in which member stars can be expected. Provided that there are no systematic deviations between trigonometric parallaxes and kinematical distances this can also be achieved within the framework of the classical convergent point method by rejecting stars with kinematical distances outside a reasonable interval (see criterion (iv) above).

5.4.2 Results

As a first step kinematical distances for all the Hipparcos members of Upper Scorpius and Upper Centaurus Lupus were calculated. The CP given by de Zeeuw et al. (1999) was used (US: $\alpha = 7^h 44^m$, $\delta = -57^\circ 32'$, UCL: $\alpha = 7^h 00^m$, $\delta = -38^\circ 37'$) together with the values for the streaming velocities of 18.2 km/s (US) and 20.9 km/s (UCL), respectively. The parallax π of an individual member star in [mas] is then computed by

$$\pi = \frac{\mu_{\text{tot}}}{S \cdot \sin \lambda} \quad ,$$

where μ_{tot} is the total proper motion of the star in [mas/a], S the streaming velocity of the association in [km/s], and λ the angular distance between the position of the star and the CP.

By definition of the sample, all stars fulfilled the membership criteria (i)–(iv). As mentioned earlier, criterion (v) is very strong and sometimes even can discard stars which are probable members based on the other criteria, and about 20% of the stars from de Zeeuw et al. (1999) would have to be rejected when a maximal difference of 40 pc is allowed between the distances derived from proper motions in right

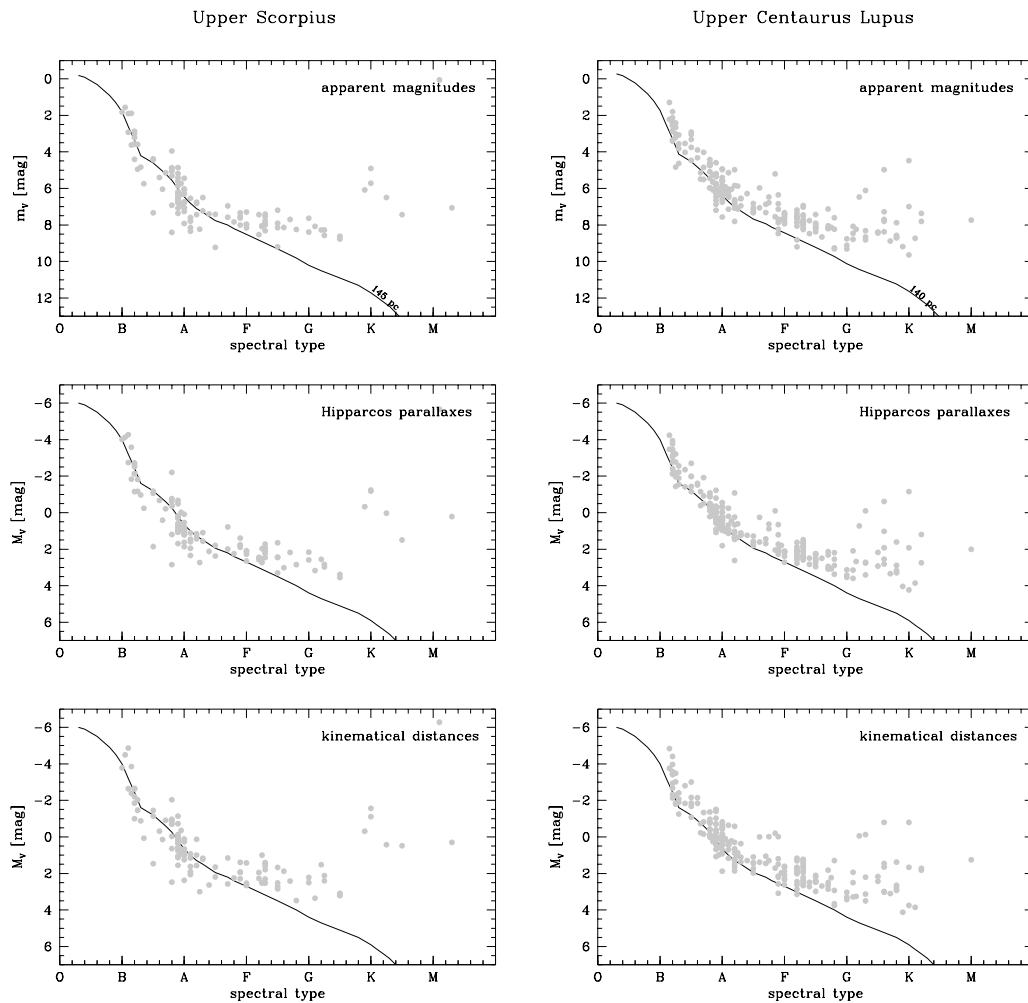


Figure 5.2: HR diagrams of the early-type stars selected as members by de Zeeuw et al. (1999) for the subgroups of US (left) and UCL (right). Spectral types and visual magnitudes were taken from the Hipparcos Catalogue, and an extinction of 1 mag has been assumed for all stars. The upper panels show apparent magnitudes and the main-sequence for mean distances of 145 pc (US) and 140 pc (UCL), respectively. The middle panels are based on absolute magnitudes calculated with the Hipparcos trigonometric parallaxes, whereas in the lower panels the newly derived kinematical distances have been used. No additional scatter is introduced by the use of kinematical distances, suggesting that the method works fine.

ascension and declination separately. Therefore these stars should not be regarded as non-members, but only the kinematical distances for them cannot be derived with high accuracy.

Fig. 5.2 shows the Hertzsprung Russell diagrams for US and UCL based on the assumption of a unique mean distance for all the stars (upper panels), absolute magnitudes calculated with Hipparcos parallaxes (middle panels) and absolute magnitudes calculated with the newly derived kinematical distances (lower panels). Spectral types and visual magnitudes were taken from the Hipparcos Catalogue, and for comparison with the main sequence an extinction of 1 mag was adopted for all stars.

The main intention of the figure is to show that the kinematical distances are on average at least as accurate as the trigonometric parallaxes since no additional scatter is introduced for the early-type stars in the lower panels of Fig. 5.2. However, there is some scatter visible among the late-type stars, but de Zeeuw et al. (1999) estimate that the majority of their kinematical G- to M-type members probably do not belong to the association. In this case the model for the calculation of the cluster parallaxes breaks down, and the computed distances have no meaning for non-member stars.

Similar considerations hold for the stars with rather small Hipparcos parallaxes. Figure 5.3 shows a

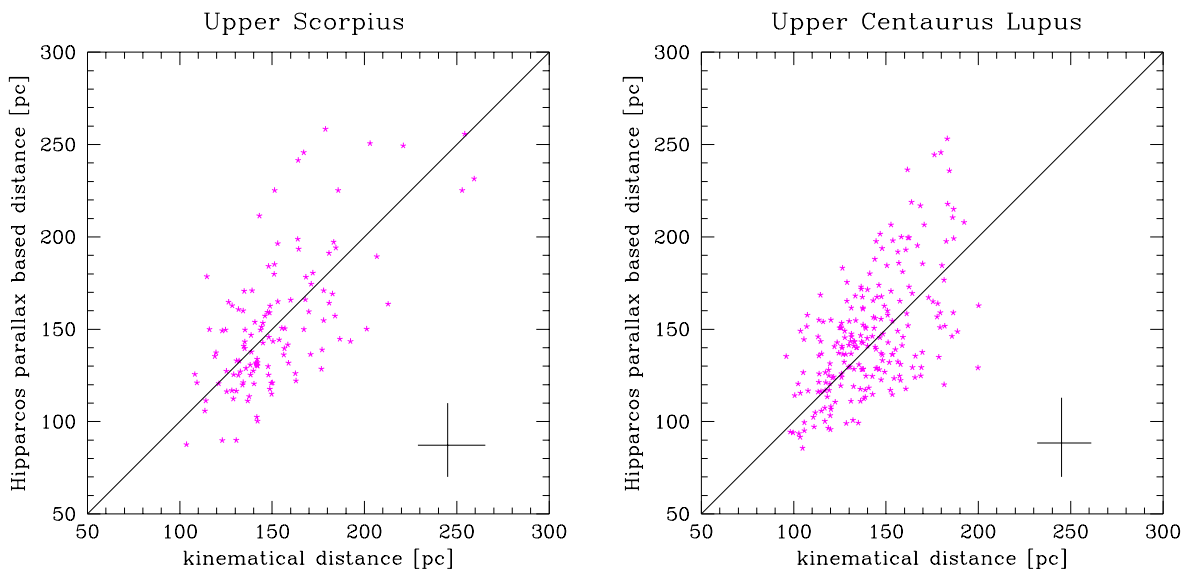


Figure 5.3: Direct comparison of kinematical distances and Hipparcos trigonometric parallaxes converted to distances for the US and UCL subgroups. A typical error bar is shown in the lower right of the figures. Whereas for the majority of the stars both methods yield consistent results within the errors, a systematic deviation is visible for more distant stars in the sense that kinematical distances are systematically smaller. It is likely that these more distant stars (according to Hipparcos) are not members of the association.

direct comparison between the calculated kinematical distances and the Hipparcos based distances. For the majority of the stars both distances are consistent within the errors, whereas for the more distant stars in the sample there seems to be a systematic difference in the sense that kinematical distances are too small.

However, this probably simply reflects the fact that the more distant stars are not members of the association, and so the CP method is not applicable for these stars. This interpretation is supported by the fact that the rather sharp limit between overall agreement and discordance between both distance estimates occurs at about 200 pc, which is yet even larger than the distance up to which member stars are expected if the association is thought to be more or less spherical (an extent of some 40 or 50 pc is estimated from the extent of the subgroups on the sky: 20° correspond to 50 pc at distances of 140–145 pc)

Finally, distances have also been calculated for the late-type stars from Tables 5.1–5.3 where possible. The same streaming velocities and convergent points have been used as for the early-type stars. Preliminary distances have been calculated for the stars under the assumption of membership to both US and UCL, and the residual angles θ between direction of proper motion and convergent point have been compared. For all the stars south of $\delta = -28^\circ$ (with the exception of RXJ 1555.4-3338, which has rather large errors in the proper motion components and likewise in θ), the solution based on the UCL parameters produced a better result, and so the division between US and UCL already made in Fig. 5.1 was kept. For the stars north of $\delta = -28^\circ$ the preferred solution was sometimes US and sometimes UCL, and although some UCL members can be expected in the US region, the distances for these stars were calculated with the assumption of US membership, since this should be more frequent in this region.

The results of the kinematical distance determinations are shown in Table 5.4. Only those stars which fulfilled all the membership criteria quoted in the previous subsection are listed. The most important criteria were the residual angle θ , which had to be smaller than 15° and is given together with its error in the first data column of Table 5.4, and the difference between the distances calculated from the proper motion components in right ascension and declination separately, which should not exceed 60 pc (as compared to 40 pc for the early-type stars, taking the larger proper motion errors for the late-type stars into account).

Altogether the method yielded reliable results for 45 out of 92 stars. The quoted distance errors reflect the errors of the proper motions as well as the errors in the assumed streaming velocity and convergent

Table 5.4: Kinematical distances calculated for late-type stars from the samples of Walter et al. (1994), Kunkel et al. (1999) and Preibisch et al. (1998a) (listed in that order) using the convergent point and streaming velocity of de Zeeuw et al. (1999). Stars north of -28° declination have been assumed to belong to Upper Scorpius (US), those south of -28° declination to Upper Centaurus Lupus (UCL), as indicated in the second column. The following columns give the residual angle θ between the direction of the proper motion and the convergent point as seen from the stars position, together with its error, and the distance with its uncertainty estimate reflecting the error in proper motion, streaming velocity and convergent point. Finally the logarithm of the effective temperature and the $\log L_*/L_{\text{bol}}$ ratio for the quoted distance are given (appropriate photometry is not available for the stars where these columns are blank).

object	CP	θ [°]	d [pc]	$\log T_{\text{eff}}$ [K]	$\log L_*/L_{\text{bol}}$
NTTS 155203-2338	US	11.4 ± 2.4	76 +10 / -8	3.768	0.183 +0.107 / -0.097
NTTS 155220-2313	US	4.9 ± 2.3	123 +16 / -13	3.498	-0.758 +0.106 / -0.097
NTTS 160946-1851	US	2.5 ± 9.9	153 +30 / -21	3.720	0.541 +0.156 / -0.128
stars younger than $\approx 3.5 \cdot 10^7$ years					
RXJ 1549.3-2600	US	0.1 ± 3.0	119 +18 / -14	3.720	0.053 +0.122 / -0.109
RXJ 1551.9-2621	US	2.0 ± 1.7	85 +11 / -9	3.780	0.041 +0.106 / -0.097
RXJ 1552.5-2633	US	-6.8 ± 7.1	73 +25 / -10	3.580	-0.792 +0.162 / -0.128
RXJ 1558.2-2328	US	11.0 ± 4.3	151 +26 / -19	3.768	0.400 +0.138 / -0.117
RXJ 1600.0-2509	US	5.3 ± 4.5	134 +20 / -16	3.780	0.046 +0.121 / -0.110
RXJ 1604.3-2130	US	5.1 ± 17.5	141 +68 / -35	3.690	-0.120 +0.342 / -0.248
RXJ 1524.2-3030	UCL	4.5 ± 3.6	123 +16 / -13	3.720	-0.158 +0.106 / -0.097
RXJ 1530.4-3218	UCL	3.4 ± 3.8	103 +14 / -11	3.751	0.437 +0.111 / -0.098
RXJ 1530.8-3021	UCL	-3.7 ± 9.4	122 +29 / -19	3.690	-0.296 +0.185 / -0.147
RXJ 1531.3-3329	UCL	-2.5 ± 2.5	117 +14 / -11	3.742	-0.202 +0.098 / -0.086
RXJ 1537.0-3136	UCL	2.0 ± 3.9	105 +14 / -11	3.751	0.064 +0.109 / -0.096
RXJ 1537.8-3045	UCL	5.8 ± 8.3	117 +25 / -17	3.662	-0.292 +0.168 / -0.136
RXJ 1544.0-3311	UCL	3.4 ± 2.0	131 +15 / -12	3.733	-0.044 +0.094 / -0.083
RXJ 1545.2-3417	UCL	-1.6 ± 4.7	179 +25 / -19	3.720	0.907 +0.114 / -0.097
RXJ 1545.8-3020	UCL	-1.8 ± 0.5	36 +4 / -3	3.675	-0.506 +0.092 / -0.076
RXJ 1548.0-2908	UCL	10.9 ± 4.1	128 +18 / -14	3.733	-0.184 +0.114 / -0.101
RXJ 1549.0-3102	UCL	4.3 ± 3.0	146 +18 / -15	3.720	-0.020 +0.101 / -0.094
RXJ 1555.4-3338	UCL	-4.1 ± 10.8	109 +29 / -19	3.643	-0.693 +0.205 / -0.166
$\approx 10^8$ years old stars					
RXJ 1550.9-2534	US	5.0 ± 4.6	162 +29 / -21	3.786	0.561 +0.143 / -0.121
RXJ 1601.3-2652	US	1.3 ± 3.5	157 +22 / -17	3.780	0.674 +0.114 / -0.100
RXJ 1529.4-2850	UCL	4.5 ± 1.0	59 +6 / -5	3.742	0.033 +0.084 / -0.077
stars younger than $\approx 3.5 \cdot 10^7$ years					
GSC 6785 476	US	14.6 ± 6.9	90 +17 / -13	3.751	-0.468 +0.150 / -0.136
GSC 6204 812	US	7.5 ± 12.8	150 +50 / -30	3.662	-0.344 +0.250 / -0.194
GSC 6784 39	US	0.4 ± 2.1	135 +18 / -14	3.751	0.157 +0.109 / -0.095
GSC 6784 997	US	10.6 ± 7.0	82 +16 / -12	3.562	-0.416 +0.155 / -0.137
GSC 6793 797	US	6.8 ± 13.1	110 +38 / -22	3.662	-0.453 +0.258 / -0.194
GSC 6213 306	US	6.6 ± 5.5	140 +24 / -18	3.733	0.208 +0.137 / -0.120
GSC 6793 569	US	2.2 ± 8.7	96 +22 / -15	3.706	-0.535 +0.179 / -0.148
GSC 6793 994	US	5.3 ± 13.6	150 +53 / -31	3.763	-0.044 +0.263 / -0.201
GSC 6793 819	US	2.5 ± 12.1	147 +46 / -28	3.720	0.271 +0.236 / -0.184
GSC 6801 186	US	-4.4 ± 10.0	121 +31 / -21	3.760	-0.258 +0.198 / -0.166
GSC 6793 1406	US	-2.9 ± 3.8	155 +24 / -18	3.751	0.177 +0.125 / -0.107
GSC 6794 156	US	1.8 ± 3.2	102 +14 / -11		
GSC 6794 337	US	-1.6 ± 10.8	108 +30 / -19		
GSC 6770 655	UCL	6.3 ± 6.8	76 +14 / -10		
$\approx 10^8$ years old stars					
GSC 6762 602	US	7.1 ± 5.4	172 +32 / -23		
GSC 6771 1281	US	6.5 ± 16.4	156 +69 / -37		
GSC 6189 101	US	5.5 ± 12.0	146 +45 / -28		
GSC 6781 1046	US	0.5 ± 3.2	117 +18 / -14		
GSC 6191 274	US	6.4 ± 10.7	146 +31 / -22		
GSC 6797 599	US	5.3 ± 4.5	134 +20 / -16		
stars older than $\approx 10^8$ years					
GSC 6212 1330	US	11.6 ± 3.5	42 +6 / -5		

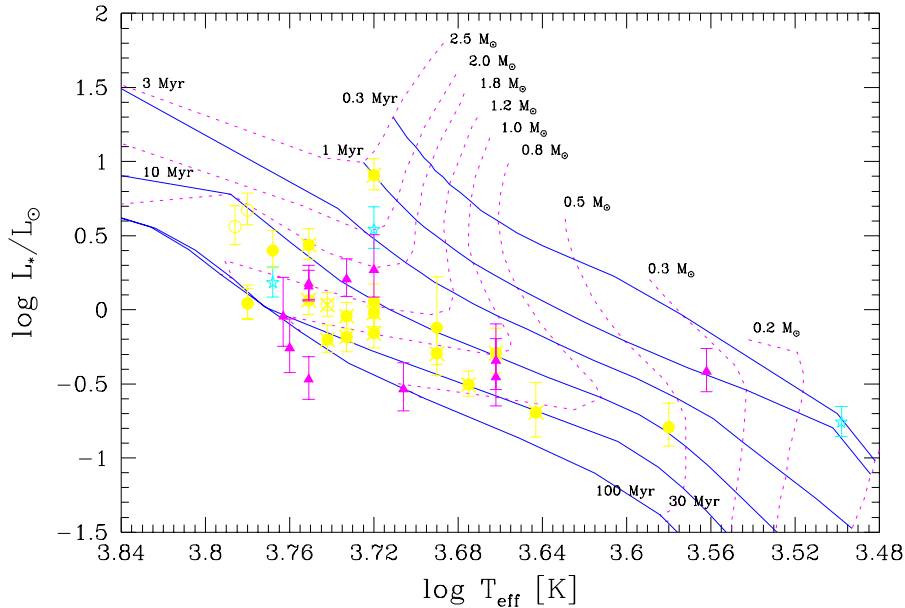


Figure 5.4: HR diagram showing the 35 stars of Table 5.4 with photometry and kinematical distance available. The symbols of the stars are the same as in Fig. 5.1, and stars south of -28° declination have again marked by additional crosses. Spectral types were converted to effective temperatures using the table by Hartigan et al. (1994), and the PMS tracks and isochrones were taken from D’Antona & Mazzitelli (1994) (for Alexander opacities and CM convection). Most of the stars have ages between 10 and 30 Myr, consistent with being members of UCL with a photometrically determined nuclear age of 12–15 Myr (de Geus et al. 1989). However, stars supposed to be members of US apparently do not have smaller ages than the UCL member stars, although the photometric age for US is around 5–8 Myr (de Geus et al. 1989).

point. The error in the streaming velocity was set to 2 km/s and dominates over the error in the position of the convergent point, which has been taken to be 5° along the great circle connecting the association with the convergent point, and 1° in the perpendicular direction (de Bruijne 1999).

Whereas in general a slightly different CP can result either in smaller or larger distances depending on the parameters of each individual star, a different streaming velocity will have a systematic effect on the distances: higher streaming velocities yield higher distances for all the stars and vice versa.

It is noted here again that the distances in Table 5.4 only make sense if the star under consideration really is a member of the association. However, all the stars for which the CP method produced a result, i.e. which can be regarded as members according to the purely kinematical membership criteria, are listed in Table 5.4, irrespective of their ages deduced from the lithium line widths.

For example, the distance of the star GSC 6212 1330, assumed to be older than 10^8 years, is likely to be wrong, as also indicated by its small value of 42 pc. Members are not expected at such small distances, besides maybe in a few exceptional cases when a member star is ejected from the association in the direction to the Sun. Nevertheless, the small distance of 36^{+4}_{-3} pc for the star RXJ 1545.8-3020 seems to be correct, as it is consistent with the Hipparcos parallax yielding a distance of 41 ± 2 pc. There are 4 more stars in Table 5.4 with kinematical distances that have also parallaxes measured by Hipparcos, and they are all consistent within their respective errors.

5.4.3 Hertzsprung-Russell diagram

Fig. 5.4 shows the HR diagram calculated with the kinematical distances of Table 5.4. Spectral types have been converted to effective temperatures according to the table by Hartigan et al. (1994) for late-type dwarfs. Similarly, bolometric corrections have also been taken from that table to derive bolometric luminosities for the stars in Table 5.3 using the photometry in Preibisch & Zinnecker (1999). For stars

of Table 5.1 and 5.2, the absolute bolometric luminosities given by Walter et al. (1994) and Kunkel et al. (1999) for a mean distance of 160 pc have been scaled with the appropriate value from Table 5.4, and the errors in the bolometric luminosities are due to the errors of the derived distances. The tracks and isochrones in Fig. 5.4 have been taken from D’Antona & Mazzitelli (1994), calculated with Alexander opacities and CM convection.

Nearly all the stars fall well above the main-sequence and can therefore really be regarded as rather young. Most of the ages fall into the range between 10 and 30 Myr. Some stars have ages of only a few Myr, while the two stars below the main-sequence (GSC 6793 569 and GSC 6801 186) are probably not members of the Scorpius Centaurus association.

However, it is not obvious from that diagram that UCL stars are on average older than US stars, although the photometric ages for the early-type members indicate an age of 12–15 Myr for UCL and only 6 Myr for US (de Geus et al. 1989). It is not a priori clear that the late-type stars have the same ages as the early-type stars, since not much is known about the formation sequence. Indeed, Walter et al. (1994) have claimed that the late-type stars in the Upper Scorpius region are significantly younger than the B-type stars, with ages around 1 Myr and a very small dispersion. This result has been questioned later on by other authors, and Martín (1998) shows that a mean distance of 125 pc instead of 160 pc would make the ages of early- and late-type stars comparable to each other, fully consistent with the ages derived from the HR diagram based on kinematical distances. Preibisch & Zinnecker (1999) draw the same conclusion taking the uncertainties caused by unresolved binaries into account. Consequently, there is no need to assume different episodes of star formation for early- and late-type stars.

5.5 Summary

Proper motions have been presented for altogether 92 stars in the Upper Scorpius and Upper Centaurus Lupus regions, of which 58 stars have been classified as very young according to their lithium line strengths. The majority of the proper motions has been taken from the ACT, TRC and STARNET proper motion catalogues, and thus they are complementary to the Hipparcos proper motions of early-type stars investigated by de Zeeuw et al. (1999).

The proper motions of the late-type stars have been compared to those of the early-type stars, and no differences have been found within the subgroups. The dispersion in proper motions is slightly larger for the late-type stars, but this can be attributed to larger proper motion errors and/or larger extent in space.

All of the stars south of -28° declination (the region called US-B) have proper motions more typical for UCL than for US and should therefore be regarded as members of UCL.

Given the CP and streaming velocity of de Zeeuw et al. (1999), kinematical distances have been calculated for the early- as well as for the late-type stars, applying several kinematical membership criteria. This procedure led to a result for the distances of 45 late-type stars, and 35 of them could be placed in the HR diagram. The corresponding ages in the range between 10 and 30 Myr are fully consistent with the photometric age of the UCL subgroup. The US subgroup should be slightly younger, but from the HR diagram no difference between the ages of US and UCL member stars is obvious.

6 Conclusions

6.1 Comparison with simulations

Hydrodynamical simulations conducted by Tenorio-Tagle et al. (1987), Franco et al. (1988) and Lépine & Duvert (1994) show that it is possible to explain the properties of nearby star forming regions by assuming that they originated from a high velocity cloud (HVC) impact on the galactic plane. Subsequent to the impact, clouds and stars will oscillate around the galactic plane due to the K_z -force, and during the passage through the plane clouds and stars can separate from each other while encountering different frictions (combing-out).

The difference in proper motions between the T Tauri stars in the central region of Taurus-Auriga and the young stars discovered south of it suggest an interpretation in terms of this kind of high velocity cloud impact model. However, detailed predictions for the motions of cloud and stars after the HVC impact are not available. The hydrodynamical simulations by Tenorio-Tagle et al. (1997), Franco et al. (1988) and Lépine & Duvert (1994) aimed at explaining the origin of star forming regions rather than their subsequent evolution.

In Section 2.3.4 some very simple considerations lead to the conclusion that it is possible that the southern stars are still bound to the cloud if the total cloud mass in the extended Taurus-Auriga region is around $2 \cdot 10^5 M_\odot$. Developing the idea of this simple model a little bit further, the paths of the stars and the cloud in the Taurus-Auriga star forming region have been traced back in time. The cloud was represented by a Plummer sphere with a Plummer radius of 20 pc and a total cloud mass of $2 \cdot 10^5 M_\odot$. The initial position and velocity of the cloud were taken to be the mean values observed for the stars in the central region of Taurus. Similarly, mean values for the southern stars have been adopted, and whereas the only force acting on the cloud was the K_z -force, the stars were subject to the K_z -force as well as to the gravitational force due to the presence of the cloud. The K_z -force per unit mass was calculated according to $K_z = (4\pi G\rho + 2(A^2 - B^2)) \cdot z$, where G is the gravitational constant, $\rho = 0.11 M_\odot/\text{pc}^3$ is the mass density of the galactic disk (Flynn & Fuchs 1994) and A and B are Oort's constants.

The results are presented in Fig. 6.1 and Fig. 6.2. Figure 6.1 shows the height z above the galactic plane of the cloud (grey) and the stars (black). Whereas the cloud oscillates around the galactic plane with a period of slightly less than 10^8 yrs, the motion due to the gravitational force of the cloud is superimposed on the oscillatory motion in the orbit of the stars.

The positions and motions of the cloud and of the stars projected on the sphere are shown in Fig. 6.2. In addition to the mean values for the cloud and the southern stars, the orbits for three individual stars of Table 2.3, namely RXJ 0324.4+0231, RXJ 0354.3+0535 and RXJ 0427.5+0616, are shown, too. These stars represent some of the more peculiar orbits in the diagram; most of the stars follow closely the thick black line representing the mean motions of the southern stars.

Nevertheless, it is remarkable that all the orbits end up in the same region in the position as well as in the proper motion diagram. The simulation was followed for 10^8 yrs backwards in time, whereas the ages of the stars are only around $3.5 \cdot 10^7$ yrs or even younger. This is in accordance with the simulations, since similar positions and proper motions for the cloud and the stars are already reached before 10–30 Myr back in time. The fact that the proper motions tend to zero and the projected positions remain more or less constant after 10^8 yrs is due to the large distance of clouds and stars in earlier times.

The model is very simple and clearly neglects a variety of effects, e.g. the interactions of the stars among each other (especially in binary or multiple systems), hydrodynamical forces, deviations from a spherical geometry of the cloud or different ages of the stars. Despite these shortcomings, the model illustrates nicely how the observed kinematics in the Taurus-Auriga association could be interpreted in the framework of a HVC impact model.

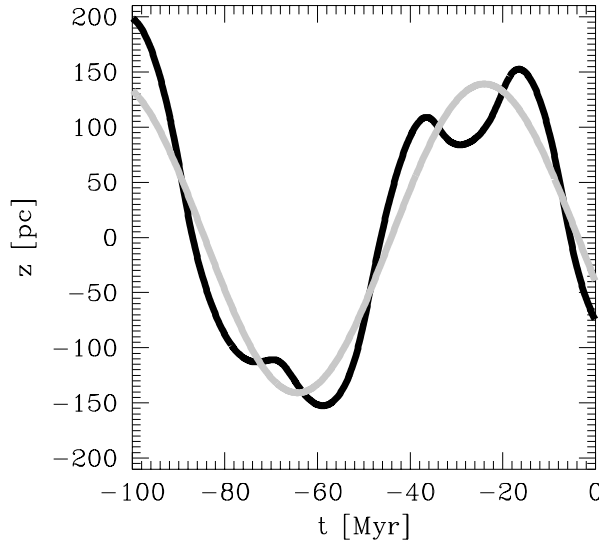


Figure 6.1: Height z above the galactic plane of a cloud (grey) with properties similar to those of the Taurus cloud and of a star (black) with initial position and proper motion reflecting the mean values for the stars discovered south of Taurus (see Chapter 2). Whereas the cloud oscillates around the galactic plane, the motion due to the gravitational force of the cloud is superimposed on a pure oscillatory motion in the orbit of the star.

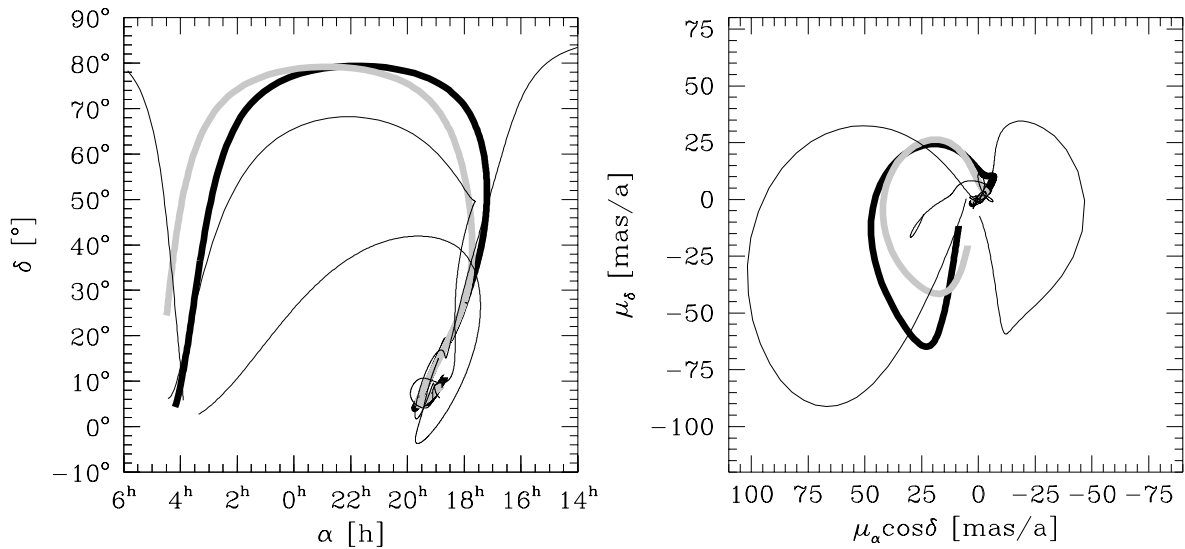


Figure 6.2: Positions (left panel) and proper motions (right panel) of a cloud (thick grey line) and of a star (thick black line) typical for those discovered south of the Taurus clouds during a simulation time of 10^8 yrs. The three thin lines represent individual orbits of stars. At the beginning, the objects are between 4^h and 5^h in right ascension in the position diagram and move quickly back to their earlier positions. Before about 10–30 Myr clouds and stars were located at approximately the same positions with similar proper motions. In earlier times objects which are now located close to the Sun have been more distant, and this is reflected in the simulations by the fact that proper motions tend to zero for larger periods back in time, so that the projected positions on the sky do not change much any more.

6.2 Comparison of the results in the Taurus-Auriga, Chamaeleon, Lupus and Scorpius-Centaurus star forming regions

The main intention of the present proper motion study of T Tauri stars was to investigate the kinematical relation between the classical T Tauri stars in the central regions of some nearby star forming regions and the more widely distributed weak-line T Tauri stars discovered with ROSAT.

The observational findings in the regions investigated in this thesis (Taurus-Auriga, Chamaeleon, Lupus and Scorpius-Centaurus) were all very similar. Certain search fields have been specified outside the adopted boundaries of these star forming regions, extending up to several tens of parsec away from the known sites of star formation: a field south of Taurus (Neuhäuser et al. 1995c, Neuhäuser et al. 1997, Magazzù et al. 1997), west of Chamaeleon τ (Alcalá et al. 1995, Alcalá et al. 1997, Covino et al. 1997), a strip perpendicular to Gould's Belt somewhat west of the Lupus clouds (Wichmann et al. 1997b) and a field southwest of Upper Scorpius (Kunkel et al. 1999) as well as a large field encompassing the whole Upper Scorpius region (Preibisch et al. 1998a).

In each of the above search fields large numbers of weak-line T Tauri stars have been identified by selecting promising candidates from the ROSAT databases and optical follow-up spectroscopy. Because of this similarity it seemed at first glance likely that the observed halos of WTTS around these star forming regions were produced by the same mechanism in all these regions, like e.g. the RATTS mechanism (Sterzik & Durisen 1995, Gorti & Bhatt 1996).

However, it turned out very clearly from the proper motion studies that the RATTS mechanism could not be the dominant process in producing these halos of WTTS. Indeed a few candidate escaper stars which could have been ejected with relative high velocities out of the denser regions can be found in the samples, but it certainly cannot be invoked for the majority of the weak-line T Tauri stars to explain their current positions.

In order to get around the problems of explaining the existence of such a large population of widely distributed WTTS, Briceño et al. (1997) suggested that the stars discovered with ROSAT might not be as young as judged from the lithium line widths, but rather belong to a population of nearby X-ray active main-sequence stars. However, their galactic evolutionary model was very simple and contained some shortcomings, and the Hipparcos parallaxes (Neuhäuser & Brandner 1998) as well as higher resolution studies (e.g. Covino et al. 1997, Wichmann et al. 1997b) demonstrated that the majority of the WTTS is really still in a pre-main sequence evolutionary phase.

The solution to the problem might be to consider a variety of mechanisms and explanations that are of mutual importance for different star forming regions.

Evidence is accumulating that at least a certain fraction of the WTTS might be members of Gould's Belt, especially those located in the extended Lupus region. Wichmann et al. (1997b) found a peak in the spatial distribution of the WTTS in their sample that coincides with the position of Gould's Belt midplane. Also, the so-called off-cloud WTTS have ages somewhat larger than the CTTS and on-cloud WTTS, and it might very well be that at least a fraction of the WTTS are indeed members of Gould's Belt. Additionally, the velocity dispersion observed in the Lupus region is rather large, which might indicate that the stars do not constitute a homogeneous sample.

So, although Gould's Belt membership is a promising scenario in the Lupus region (and maybe also in the Scorpius-Centaurus and Orion regions), it encounters serious problems in the Chamaeleon and Taurus regions, where Gould's Belt is not so close to the specified search fields.

According to the present model for Gould's Belt (see e.g. Pöppel 1997) the centre of Gould's Belt is not at the Sun, but rather close to the Taurus region, whereas the other star forming regions are positioned on a ring outside at distances up to 450 pc (Comeron et al. 1994). Guillot et al. (1998) argue for a filled plane of stars rather than a ring for the geometry of Gould's Belt, which could help to explain a possible connection of the Taurus region to Gould's Belt.

However, the model developed in Section 2.3.4 and compared with simulations in the previous section can easily explain the observed motions of the southern stars relative to the stars in the central Taurus clouds and therefore can be considered as a promising alternative. It assumes that the southern stars are

still bound to the clouds while oscillating around the galactic plane, in line with models that invoke high velocity cloud impacts on the galactic plane as trigger for star formation (Franco et al. 1988, Lépine & Duvert 1994).

The case for the Chamaeleon region is again different. Feigelson (1996) has put forward a model where star formation occurs in small cloudlets. Stars originating from the same cloudlet should have very similar velocities with a small dispersion, whereas the mean motions of the cloudlets reflect the turbulent structure of the giant parental molecular cloud. Although at present there are not many stars with known proper motions from the same cloudlet, the overall distribution of proper motions in the proper motion diagram is consistent with this scenario. Note also that Mizuno et al. (1998) have discovered 25 small dense clouds widely distributed in the Chamaeleon region, giving strong support to the cloudlet model of star formation by Feigelson (1996).

Finally, the observed kinematics in the Scorpius-Centaurus region is fully consistent with membership of the late-type stars to the association, and no significant kinematical differences between the early-type members and the T Tauri stars could be found. The majority of the T Tauri stars in the region called US-B belong to Upper Centaurus Lupus rather than to Upper Scorpius. Additionally, a search for wider distributed WTTS around the Upper Scorpius region showed that the WTTS were preferentially found close to the centre of the association, so that there is no need to explain a large separation to their assumed birthplaces like in the T associations studied.

6.3 Outlook

The results of the previous chapters demonstrated once more that astrometry is a very powerful tool from which one can expect important contributions for disciplines not intrinsically related to it, like e.g. star formation.

The work of this thesis has benefited greatly from the results of the Hipparcos Space Astrometry Mission, which provides the most accurate absolute proper motions and largest sample of trigonometric parallaxes ever available. For example, the discovery of a separate kinematical subgroup located between the Cha I and Cha II clouds at only half the assumed distance of the cloud material in the Chamaeleon region was facilitated by the availability of a handful Hipparcos parallaxes for stars in this subgroup as well as in the Cha I cloud. Similarly, the derivation of kinematical distances with the convergent point method for faint late-type stars in the Scorpius-Centaurus association was possible only because a large fraction of early-type member stars have been observed by Hipparcos, so that the distance, the convergent point and the streaming velocity could be determined with very high accuracies.

The availability of proper motion catalogues like STARNET covering the whole sky down to reasonable faint magnitudes also was essential for this study. STARNET contains 36 times as many stars as Hipparcos and about 4 times as many stars as ACT or TRC, and one could easily imagine how small the samples of typically about one hundred stars in a region would have been without STARNET. STARNET proper motions were extremely helpful to withdraw the RATTS hypothesis e.g. for the stars south of Taurus-Auriga and again they were useful for the determination of the kinematical distances in the Scorpius-Centaurus association.

The ACT and TRC catalogues play an intermediate role between Hipparcos and STARNET with respect to numbers of stars and accuracies and completed the Hipparcos and STARNET data. With the completion of the Tycho2 Catalogue proper motions with accuracies of ≈ 2.5 mas/a (comparable to ACT and TRC) will be available for a larger number of then 2.5 million stars (Høg et al. 1998).

On the other hand, some issues could not be clarified with the Hipparcos data. For example, it would be very interesting to know the parallaxes for at least some of the young stars south of the Taurus clouds in order to fix their space motions with respect to the stars in the centre of the association. If they were at the same distance as the stars in the centre the two populations would approach each other. If they were however nearer than previously thought they would have similar space velocities, but also their ages as derived from the Hertzsprung-Russell diagram would increase.

Important contributions to the solutions of these outstanding problems can be expected from planned future space missions like DIVA (Bastian 1998, Röser 1999) or GAIA (Perryman et al. 1997, Lindegren & Perryman 1997).

With the current mission design for DIVA about 50 to 100 times as many stars as with Hipparcos could be observed, about 2 times as many as are included in the STARNET catalogue. This means that nearly all of the presently known T Tauri stars in nearby star forming regions will be observed with DIVA. Precise trigonometric parallaxes will be available at least for all stars brighter than 13^{th} mag, as well as proper motions with accuracies around 2 mas/a. In combination with the Hipparcos data, much more precise proper motions can be obtained, and this will probably help to resolve the internal velocity dispersion of small groups of stars. The launch of DIVA is planned for the year 2003, and the results could be available in 2008 (for further details, see Röser 1999).

Astrometry on the micro-arcsecond level is within reach with the GAIA mission, planned for a decade or even more later than DIVA. In addition to very accurate trigonometric parallaxes and proper motions for possibly up to one billion stars, GAIA will also provide radial velocities for a large fraction of the brighter stars, so that the whole 3-dimensional position and velocity information will be available.

The results of the DIVA and GAIA missions could clearly help to revolutionize our understanding of many aspects of galactic as well as extragalactic dynamics, including some important issues of star formation.

References

- Alcalá, J.M., Covino, E., Franchini, M., Krautter, J., Terranegra, L., Wichmann, R., 1993, A&A 272, 225
- Alcalá, J.M., Krautter, J., Schmitt, J.H.M.M., Covino, E., Wichmann, R., Mundt, R., 1995, A&AS 114, 109
- Alcalá, J.M., Terranegra, L., Wichmann, R., Chavarría-K., C., Krautter, J., Schmitt, J.H.M.M., Moreno-Corral, M.A.; de Lara, E.; Wagner, R.M., 1996, A&AS 119, 7
- Alcalá, J.M., Krautter, J., Covino, E., Neuhäuser, R., Schmitt, J.H.M.M., Wichmann, R., 1997, A&A 319, 184
- Alcalá, J.M., Chevarría-K., C.; Terranegra, L., 1998, A&A 330, 1017
- Ambartsumian, V.A., 1947, *Stellar Evolution and Astrophysics*, Academy of Science of Armenia, Erevan
- van den Ancker, M.E., de Winter, D., Thé, P.S., 1996, A&A 313, 517
- Appenzeller, I., Jankovics, I., Krautter, J., 1983, A&AS 53, 291
- Barbier-Brossat, M., 1989, A&AS 80, 67
- Bastian, U., Finkenzeller, U., Jaschek, C., Jaschek, M., 1983, A&A 126, 438
- Bastian, U., Röser, S., Yagudin, L.I., Nesterov, V.V., Polozhentsev, D.D., Potter, Kh.I., Wielen, R., Yatskiv, Ya.S., 1993, *PPM Star Catalogue*, Vols. III & IV, Spektrum Akademischer Verlag, Heidelberg
- Bastian, U., 1998, *The Small Astrometric Interferometry Satellite DIVA*, Frühjahrstagung der Astron. Ges. Gotha, 1998
- Beckwith, S., Sargent, A., 1996, Nature 383, 139
- Bertiau, F.C., 1958, ApJ 128, 533
- Bessell, M.S., Eggen, O.J., 1972, ApJ 177, 209
- Blaauw, A., 1946, PhD thesis, University of Groningen
- Blaauw, A., 1991, in: *The Physics of Star Formation and Early Stellar Evolution*, eds. Ch.J. Lada & N.D. Kylafis, p. 125
- Bodenheimer, P., 1965, ApJ 142, 451
- Boulanger, E., Bronfman, L., Dame, T.M., Thaddeus P., 1998, A&A 332, 273
- Bouvier, J., Wichmann, R., Grankin, K., Allain, S., Covino, E., Fernández, M., Martín, E.L., Terranegra, L., Catalano, S., Marilli, E., 1997, A&A 318, 495
- Brandner, W., 1992, Diploma thesis, Julius-Maximilians-Universität Würzburg
- Brandner, W., Alcalá, J.M., Kunkel, M., Moneti, A., Zinnecker, H., 1996, A&A 307, 121
- Brandner, W., Köhler, R., 1998, ApJ 499, L79
- Brandner, W., Zinnecker, H., 1997, A&A 321, 220
- Briceño, C., Hartmann, L.W., Stauffer, J.R., Gagné, M., Stern, R.A., Caillault, J.-P., 1997, AJ 113, 740
- Brown, A.G.A., Dekker, G., de Zeeuw, P.T., 1997, MNRAS 285, 479

- de Bruijne, J.H.J., 1999, MNRAS, submitted
- Carkner, L., Feigelson, E.D., Koyama, K., Montmerle, T., Reid, N.I., 1996, ApJ 464, 286
- Casanova, S., Montmerle, Th., Feigelson, E.D., André, Ph., 1995, ApJ 439, 752
- Cohen, M., Kuhl, L.V., 1979, ApJ 227, L105
- Comerón, F., Torra, J., Gómez, A.E., 1994, A&A 286, 789
- Corbin, T.E., Urban, S.E., Warren, W.H., 1991, *Astrographic Catalogue Reference Stars*, NASA, NSSDC 91-10
- Covino, E., Alcalá, J.M., Allain, S., Bouvier, J., Terranegra, L., Krautter, J., 1997, A&A 328, 187
- D'Antona, F., Mazzitelli, I., 1994, ApJS 90, 467
- Delhaye, J., 1965, in: *Galactic Structure*, eds. A. Blaauw & M. Schmidt, University of Chicago Press, 61
- Dubath, P., Reipurth, B., Mayor, M., 1996, A&A 308, 107
- Duquennoy, A., Mayor, M., 1991, A&A 248, 485
- Elias, J.H., 1978, ApJ 224, 857
- ESA, 1997, *The Hipparcos and Tycho Catalogues*, ESA SP-1200
- Favata, F., Micela, G., Sciortino, S., 1997, A&A 326, 647
- Feigelson, E.D., Casanova, S., Montmerle, T., Guibert, J., 1993, ApJ 416, 623
- Feigelson, E.D., DeCampi, W.M., 1981, ApJ 243, L89
- Feigelson, E.D., Kriss, G.A., 1981, ApJ 248, L35
- Feigelson, E.D., Kriss, G.A., 1989, ApJ 338, 262
- Feigelson, E.D., 1996, ApJ 468, 306
- Finkenzeller, U., Jankovics, I., A&AS 57, 285, 1984
- Franco, J., Tenorio-Tagle, G., Bodenheimer, P., Różycka, M., Mirabel, I.F., 1988, ApJ 333, 826
- Fricke, W., Schwan, H., Lederle, T., 1988, *Fifth Fundamental Catalogue (FK5)*, Veröffentlichungen Astronomisches Rechen-Institut Heidelberg No. 32
- Frink, S., Röser, S., 1996, Astron. Ges., Abstr. Ser. 12, p. 80
- Frink, S., Röser, S., Neuhäuser, R., Sterzik, M.F., 1997, A&A 325, 613
- Frink, S., Röser, S., Alcalá, J.M., Covino, E., Brandner, W., 1998, A&A 338, 442
- de Geus, E.J., de Zeeuw, P.T., Lub, J., 1989, A&A 216, 44
- de Geus, E.J., Lub, J., van der Grift, E., 1990, A&AS 85, 915
- Ghez, A.M., McCarthy, D.W., Patience, J.L., Beck, T.L., 1997, ApJ 481, 378
- Gliese, W., Jahreiß, H., 1991, *Preliminary Version of the Third Catalogue of Nearby Stars*, on: The Astronomical Data Center CD-ROM: Selected Astronomical Catalogs, Vol. I; eds. L.E. Brodzmann & S.E. Gesser, NASA/Astronomical Data Center, Goddard Space Flight Center, Greenbelt, MD
- Gomez, M., Jones, B.F., Hartmann, L., Kenyon, S.J., Stauffer, J.R., Hewett, R., Reid, I.N., 1992, AJ 104, 762
- Gorti, U., Bhatt, H.C., 1996, MNRAS 278, 611
- Gottlieb, D.M., Upson, W.L., 1969, ApJ 157, 611
- Greenstein, J.L., 1937, Ann. Harvard Obs., 105, 359

- Gregorio-Hetem, J., Lépine, J.R.D., Quast, G.R., Torres, C.A.O., de la Reza, R., 1992, AJ 103, 549
- Guenther, E., Lehmann, H., 1998, ASP Conf. Ser. 154, *The Tenth Cambridge Workshop on Cool Stars, Stellar Systems and the Sun*, eds. R.A. Donahue & J.A. Bookbinder, p. 1693
- Guenther, E., Lehmann, H., Emerson, J.P., Staude, J., 1999, A&A 341, 768
- Guillout, P., Sterzik, M.F., Schmitt, J.H.M.M., Motch, C., Neuhäuser, R., 1998, A&A 337, 113
- Hartigan, P., 1993, AJ 105, 1511
- Hartigan, P., Strom, K.M., Strom, S.E., 1994, ApJ 427, 961
- Hartley, M., Tritton, S.B., Manchester, R.N. et al., 1986, A&AS 63, 27
- Hartmann, L., Jones, B.F., Stauffer, J.R., Kenyon, S.J., 1991, AJ 101, 1050
- Heckmann, O., Dieckvoss, W., 1975, *AGK3: Star Catalogue of Positions and Proper Motions North of 2°5 Declination*, Sternwarte Hamburg-Bergedorf
- Henize, K.G., 1954, ApJ 119, 459
- Henize, K.G., 1963, AJ 68, 280
- Henize, K.G., Mendoza V., E.E., 1973, ApJ 180, 115
- Herbig, G.H., 1962, Adv. Astron. Astrophys. 1, 47
- Herbig, G.H., Rao, N.K., 1972, ApJ 174, 401
- Herbig, G.H., 1973, ApJ 128, 129
- Herbig, G.H., 1977, ApJ 214, 747
- Herbig, G.H., 1978, in: *Problems of Physics and Evolution of the Universe*, ed. L. Mirzoyan, Academy of Science of Armenia, Erevan, p. 171
- Herbig, G.H., 1985, in: *Birth and Infancy of Stars*, eds. R. Lucas, A. Omont, R. Stora, Amsterdam, North-Holland, p. 535
- Herbig, G.H., Bell, K.R., 1988, Lick Obs. Bull. 43
- Hoffmeister, C., 1962, Zeitschr. Astrophys. 55, 290
- Høg, E., Kuzmin, A., Bastian, U., Fabricius, C., Kuimov, K., Lindegren, L., Makarov, V.V., Röser, S., 1998, A&A 335, L65
- Hoogerwerf, R., Aguilar, L.A., 1999, MNRAS, submitted
- Hughes, J., Hartigan, P., Clampitt, L., 1993, AJ 105, 571
- Hughes, J., Hartigan, P., Krautter, J., Kelemen, J., 1994, AJ 108, 1071
- Jenkner, H., Lasker, B.M., Sturch, C.R., McLean, B.J., Shara, M.M., Russell, J.L., 1990, AJ 99, 2082
- Jones, D.H.P., 1971, MNRAS 152, 231
- Jones, B.F., Herbig, G.H., 1979, AJ 84, 1872
- Joy, A.H., 1945, ApJ 102, 168
- Kapteyn, J.C., 1914, ApJ 40, 43
- Kenyon, S.J., Dobrzycka, D., Hartmann, L., 1994, AJ 108, 1872
- Kovalevsky, J., 1997, ESA-SP 402, 11
- Koyama, K., Hamaguchi, K., Ueno, S., Kobayashi, N., Feigelson, E.D., 1996, PASJ 48, L87
- Krautter, J., Kelemen, J., 1987, Mitt. Astron. Ges. 70, 397

- Krautter, J., 1991, ESO Scientific Report No. 11, *Low Mass Star Formation in Southern Molecular Clouds*, ed. B. Reipurth, p. 127
- Krautter, J., Wichmann, R., Schmitt, J.H.M.M., Alcalá, J.M., Neuhäuser, R., Terranegra, L., 1997, A&AS 123, 329
- Kroupa, P., 1995, MNRAS 277, 1522
- Kroupa, P., 1998, MNRAS 298, 231
- Ku, W.H.-M., Chanan, G.A., 1979, ApJ 234, L59
- Kunkel, M. et al. 1999, in preparation
- Lasker, B.M., Sturch, C.R., McLean, B.J., Russell, J.L., Jenkner, H., Shara, M.M., 1990, AJ 99, 2019
- Launhardt, R., Henning, T., 1997, A&A 326, 329
- Lawson, W.A., Feigelson, E.D., Huenemoerder, D.P., 1996, MNRAS 280, 1071
- Lépine, J.R.D., Duvert, G., 1994, A&A 286, 60
- van Leeuwen, F., Alpenaar, P., Brand, J., 1986, A&AS 65, 309
- Lindblad, P.O., Westin, T.N.G., 1985, in: *Birth and Evolution of Massive Stars and Stellar Groups*, eds. W. Boland & H. van Woerden, p. 33
- Lindgren, L., 1992, European International Space Year Conference, Satellite Symposium 3, p. 3
- Lindgren, L., Kovalevsky, J., 1995, A&A 304, 189
- Lindgren, L., Perryman, M.A.C., 1997, ESA-SP 402, 799
- Lindgren, L., Mignard, F., Söderhjelm, S., Badiali, M., Bernstein, H.H., Lampens, P., Pannunzio, R., Arenou, F., Bernacca, P.L., Falin, J.L., Froeschlé, M., Kovalevsky, J., Martin, C., Perryman, M.A.C., Wielen, R., 1997, A&A 323, L53
- Luyten, W.J., 1979, NLTT Catalogue, Minneapolis, University of Minnesota
- Magazzù, A., Martín, E.L., Sterzik, M.F., Neuhäuser, R., Covino, E., Alcalá, J.M., 1997, A&AS 124, 449
- Martín, E.L., 1998, AJ 115, 351
- Martín, E.L., Magazzù, A., 1999, accepted by A&A
- McCuskey, S.W., 1939, ApJ 89, 568
- Morse, J.A., Mathieu, R.D., Levine, S.E., 1991, AJ 101, 1495
- Murphy, D.C., Cohen, R., May, J., 1986, A&A 167, 234
- Neuhäuser, R., Sterzik, M.F., Schmitt, J.H.M.M., Wichmann, R., Krautter, J., 1995a, A&A 295, L5
- Neuhäuser, R., Sterzik, M.F., Schmitt, J.H.M.M., Wichmann, R., Krautter, J., 1995b, A&A 297, 391
- Neuhäuser, R., Sterzik, M.F., Torres, G., Martín E.L., 1995c, A&A 299, L13
- Neuhäuser, R., Preibisch, Th., 1997, A&A 322, L37
- Neuhäuser, R., Torres, G., Sterzik, M.F., Randich, S., 1997, A&A 325, 647
- Neuhäuser, R., Brandner, W., 1998, A&A 330, L29
- Neuhäuser, R. et al., 1999, in preparation
- Martín E.L., 1998, AJ 115, 351
- Palla, F., Galli, D., 1997, ApJ 476, L35
- Perryman, M.A.C., Lindgren, L., Turon, C., 1997, ESA-SP 402, 743

- Perryman, M.A.C., Brown, A.G.A., Lebreton, Y., Gómez, A., Turon, C., Cayrel de Strobel, G., Mermilliod, J.C., Robichon, N., Kovalevsky, J., Crifo, F., 1998, *A&A* 331, 81
- Petr, M.G., Coudé du Foresto, V., Beckwith, S.V.W., Richichi, A., McCaughrean, M.J., 1998, *ApJ* 500, 825
- Petrie, R.M., 1961, *MNRAS* 123, 501
- Pfau, W., Hoff, W., Relke, H., 1996, MPE Report 263, 59
- Plaskett, J.S., Pearce, J.A., 1934, *MNRAS* 94, 679
- Pöppel, W., 1997, *Fund. Cosm. Phys.* 18, 1
- Preibisch, Th., Smith, M.D., 1997, *A&A* 322, 825
- Preibisch, Th., Guenther, E., Zinnecker, H., Sterzik, M., Frink, S., Röser, S., 1998a, *A&A* 333, 619
- Preibisch, Th., Zinnecker, H., Guenther, E., Sterzik, M., Frink, S., Röser, S., 1998b, *Astron. Ges., Abstr. Ser.* 14, 16
- Preibisch, Th., Zinnecker, H., 1999, *AJ*, submitted
- Racine, R., 1968, *AJ* 73, 233
- Rasmuson, N.H., 1921, *Lund Medd., Ser. II*, 26, 1
- Reipurth, B., Zinnecker, W., 1993, *A&A* 278, 81
- Relke, H., Pfau, W., 1999, in preparation
- Röser, S., Bastian, U., 1991, *PPM Star Catalogue*, Vols. I & II, Spektrum Akademischer Verlag, Heidelberg
- Röser, S., Bastian, U., Kuzmin, A., 1994, *A&AS* 105, 301
- Röser, S., 1996, *IAU Symp.* 172, 481
- Röser, S., Morrison, J., Bucciarelli, B., Lasker, B., McLean, B., 1996, *IAU Symp.* 179, 420
- Röser, S., 1999, *DIVA - Beyond Hipparcos and Towards GAIA*, *Reviews in Modern Astronomy* 12
- Ruciński, S.M., Krautter, J., 1983, *A&A* 121, 217
- Russell, J.L., Lasker, B.M., McLean, B.J., Sturch, C.R., Jenkner, H., 1990, *AJ* 99, 2059
- SAO staff, 1966, *Smithsonian Astrophysical Observatory Star Catalog*, Smithsonian Astrophysical Observatory
- Schilbach, E., Robichon, N., Souchay, J., Guibert, J., 1995, *A&A* 299, 696
- Schwan, H., 1990, *A&A* 228, 69
- Schwan, H., 1991, *A&A* 243, 386
- Schwartz, R.D., 1977, *ApJS* 35, 161
- Schwartz, R.D., 1991, *ESO Scientific Report No.* 11, 93
- Sciortino, S., Damiani, F., Favata, F., Micela, G., 1998, *A&A* 332, 825
- Smart, W.M., 1939, *MNRAS* 100, 60
- Sterzik, M.F., Alcalá, J.M., Neuhäuser, R., Schmitt, J.H.M.M., 1995, *A&A* 297, 418
- Sterzik, M.F., Durisen, R.H., 1995, *A&A* 304, L9
- Strom, S.E., Strom, K.M., Edwards, S., 1987, in: *Galactic and Extragalactic Star Formation*, eds. R.E. Pudritz & M. Fich, p. 53
- Strom, K.M., Strom, S.E., 1994, *ApJ* 424, 237

- Strom, K.M., Strom, S.E., Edwards, S., Cabrit, S., Skrutskie, M.F., 1989, AJ 97, 1451
- Tachihara, K., Dobashi, K., Mizuno, A., Ogawa, H., Fukui, Y., 1986, PASJ 48, 489
- Tenorio-Tagle, G., Franco, J., Bodenheimer, P., Rozyczka, M., 1987, A&A 179, 219
- Terranegra, L., Morale, F., Spagna, A., Massone, G., Lattanzi, M.G., 1999, A&A 341, L79
- The, P.-S., 1962, Contr. Bosscha Obs. Lembang, No. 15
- Torres, C.A.O., Quast, G., de la Reza, R., Gregorio-Hetem, J., Lépine, J.R.D., 1995, AJ 109, 2146
- Ungerechts, H., Thaddeus, P., 1987, ApJS 63, 645
- Urban, S.E., Corbin, Th.E., Wycoff, G.L., 1997, *The ACT Reference Catalog*, U.S. Naval Observatory, Washington, D.C.
- Walter, F.M., Kuhl, L.V., 1981, ApJ 250, 254
- Walter, F.M., 1986, ApJ 306, 573
- Walter, F.M., Brown, A., Linsky, J.L., Rydgren, A.E., Vrba, F., Roth, M., Carrasco, L., Chugainov, P.F., Shakovskaya, N.I., Imhoff, C.L., 1987, ApJ 314, 297
- Walter, F.M., 1992, AJ 104, 758
- Walter, F.M., Vrba, F.J., Mathieu, R.D., Brown, A., Myers, P.C., 1994, AJ 107, 692
- Weaver, W.B., 1983, MNRAS 205, 389
- Whittet, D.C.B., Prusti, T., Franco, G.A.P. et al., 1997, A&A 327, 1194
- Wielen, R., 1997, A&A 325, 367
- Wichmann, R., Krautter, J., Schmitt, J.H.M.M., Neuhäuser, R., Alcalá, J.M., Zinnecker, H., Wagner, R.M., Mundt, R., Sterzik, M.F., 1996, A&A 312, 439
- Wichmann, R., Krautter, J., Covino, E., Alcalá, J.M., Neuhäuser, R., Schmitt, J.H.M.M., 1997a, A&A 320, 185
- Wichmann, R., Sterzik, M., Krautter, J., Metanomski, A., Voges, W., 1997b, A&A 326, 211
- Wichmann, R., Bouvier, J., Allain, S., Krautter, J., 1998a, A&A 330, 521
- Wichmann, R., Bastian, U., Krautter, J., Jankovics, I., Ruciński, S.M., 1998b, MNRAS 301, L39
- Wichmann, R., Covino, E., Alcalá, J.M., Krautter, J., Allain, S., Hauschildt, P., 1999a, submitted to MNRAS
- Wichmann, R. et al. 1999b, in preparation
- Wilson, R.E., 1953, *General Catalogue of Stellar Radial Velocities*, Carnegie Inst. Washington, Publ. 601
- Yun, J.L., Moreira, M.C., Alves, J.F., Storm, J., 1997, A&A 320, 167
- de Zeeuw, P.T., Hoogerwerf, R., de Bruijne, J.H.J., Brown, A.G.A., Blaauw, A., 1999, AJ 117, 354

A Appendix

The Appendix contains those stars investigated in the main part of this work which are present in more than one of the Hipparcos, PPM, ACT, TRC and STARNET proper motion catalogues. All these multiple proper motions are listed together with their formal errors for comparison, and the catalogue entry which is used for the kinematical analysis is flagged by an arrow (\rightarrow).

If all proper motions for a particular star agree within the errors the most accurate proper motion is selected, taking into account also the flags from the source catalogues indicating problems with the proper motion. Note that the quoted ACT proper motion errors do not contain the contribution from systematic uncertainties of the order of $1-2\text{ mas/a}$ which has to be added quadratically for comparison with the proper motion errors from the other catalogues. On the other hand, if there were discrepancies between the proper motions in individual catalogues preference was given to proper motions based on larger epoch differences, since such discrepancies are often due to orbital motion of multiple stars (Wielen 1997).

An asterisk (*) after a star name refers to additional notes at the bottom of the table.

Taurus-Auriga

Table A.1: Stars from Table 2.1 (TTS in Taurus known before ROSAT).

[mas/a]	μ_α	μ_δ	$\frac{\sigma_{\mu_\alpha}}{\cos \delta}$	σ_{μ_δ}	[mas/a]	μ_α	μ_δ	$\frac{\sigma_{\mu_\alpha}}{\cos \delta}$	σ_{μ_δ}	
SAO 76411A					T Tau N					
PPM 93187	45.	-57.	3.6	3.7	→ HIP 20390	16.39	-12.48	1.88	1.62	
→ T 1262 1647	49.3	-51.4	1.8	1.8	PPM 119824	14.	-10.	2.6	2.5	
SAO 76428					A 1272	470	11.4	-13.2	2.38	2.27
PPM 93216	8.	-25.	3.7	3.8	T 1272	470	16.3	-14.5	2.1	2.1
→ A 1262 421	6.0	-15.4	3.13	0.85	S 1272	470	12.	-11.	4.4	4.4
S 1262 421	6.	-23.	4.4	4.4	DF Tau*					
V773 Tau*					→ HIP 20777	16.07	-26.38	6.25	4.26	
HIP 19762	0.74	-24.89	2.55	1.89	A 1820 1418	3.9	-20.1			
→ A 1827 1236	10.3	-20.7	2.57	3.84	S 1820 525	1.	-9.	3.9	3.9	
T 1827 1236	12.1	-18.2	2.7	4.9	NTTS 042417+1744					
S 1827 1236	9.	-22.	4.9	5.0	→ A 1269 913	0.2	-14.6	0.92	1.07	
V410 Tau					T 1269 913	0.8	-12.4	2.1	1.8	
→ HIP 20097	6.87	-27.44	2.38	1.77	S 1269 913	2.	-17.	3.3	3.3	
A 1827 8	5.1	-33.1	4.08	4.29	UX Tau A*					
T 1827 8	7.7	-31.3	4.2	2.1	HIP 20990	9.04	-27.42	5.08	3.78	
S 1827 8	14.	-32.	5.0	5.0	PPM 119959	2.	-6.	4.4	4.4	
BP Tau					→ A 1269 225	8.2	-12.4			
→ HIP 20160	6.04	-33.13	5.43	3.94	S 1269 225	-2.	-13.	3.7	3.7	
A 1827 554	4.9	-31.9			NTTS 043220+1815					
S 1827 554	8.	-29.	3.9	3.9	→ A 1270 1331	0.9	-11.0	0.99	2.89	
RY Tau*					T 1270 1331	1.9	-11.8	1.7	1.7	
→ HIP 20387	10.33	-23.05	2.62	1.89	S 1270 1331	-2.	-13.	3.3	3.3	
A 1828 129	12.9	-31.3	2.78	6.57	SU Aur*					
T 1828 129	12.6	-38.0	7.6	6.4	HIP 22925	0.20	-21.69	2.24	1.28	
S 1828 129	13.	-28.	3.9	3.9	PPM 69760	7.	-27.	5.0	4.9	
HDE 283572					→ A 2387 977	4.6	-27.9	0.95	1.82	
→ HIP 20388	8.54	-27.45	1.57	1.14	T 2387 977	2.4	-27.4	2.2	1.6	
PPM 93450	4.	-33.	2.8	3.0	S 2387 977	-17.	-25.	4.2	4.2	
A 1828 481	11.1	-29.8	1.18	2.69	RW Aur A*					
T 1828 481	9.9	-32.4	3.9	2.8	HIP 23873	11.23	-21.92	7.36	3.91	
S 1828 481	8.	-31.	3.6	3.6	PPM 69942	-12.	-31.	5.4	5.4	
					→ A 2389 955	1.4	-23.3	1.00	0.95	
					T 2389 955	7.5	-26.4	3.1	2.3	
					S 2389 955	-11.	-24.	4.3	4.3	

- V773 Tau VIM solution in Hipparcos. This might indicate a possible double or multiple system, and the given parameters correspond to the photocentre.
- RY Tau VIM solution in Hipparcos. This might indicate a possible double or multiple system, and the given parameters correspond to the photocentre.
- DF Tau The GSC identification of this star is doubtful. The entry should correspond to HIP 20777 (which has a VIM solution in the Hipparcos Catalogue, too), but it is not clear whether the GSC counterpart is GSC 1820 418 or GSC 1820 525.
- UX Tau A The Hipparcos solution for this star is again a VIM solution referring to the photocentre; however, errors are rather large and the parallax is significantly negative. Therefore this solution is not used here for this known double star.
- SU Aur Flagged as possibly double in the Hipparcos Catalogue. The proper motions in right ascension are different in different catalogues, proving this suspicion.
- RW Aur A Flagged as possibly double in the Hipparcos Catalogue. A stochastic solution is given, and the period is suggested to be 2.535 d.

Table A.2: Stars from Table 2.2 (ROSAT stars discovered in the central part of the Taurus-Auriga association), based on the list of Wichmann et al. (1996).

	[mas/a]	μ_α	μ_δ	$\frac{\sigma_{\mu_\alpha}}{\cos \delta}$	σ_{μ_δ}		[mas/a]	μ_α	μ_δ	$\frac{\sigma_{\mu_\alpha}}{\cos \delta}$	σ_{μ_δ}		
HD 285281							RXJ 0432.7+1853						
	A 1258	894	3.9	-10.1	0.97	0.90		PPM 120001	0.	-28.	4.5	4.5	
→	T 1258	894	6.0	-14.0	1.6	1.6	→	A 1274	1501	-2.4	-13.7	1.01	1.18
	S 1258	894	9.	-17.	3.9	3.9		T 1274	1501	-3.1	-11.9	1.6	1.6
HD 284135								S 1274	1501	-1.	-21.	3.5	3.5
	PPM 93240	2.	-25.	3.5	3.5		HD 283798*						
→	A 1814	409	3.9	-14.9	0.87	0.86	→	HIP 21852	-0.79	-20.56	1.35	1.04	
	T 1814	409	2.4	-15.4	1.9	1.7		PPM 93702	-4.	-25.	2.2	2.1	
	S 1814	409	1.	-24.	3.0	3.0		A 1838	81	-3.4	-20.7	0.89	1.52
HD 284149								T 1838	81	-0.5	-22.6	1.8	2.2
	HIP 19176	6.40	-15.40	1.65	1.24			S 1838	81	-106.	62.	5.0	5.0
	PPM 93259	11.	-16.	3.6	3.7		RXJ 0444.9+2717*						
→	A 1258	257	8.0	-15.4	1.64	2.87		A 1839	643	2.2	-25.9	8.33	4.56
	T 1258	257	7.6	-13.0	1.6	2.7	→	T 1839	643	15.4	-20.6	5.8	5.3
	S 1258	257	9.	-17.	2.9	2.9		S 1839	643	-2.	-17.	5.1	5.1
RXJ 0409.2+2901							HD 30171						
→	A 1826	877	23.9	-32.0	2.65	1.89		PPM 120221	18.	-19.	3.7	3.7	
	T 1826	877	22.1	-27.3	2.6	3.0	→	A 1267	425	13.2	-17.5	0.95	0.94
	S 1826	877	38.	-36.	3.5	3.5		T 1267	425	12.5	-19.6	1.7	1.9
RXJ 0415.4+2044								S 1267	425	14.	-24.	4.2	4.2
→	A 1263	1027	3.0	-13.8	3.24	4.02	HD 31281						
	T 1263	1027	1.8	-17.0	1.6	3.5		PPM 120390	-6.	-26.	3.7	3.8	
	S 1263	1027	9.	-13.	4.6	4.6	→	A 1284	1193	-3.3	-18.0	0.87	0.87
BD+17 724B*								T 1284	1193	0.4	-16.8	2.2	1.6
	HIP 20782	-6.24	-33.28	25.67	20.88			S 1284	1193	-8.	-27.	3.8	3.8
	PPM 119907	2.	-7.	3.8	3.8		HD 286179						
→	A 1269	271	2.1	-15.3	0.90	0.89	→	A 1281	1215	-1.5	-17.1	2.29	1.04
RXJ 0430.8+2113								T 1281	1215	1.2	-18.2	2.0	2.7
	A 1277	574	30.0	-25.6	2.02	1.25		S 1281	1215	-5.	-20.	5.1	5.1
→	T 1277	574	30.4	-27.3	1.9	2.1	RXJ 0457.1+3142						
	S 1277	574	24.	-26.	4.4	4.4	→	A 2388	857	-11.2	-14.2	1.24	1.13
HD 284496								T 2388	857	-9.5	-10.9	2.3	2.3
→	A 1277	1238	1.2	-13.6	1.56	2.13		S 2388	857	-4.	-16.	4.4	4.4
	T 1277	1238	4.1	-14.1	2.5	2.1	RXJ 0457.2+1524						
	S 1277	1238	-5.	-8.	4.4	4.4	→	A 1281	1288	8.4	-17.6	1.04	3.45
								T 1281	1288	10.7	-19.9	1.7	2.7
								S 1281	1288	2.	-19.	4.9	4.9

BD+17 724B

Hipparcos could attribute the variability to duplicity, and the entry HIP 20782 corresponds to the B-component. However, the errors of the derived parameters in this solution, without constraints on parallax or proper motions, are quite large (the parallax is not significant), and preference is given to the ACT proper motion.

HD 283798

The STARNET proper motion for this star is quite different from that in the other catalogues, which are in reasonable agreement. It is likely that the rather high STARNET proper motion is spurious, caused by a misidentification of the stars in AC and GSC.

RXJ 0444.9+2717

The proper motions in ACT, TRC and STARNET are slightly different in right ascension and in declination, suggesting the possibility that we may deal with a double or multiple system.

Table A.3: Stars from Table 2.3 (stars south of Taurus), based on the lists of Neuhäuser et al. (1995c, 1997) and Magazzú et al. (1997).

	[mas/a]	μ_α	μ_δ	$\frac{\sigma_{\mu_\alpha}}{\cos \delta}$	σ_{μ_δ}		[mas/a]	μ_α	μ_δ	$\frac{\sigma_{\mu_\alpha}}{\cos \delta}$	σ_{μ_δ}
RXJ 0210.4-1308SW							BD+11 533				
→	PPM 211168	57.	-27.	2.9	3.0	→	HIP 18117	6.52	-16.60	1.79	1.50
	A 5283 1690	57.8	-30.5	2.70	0.90		PPM 119425	13.	-28.	4.9	4.8
	T 5283 1690	52.8	-30.0	2.5	1.9		A 661 452	6.8	-18.5	1.98	2.64
	S 5283 1690	54.	-24.	4.0	4.0		T 661 452	6.7	-17.6	2.1	2.3
							S 661 452	9.	-25.	4.4	4.4
RXJ 0212.3-1330							RXJ 0354.3+0535				
	PPM 211212	156.	-77.	3.0	3.1	→	A 72 921	-0.3	-6.7	1.01	0.98
	A 5283 876	162.6	-80.3	3.94	4.00		T 72 921	-2.2	-10.2	2.5	2.0
→	T 5283 876	163.9	-82.2	1.6	1.6		S 72 921	-3.	-3.	3.9	3.9
	S 5283 876	160.	-81.	4.1	4.1						
HD 15526							RXJ 0357.3+1258				
	PPM 211594	44.	-12.	2.7	2.7	→	A 665 150	22.8	-21.9	2.13	1.48
→	A 5284 686	43.6	-11.1	2.43	1.21		T 665 150	23.7	-24.0	3.4	1.7
	T 5284 686	41.9	-10.8	2.3	1.6		S 665 150	23.	-19.	5.2	5.2
	S 5284 686	47.	-13.	3.8	3.8						
RXJ 0248.3-1117							BD+07 582*				
→	PPM 710125	9.	-13.	3.6	3.6	→	PPM 147110	-12.	-39.	4.6	4.6
	S 5289 1010	11.	-12.	3.8	3.8		T 659 1081	2.2	-26.3	1.7	2.4
							S 659 1081	12.	-6.	3.5	3.5
RXJ 0309.1+0324							HD 286753				
	A 58 166	29.1	-3.2	4.26	1.04	→	A 676 1123	28.7	-24.9	1.09	1.09
→	T 58 166	27.8	-6.6	1.7	2.6		T 676 1123	27.3	-23.6	1.9	2.1
	S 58 166	29.	-9.	3.5	3.4		S 676 1123	27.	-23.	3.4	3.4
RXJ 0312.8-0414NW							RXJ 0427.5+0616				
	A 4711 684	1.5	-9.3	4.81	1.29	→	A 81 1414	5.5	1.4	1.43	1.02
→	T 4711 684	1.6	-11.5	3.8	1.6		T 81 1414	5.3	0.8	1.6	2.0
							S 81 1414	1.	0.	3.5	3.5
RXJ 0317.9+0231							BD+00 760				
→	A 59 24	-19.7	-66.2	1.19	2.74		PPM 147574	54.	-7.	3.8	3.9
	T 59 24	-19.5	-64.6	2.4	3.9		A 75 1529	58.5	-7.1	5.31	0.93
	S 59 24	-16.	-63.	4.2	4.2	→	T 75 1529	59.5	-7.2	2.1	1.7
							S 75 1529	59.	-8.	3.3	3.3
RXJ 0336.0+0846*							RXJ 0429.9+0155				
	HIP 16786	26.30	23.86	8.52	5.37	→	A 75 1	3.6	-3.4	1.07	1.04
→	A 657 726	17.2	22.1				T 75 1	4.2	-4.3	3.8	2.4
	S 657 726	3.	25.	7.4	7.4		S 75 1	-2.	-5.	3.7	3.7
RXJ 0343.6+1039							RXJ 0435.5+0455				
→	A 660 825	-7.2	-28.3	1.10	1.32	→	A 90 936	-6.2	-0.5	1.48	1.02
	T 660 825	-3.9	-29.7	1.9	3.7		T 90 936	-6.0	-1.1	1.6	2.0
	S 660 825	-8.	-29.	3.8	3.8		S 90 936	-12.	1.	3.0	3.0
RXJ 0348.5+0832							BD+05 706				
→	A 658 922	23.1	-21.9	1.10	1.48		PPM 147827	0.	-6.	5.2	5.2
	T 658 922	20.3	-20.4	3.6	5.0		A 91 830	4.6	-7.5	2.31	0.97
	S 658 922	31.	-12.	4.0	4.0	→	T 91 830	1.4	-8.1	1.8	1.8
							S 91 830	2.	-5.	3.9	3.9
BD+12 511*											
	HIP 17878	-35.11	42.34	5.76	3.99						
	PPM 119389	-40.	45.	4.0	3.9						
→	T 664 694	-42.0	43.2	1.7	1.7						

Table A.3: continued.

	[mas/a]	μ_α	μ_δ	$\frac{\sigma_{\mu_\alpha}}{\cos \delta}$	σ_{μ_δ}		[mas/a]	μ_α	μ_δ	$\frac{\sigma_{\mu_\alpha}}{\cos \delta}$	σ_{μ_δ}	
	BD+08 742						RXJ 0442.9+0400					
	PPM 147838	33.	-31.	5.6	5.3		A 91	702	18.8	-18.7	1.86	1.08
	A 682	674	28.7	-25.4	7.51	4.80	T 91	702	14.1	-17.9	4.9	2.2
→	T 682	674	27.9	-25.5	4.6	1.7	S 91	702	16.	-16.	3.6	3.6
	S 682	674	40.	-19.	6.6	6.6		HD 287017				
	RXJ 0442.6+1018						PPM 147895	57.	-75.	4.5	4.3	
	A 686	1246	23.9	-15.3	1.05	1.04	A 687	419	51.9	-65.4	3.90	11.19
→	T 686	1246	25.2	-14.9	1.6	1.9	→ T 687	419	52.9	-64.3	1.7	1.6
	S 686	1246	34.	-29.	5.2	5.2	S 687	419	57.	-72.	5.1	5.1

RXJ 0336.0+0846 The proper motions in right ascension are quite different between the catalogues, suggesting a double or multiple system. Indeed the star is flagged as 'suspected non-single' in Hipparcos and 'dubious astrometric reference star' in Tycho.

BD+12 511 The components of this known double star were solved independently in Hipparcos. The TRC solution however is much more precise and therefore preferred.

BD+07 582 This known double star has two entries in PPM, but only one in TRC and STARNET. The proper motions are quite different, maybe because the components have not been resolved. In order to avoid these difficulties the PPM proper motions have been chosen.

Chamaeleon

Table A.4: Stars from Table 3.1 (stars known before ROSAT in the Chamaeleon region).

	[mas/a]	μ_α	μ_δ	$\frac{\sigma_{\mu_\alpha}}{\cos \delta}$	σ_{μ_δ}		[mas/a]	μ_α	μ_δ	$\frac{\sigma_{\mu_\alpha}}{\cos \delta}$	σ_{μ_δ}
HD 97048						CV Cha*					
→	HIP 54413	-92.19	-1.70	0.82	0.78		HIP 54738	-102.32	-20.11	9.52	9.05
	PPM 370994	-115.	4.	2.7	3.1		HIP 54744	-102.32	-20.11	9.52	9.05
	A 9414 795	-101.7	1.0	5.40	4.85		A 9410 60	-87.8	7.7	6.44	3.99
	T 9414 795	-89.8	-0.6	1.9	1.6	→	T 9410 60	-100.3	2.5	2.1	2.9
HD 97300						CHXR 8					
→	HIP 54557	-94.07	-1.04	1.03	0.89		A 9414 444	-114.9	13.4	2.69	3.77
	PPM 371004	-115.	4.	2.7	3.1	→	T 9414 444	-96.5	6.1	2.0	3.5
	A 9410 2805	-95.4	4.2	3.95	1.67		S 9414 444	-104.	10.	4.2	4.2
	T 9410 2805	-93.7	0.5	1.6	1.6	T Cha*					
Sz 6						→	HIP 58285	-214.50	-9.87	5.08	3.79
→	HIP 53691	-97.03	1.64	2.07	1.76		A 9419 1187	-216.9	-9.3		
	A 9414 186	-112.8	8.2				S 9419 1187	-242.	-9.	4.8	4.8
	S 9414 186	-135.	5.	4.3	4.3	Sz 19*					
→	HIP 54365	-113.29	3.27	3.07	2.91	→	HIP 54365	-113.29	3.27	3.07	2.91
	A 9414 743	-120.8	8.3	3.14	2.17		A 9414 743	-120.8	8.3	3.14	2.17
	T 9414 743	-108.8	10.9	1.6	6.1		T 9414 743	-108.8	10.9	1.6	6.1
	S 9414 743	-106.	45.	4.4	4.5		S 9414 743	-106.	45.	4.4	4.5

- Sz 19 Flagged as possibly double in the Hipparcos Catalogue, where a stochastic solution is given. The proper motions in declination are rather different between the catalogues.
- CV Cha The Hipparcos solution is classified as poor, although two separate entries for this visual binary with a separation of $8''48$ are given. The TRC solution is therefore preferred.
- T Cha Flagged as possibly double in the Hipparcos Catalogue.

Table A.5: Stars from Table 3.2 (stars discovered with ROSAT in the Chamaeleon region).

	[mas/a]	μ_α	μ_δ	$\frac{\sigma_{\mu_\alpha}}{\cos \delta}$	σ_{μ_δ}		[mas/a]	μ_α	μ_δ	$\frac{\sigma_{\mu_\alpha}}{\cos \delta}$	σ_{μ_δ}
RXJ 0837.0-7856						RXJ 0917.2-7744					
	A 9402 921	-147.3	26.2	1.49	1.83		A 9399 2104	-159.9	13.0	2.16	0.87
→	T 9402 921	-153.9	27.6	2.1	1.6	→	T 9399 2104	-174.2	11.2	2.3	1.7
	S 9402 921	-321.	59.	3.7	3.7		S 9399 2104	-180.	7.	3.2	3.2
RXJ 0849.2-7735						RXJ 0919.4-7738N*					
	PPM 370092	-41.	15.	2.7	3.2	→	HIP 45734	-501.70	70.40	1.31	1.15
	A 9399 1491	-36.1	19.9	2.15	2.67		PPM 370271	-509.	69.	2.3	2.6
→	T 9399 1491	-46.1	19.7	2.9	2.1		T 9399 2451	-508.0	62.5	1.6	2.1
	S 9399 1491	-49.	16.	4.6	4.6	RXJ 0928.5-7815					
RXJ 0850.1-7554							PPM 370343	-109.	19.	2.2	2.5
	A 9395 2139	-79.5	31.1	2.21	1.47	→	A 9400 1990	-118.5	17.7	1.00	2.41
→	T 9395 2139	-76.0	32.7	1.7	2.0		T 9400 1990	-123.3	18.3	2.0	3.7
	S 9395 2139	-85.	35.	3.8	3.8	RXJ 0928.5-7815					

Table A.5: continued.

	[mas/a]	μ_α	μ_δ	$\sigma_{\mu_\alpha \cos \delta}$	σ_{μ_δ}		[mas/a]	μ_α	μ_δ	$\sigma_{\mu_\alpha \cos \delta}$	σ_{μ_δ}
RXJ 0936.3-7820						RXJ 1207.9-7555					
→	HIP 47135	-360.66	49.76	0.70	0.64		PPM 785598	-637.	-14.	3.3	3.3
	PPM 370394	-354.	55.	2.4	2.7		A 9412 2105	-639.1	-7.7	3.18	0.86
	A 9400 1713	-358.2	51.1	1.38	3.19	→	T 9412 2105	-636.0	-6.7	1.6	2.9
	T 9400 1713	-365.3	53.0	2.4	1.7		S 9412 2105	-624.	-15.	3.7	3.7
	S 9400 1713	-345.	59.	3.5	3.5	RXJ 1217.4-8035					
RXJ 0951.9-7901						RXJ 1220.6-7539					
	PPM 370508	-164.	40.	3.0	3.5		PPM 377437	16.	-9.	2.2	2.6
→	A 9404 195	-149.4	39.5	0.98	2.67	→	A 9420 439	-5.7	-11.3	2.74	2.33
	T 9404 195	-129.8	38.6	1.7	2.3		T 9420 439	24.5	-8.4	2.1	3.2
	S 9404 195	-145.	38.	4.3	4.3		S 9420 439	28.	-3.	3.7	3.7
RXJ 0952.7-7933						RXJ 1223.5-7740					
	PPM 370518	-75.	9.	2.7	3.2		PPM 371482	-296.	10.	2.1	2.5
	A 9404 1702	-82.2	6.5	1.69	2.13	→	A 9416 555	-306.6	12.2	0.84	0.88
→	T 9404 1702	-76.7	4.7	1.6	2.4		T 9416 555	-299.5	8.8	2.6	1.7
	S 9404 1702	-69.	9.	3.7	3.7		S 9416 555	-295.	12.	3.3	3.3
RXJ 1009.6-8105						RXJ 1225.3-7857					
	PPM 377161	121.	-19.	2.7	3.2		PPM 371498	-146.	-22.	2.6	3.0
	A 9409 1040	86.4	-24.6	2.41	0.87	→	A 9420 742	-123.4	-23.1	4.20	1.03
→	T 9409 1040	104.4	-24.4	1.6	2.1		T 9420 742	-124.3	-21.7	4.9	1.7
	S 9409 1040	136.	-19.	3.6	3.6		S 9420 742	-111.	-26.	4.1	4.1
RXJ 1039.5-7538S*						RXJ 1233.5-7523					
→	HIP 52172	13.26	16.75	1.64	1.40		HIP 61284	-369.64	13.48	1.13	1.10
	T 9397 1228	10.9	21.2	2.6	4.1	→	PPM 371552	-384.	13.	2.4	2.8
RXJ 1125.8-8456*						RXJ 1239.4-7502					
	HIP 55746	-545.22	12.13	0.65	0.55		A 9412 190	-383.2	16.0	0.84	0.84
	PPM 377341	-482.	12.	2.1	2.4	→	T 9412 190	-384.5	17.6	1.7	2.3
	A 9511 1593	-555.5	12.2	0.87	1.35		S 9412 190	-376.	10.	3.6	3.6
→	T 9511 1593	-511.7	10.9	1.8	2.1	RXJ 1307.3-7602					
	S 9511 1593	-388.	9.	3.2	3.2		PPM 785854	-78.	10.	2.8	2.8
RXJ 1158.5-7754a						RXJ 1349.2-7549E					
→	HIP 58400	-197.82	-0.83	1.36	1.15		PPM 372040	-265.	-33.	2.5	2.9
	A 9415 1238	-200.1	-4.4			→	A 9426 682	-267.3	-31.2	1.97	1.19
	S 9415 1238	-220.	-7.	3.9	3.9		T 9426 682	-252.9	-35.1	2.8	1.6
RXJ 1159.7-7601						RXJ 1307.3-7602					
→	HIP 58490	-165.21	-4.74	1.73	1.48		S 9413 2147	-86.	10.	3.2	3.2
	A 9411 2191	-199.5	-7.7	8.73	2.93	RXJ 1307.3-7602					
	T 9411 2191	-188.8	-8.2	2.9	1.9		PPM 785854	-78.	10.	2.8	2.8
	S 9411 2191	-224.	-20.	3.8	3.8	→	A 9413 2147	-57.6	7.4	0.88	2.01
RXJ 1201.7-7859						RXJ 1307.3-7602					
	PPM 785565	-195.	-5.	3.4	3.4		T 9413 2147	-62.2	4.7	2.6	2.7
→	A 9420 1420	-213.2	-5.5	0.84	0.84		S 9413 2147	-86.	10.	3.2	3.2
	T 9420 1420	-208.4	-6.3	1.6	1.7	RXJ 1307.3-7602					
	S 9420 1420	-229.	-8.	4.0	4.0		PPM 785854	-78.	10.	2.8	2.8

RXJ 0919.4-7738N Duplicity was also seen by Hipparcos. The entry corresponds to the A-component.

RXJ 1039.5-7538S Solved as a double star with identical proper motion and parallax in the Hipparcos Catalogue. The solution is classified as good.

RXJ 1125.8-8456 Hipparcos has detected an acceleration of $\mu_\alpha = 4.05 \pm 5.34 \text{ mas/a}^2$ and $\mu_\delta = 1.72 \pm 1.25 \text{ mas/a}^2$.

Lupus

Table A.6: Stars from Table 4.1 (stars known before ROSAT in the Lupus region).

	[mas/a]	μ_α	μ_δ	$\frac{\sigma_{\mu_\alpha}}{\cos \delta}$	σ_{μ_δ}		[mas/a]	μ_α	μ_δ	$\frac{\sigma_{\mu_\alpha}}{\cos \delta}$	σ_{μ_δ}
Sz 68						RY Lup					
→	HIP 77157	-16.79	-20.20	2.17	1.61	→	HIP 78317	-12.28	-22.12	3.13	2.04
	A 7336 1114	-25.2	-22.2	2.55	3.43		A 7842 532	-16.2	-20.7	3.39	3.16
	T 7336 1114	-21.3	-18.7	1.9	4.3		T 7842 532	-11.8	-22.2	2.7	2.7
	S 7336 552	-109.	189.	5.5	5.5	HR 5999*					
Sz 82*						→	HIP 79080	-12.32	-24.25	.85	.72
	HIP 78053	-71.84	-49.97	15.41	7.31		PPM 2947	-8.	-29.	3.1	3.6
→	S 7838 962	-6.	-23.	6.8	6.8		T 7851 1818	-10.8	-22.0	1.8	2.6
Sz 83						HR 6000*					
→	HIP 78094	-13.58	-23.16	3.80	2.14	→	HIP 79081	-8.31	-22.46	.80	.67
	A 7838 546	-13.9	-27.0	1.43	1.15		PPM 2947	-16.	-20.	4.3	4.4
	T 7838 546	-12.2	-30.4	1.6	2.6		T 7851 1817	-7.9	-23.7	1.9	2.2
	S 7838 546	-14.	-28.	5.3	5.3						

Sz 82 A double star separated by $19''$ solved as a closer binary with $4''4$ separation with identical proper motions and parallax in the Hipparcos Catalogue. The solution however is classified as poor, and therefore the STARNET proper motion is preferred.

HR 5999 Flagged as possibly double in the Hipparcos Catalogue. Duplicity is also suspected in the Tycho Catalogue.

HR 6000 The duplicity is clearly indicated from the Tycho data, and indeed this early-type star has a T Tauri companion.

Table A.7: Stars from Table 4.2, based on the lists of Krautter et al. (1997) and Wichmann et al. (1997b).

	[mas/a]	μ_α	μ_δ	$\frac{\sigma_{\mu_\alpha}}{\cos \delta}$	σ_{μ_δ}		[mas/a]	μ_α	μ_δ	$\frac{\sigma_{\mu_\alpha}}{\cos \delta}$	σ_{μ_δ}
RXJ 1412.2-1630						RXJ 1508.7-4400					
→ A 6138	383	-7.0	-6.9	1.11	3.75	A 7833	2559	-28.4	-24.3	3.05	1.33
T 6138	383	-12.0	-9.3	3.4	1.6	→ T 7833	2559	-31.4	-20.0	2.2	3.1
S 6138	383	-9.	-5.	3.4	3.4	S 7833	2559	-34.	-21.	4.7	4.7
RXJ 1419.3-2322						RXJ 1509.3-4420					
PPM 262779	44.	-29.	2.9	2.9		PPM 760905	-6.	-12.	3.9	3.9	
→ A 6731	58	43.6	-30.7	1.15	2.86	A 7833	1240	0.6	-5.6	3.02	4.27
T 6731	58	46.0	-28.6	1.7	3.2	→ T 7833	1240	-1.4	-1.8	1.7	2.5
S 6731	58	43.	-29.	6.0	6.0	S 7833	1240	-1.	-7.	4.1	4.1
RXJ 1450.4-3507						RXJ 1512.8-4508					
A 7305	380	-17.7	-18.4	6.26	1.18	→ A 8294	2230	-31.4	-21.3	2.50	1.26
→ T 7305	380	-17.0	-19.1	4.5	1.6	T 8294	2230	-31.9	-17.9	2.5	1.6
S 7305	380	-18.	-16.	6.0	6.0	S 8294	2230	-28.	-29.	4.4	4.4
RXJ 1457.3-3613						RXJ 1514.2-4103					
PPM 293266	-30.	-16.	2.9	3.0		→ HIP 74565	-26.22	-31.35	2.19	1.59	
A 7310	2431	-34.0	-20.3	3.56	2.87	A 7826	3005	-28.4	-28.4	2.47	3.80
→ T 7310	2431	-29.0	-24.6	1.6	2.6	T 7826	3005	-18.7	-28.1	2.4	1.7
S 7310	2431	-35.	-25.	4.9	4.9	S 7826	3005	-35.	-28.	4.9	4.9
RXJ 1458.6-3541						RXJ 1514.7-3445					
PPM 746423	-32.	-24.	5.3	5.0		PPM 293615	-20.	-20.	2.8	2.6	
→ A 7310	503	-25.8	-26.0	1.18	1.14	→ A 7320	427	-21.1	-21.5	3.61	1.30
T 7310	503	-28.7	-23.8	2.7	2.0	T 7320	427	-21.3	-18.9	3.2	2.5
S 7310	503	-27.	-28.	5.7	5.7	S 7320	427	-22.	-19.	5.7	5.7
RXJ 1459.3-4013						RXJ 1518.4-3738					
PPM 760774	-43.	-29.	5.0	4.8		→ A 7822	158	-22.8	-29.4	2.50	1.22
→ A 7824	1291	-34.4	-26.5	3.59	1.11	T 7822	158	-20.5	-29.4	2.5	1.9
T 7824	1291	-34.6	-27.2	4.3	3.8	S 7822	158	-36.	-37.	5.9	5.9
S 7824	1291	-36.	-19.	5.3	5.3	RXJ 1518.8-4050					
RXJ 1500.8-4331						→ A 7826	2975	-21.6	-22.7	3.37	3.16
→ A 7833	2037	-28.4	-19.3	2.19	1.02	T 7826	2975	-17.7	-21.8	5.1	1.6
T 7833	2037	-38.8	-19.2	1.7	3.6	S 7826	2975	-29.	-25.	5.0	5.0
S 7833	2037	-31.	-27.	4.4	4.4	RXJ 1519.6-4760					
RXJ 1501.2-4121						A 8298	1675	-45.6	-32.1	3.68	4.28
→ A 7829	504	-20.6	-16.3	1.68	3.74	→ T 8298	1675	-49.5	-39.2	1.6	3.2
T 7829	504	-14.8	-15.5	2.0	4.2	S 8298	1675	-50.	-32.	3.8	3.8
S 7829	504	-24.	-14.	3.9	3.9	RXJ 1525.0-3604					
RXJ 1507.2-3505						→ A 7325	212	-17.1	-28.8	2.50	1.28
A 7319	749	-40.6	-28.9	1.55	3.08	T 7325	212	-15.7	-29.5	2.3	1.6
→ T 7319	749	-42.6	-30.8	1.6	1.8	S 7325	212	-21.	-30.	5.9	5.9
S 7319	749	-49.	-32.	5.6	5.6	RXJ 1525.3-3845					
RXJ 1507.9-4515						PPM 293824	-48.	-34.	3.2	3.5	
A 8293	642	37.8	-2.4	3.91	1.43	→ T 7835	2569	-43.1	-30.7	2.3	1.6
→ T 8293	642	36.5	-0.3	3.3	2.3	S 7835	2569	-42.	-35.	5.9	5.9
S 8293	642	33.	-8.	4.3	4.3	RXJ 1526.0-4501					
RXJ 1508.6-4423						A 8295	1530	-28.9	-19.7	1.39	2.96
A 7833	2400	-24.6	-17.2	3.97	3.75	→ T 8295	1530	-19.2	-21.4	1.9	1.9
→ T 7833	2400	-25.2	-7.7	1.8	1.6	S 8295	1530	-23.	-19.	4.8	4.8
S 7833	2400	-24.	-13.	4.1	4.1	RXJ 1526.0-4501					

Table A.7: continued.

	[mas/a]	μ_α	μ_δ	$\sigma_{\cos \delta}^{\mu_\alpha}$	σ_{μ_δ}		[mas/a]	μ_α	μ_δ	$\sigma_{\cos \delta}^{\mu_\alpha}$	σ_{μ_δ}		
RXJ 1529.6-3546						RXJ 1603.8-3938							
	PPM 293919	-32.	-24.	3.6	3.5		A 7855	1106	-30.9	-28.2	6.44	2.17	
→	A 7326	928	-27.4	-27.0	4.94	2.04	→	T 7855	1106	-24.4	-30.6	5.8	2.3
	T 7326	928	-22.1	-25.0	2.5	4.1		S 7855	1106	-26.	-32.	5.4	5.4
	S 7326	928	-22.	-35.	5.2	5.2	RXJ 1604.5-3207						
RXJ 1531.3-3329						→	A 7334	429	-21.1	-25.5	3.45	2.83	
→	A 7318	593	-26.4	-30.7	1.80	1.41		T 7334	429	-12.4	-30.9	4.7	1.7
	T 7318	593	-30.2	-34.1	3.5	5.2		S 7334	429	-21.	-27.	4.8	4.8
	S 7318	593	-23.	-32.	6.1	6.1	RXJ 1605.0-3857						
RXJ 1534.1-3916						→	HIP 78774		-34.13	-46.60	1.40	1.26	
→	A 7836	1509	-35.1	-28.5	1.75	2.76		PPM 294630		-45.	-50.	2.7	3.1
	T 7836	1509	-27.9	-29.3	4.4	4.7		A 7851	305	-38.5	-49.1	1.05	1.39
	S 7836	1509	-30.	-28.	4.0	4.0		T 7851	305	-38.5	-46.0	2.1	2.3
RXJ 1538.7-4411							S 7851	305	-50.	-46.	5.3	5.3	
→	PPM 761327		-33.	-26.	3.9	3.9	RXJ 1605.7-3905						
	A 7848	1659	-33.0	-29.4	4.54	5.88		PPM 747449		-36.	-32.	5.1	4.8
	T 7848	1659	-28.9	-18.5	1.6	3.1	→	A 7851	1	-23.9	-31.6	1.29	1.04
	S 7848	1659	-29.	-28.	4.0	4.0		T 7851	1	-21.9	-29.5	2.8	1.9
RXJ 1544.0-3311							S 7851	1	-31.	-38.	5.3	5.3	
→	A 7331	782	-25.5	-25.7	1.19	1.13	RXJ 1608.9-3905						
	T 7331	782	-22.8	-29.9	1.8	1.7		A 7851	426	-14.6	-28.3	2.44	2.97
	S 7331	782	-28.	-24.	5.4	5.4	→	T 7851	426	-12.8	-28.9	1.6	1.6
RXJ 1545.9-4222							S 7851	426	-12.	-33.	5.0	5.0	
	PPM 761408		-41.	-32.	3.9	3.9	RXJ 1621.2-4030						
	A 7845	1174	-28.4	-28.6	2.83	0.94	→	PPM 321619		-12.	-27.	2.9	2.9
→	T 7845	1174	-23.3	-25.8	1.7	1.9		A 7857	648	-16.9	-26.9	1.34	0.98
	S 7845	1174	-36.	-30.	3.5	3.5		T 7857	648	-10.7	-24.9	2.7	2.1
RXJ 1549.7-3925*							S 7857	648	-9.	-28.	4.1	4.1	
→	HIP 77524		-31.66	-25.17	1.99	1.79	RXJ 1623.5-4030						
	A 7841	92	-27.6	-26.4	1.24	1.11		PPM 294997		-21.	-25.	3.8	3.7
	T 7841	92	-27.6	-25.9	2.6	1.6		A 7857	514	-16.2	-24.0	2.33	0.97
	S 7841	92	-23.	-27.	4.2	4.2	→	T 7857	514	-15.1	-28.6	1.9	1.8
RXJ 1559.8-3628*							S 7857	514	-17.	-29.	4.2	4.2	
	HIP 78345		-20.15	-48.89	2.79	2.57	HD 147454						
	A 7341	574	-36.9	-44.9				PPM 294998		-30.	-25.	3.0	2.9
→	S 7341	574	-31.	-43.	6.0	6.0	→	A 7352	572	-24.9	-24.9	1.44	1.89
RXJ 1601.1-3320							T 7352	572	-17.9	-28.7	1.8	2.8	
→	A 7333	719	-13.2	-20.4	2.85	2.24		S 7352	572	-26.	-18.	4.4	4.4
	T 7333	719	-10.3	-24.3	1.9	4.7	SAO 207620						
	S 7333	719	-19.	-19.	4.6	4.6		PPM 295001		-24.	-26.	3.0	2.9
RXJ 1603.8-4355*						→	A 7352	908	-19.1	-31.1	3.49	1.71	
→	HIP 78684		-19.62	-25.52	2.43	1.93		T 7352	908	-15.3	-35.6	2.5	2.9
	PPM 321316		-20.	-28.	2.9	3.0		S 7352	908	-22.	-23.	4.4	4.4
	A 7863	1629	-19.4	-22.5	2.51	0.91	SAO 207620						
	T 7863	1629	-20.6	-20.1	1.7	1.6		PPM 295001		-24.	-26.	3.0	2.9
	S 7863	1629	-22.	-24.	4.0	4.0	→	A 7352	908	-19.1	-31.1	3.49	1.71

RXJ 1549.7-3925 Flagged as possibly double in the Hipparcos Catalogue.

RXJ 1559.8-3628 Flagged as possibly double in the Hipparcos Catalogue.

RXJ 1603.8-4355 Double star processing in the Hipparcos Catalogue. The solution corresponds to the photo-centre and is classified as good, with a separation of $0''.290$ for the components.

Scorpius-Centaurus

Table A.8: Stars from Table 5.1 (based on the list of Walter et al. 1994).

	[mas/a]	μ_α	μ_δ	$\frac{\sigma_{\mu_\alpha}}{\cos \delta}$	σ_{μ_δ}		[mas/a]	μ_α	μ_δ	$\frac{\sigma_{\mu_\alpha}}{\cos \delta}$	σ_{μ_δ}
NTTS 155203-2338						NTTS 160946-1851					
	PPM 264851	-33.	-34.	3.3	3.2		PPM 231356	-13.	-27.	4.7	4.6
→	A 6779 1372	-34.1	-39.4	2.20	1.58		A 6209 1316	-14.9	-28.6	4.72	6.89
	T 6779 1372	-34.1	-40.2	4.5	3.0	→	T 6209 1316	-12.4	-22.2	4.7	2.3
	S 6779 1372	-28.	-47.	6.1	6.1		S 6209 1316	-18.	-25.	6.5	6.5
NTTS 155220-2313						NTTS 161431-2256					
→	HIP 77960	-17.89	-26.46	1.31	0.98		PPM 265362	-13.	-22.	4.1	4.0
	PPM 264862	-15.	-22.	2.7	2.6	→	T 6793 501	-12.8	-17.1	2.3	5.6
	A 6779 791	-18.2	-23.6	1.44	4.54		S 6793 501	-16.	-14.	5.4	5.4
	T 6779 791	-21.2	-24.0	2.2	2.3						
	S 6779 791	-10.	-36.	5.5	5.5						

Table A.9: Stars from Table 5.2 (based on the list of Kunkel et al. 1999).

	[mas/a]	μ_α	μ_δ	$\frac{\sigma_{\mu_\alpha}}{\cos \delta}$	σ_{μ_δ}		[mas/a]	μ_α	μ_δ	$\frac{\sigma_{\mu_\alpha}}{\cos \delta}$	σ_{μ_δ}
RXJ 1524.2-3030						RXJ 1535.2-2828*					
	A 7313 421	-26.1	-28.9	1.17	3.38	→	HIP 76304	14.33	-75.24	1.01	0.86
→	T 7313 421	-28.6	-25.7	1.9	2.6		PPM 264418	19.	-74.	2.7	2.6
	S 7313 421	-32.	-27.	6.0	6.0		A 6776 381	21.6	-75.7	3.22	1.65
RXJ 1528.7-3117*						RXJ 1537.0-3136					
→	HIP 75769	27.99	40.14	2.75	3.12	→	PPM 294055	-31.	-32.	2.9	2.7
	PPM 293902	19.	44.	2.7	2.6		T 7327 1934	-34.1	-32.0	6.5	3.8
	A 7314 1305	26.0	58.2	1.03	1.33	RXJ 1538.2-3229					
	S 7314 1305	29.	46.	4.5	4.5		PPM 747046	-42.	-30.	4.6	4.4
RXJ 1529.4-2850*						→	A 7331 52	-41.3	-24.3	3.20	2.90
→	HIP 75836	-57.80	-54.02	1.37	1.26		T 7331 52	-40.2	-22.4	2.3	2.1
	PPM 264316	-64.	-55.	2.7	2.6		S 7331 52	-41.	-26.	5.2	5.2
	A 6776 1380	-59.4	-55.4	3.63	2.66	RXJ 1539.4-2958					
	T 6776 1380	-60.1	-52.9	1.7	1.7	→	HIP 76675	2.17	39.88	1.45	1.18
	S 6776 1380	-69.	-64.	5.8	5.8		PPM 294091	-2.	42.	2.9	3.0
RXJ 1530.4-3218*							A 7335 861	-0.6	40.8	4.18	3.64
→	HIP 75924	-33.48	-31.72	2.82	2.77		T 7335 861	7.6	38.1	3.1	2.8
	PPM 293929	-32.	-31.	2.8	2.6		S 7335 861	-1.	43.	5.8	5.8
	A 7318 1482	-28.4	-21.4	3.37	1.05	RXJ 1544.0-3311					
	S 7318 1482	-32.	-36.	5.4	5.4	→	A 7331 782	-25.5	-25.7	1.19	1.13
RXJ 1531.3-3329							T 7331 782	-22.8	-29.9	1.8	1.7
→	A 7318 593	-26.4	-30.7	1.80	1.41		S 7331 782	-28.	-24.	5.4	5.4
	T 7318 593	-30.2	-34.1	3.5	5.2						
	S 7318 593	-23.	-32.	6.1	6.1						

Table A.9: continued.

	[mas/a]	μ_α	μ_δ	$\frac{\sigma_{\mu_\alpha}}{\cos \delta}$	σ_{μ_δ}		[mas/a]	μ_α	μ_δ	$\frac{\sigma_{\mu_\alpha}}{\cos \delta}$	σ_{μ_δ}
RXJ 1545.2-3417						RXJ 1551.9-2621					
→	HIP 77157	-16.79	-20.20	2.17	1.61		PPM 264787	-27.	-39.	3.1	2.9
	A 7336 1114	-25.2	-22.2	2.55	3.43	→	A 6786 1545	-24.5	-39.0	1.05	2.11
	T 7336 1114	-21.3	-18.7	1.9	4.3		T 6786 1545	-24.3	-43.0	1.7	1.6
RXJ 1545.8-3020						RXJ 1555.8-2512					
→	HIP 77199	-78.97	-99.66	1.13	0.93		PPM 264873	-26.	-17.	4.1	3.6
	PPM 294230	-77.	-112.	2.6	2.6	→	A 6783 2045	-27.3	-17.1	2.20	1.07
	A 7328 388	-81.9	-104.1	1.05	2.93		T 6783 2045	-29.1	-13.6	3.4	1.6
	T 7328 388	-84.1	-103.9	1.7	2.8	RXJ 1558.2-2328					
	S 7328 388	-82.	-108.	5.9	5.9		PPM 264931	-18.	-26.	3.0	2.9
RXJ 1546.1-2804							A 6779 780	-11.6	-20.1	2.93	1.93
	PPM 264663	-68.	-26.	2.7	2.6	→	T 6779 780	-16.9	-20.1	1.6	2.8
→	T 6786 811	-70.4	-23.3	4.7	2.6		S 6779 780	-14.	-27.	5.6	5.6
	S 6786 811	-68.	-14.	8.9	8.9	RXJ 1600.0-2509					
RXJ 1548.0-2908							PPM 264970	-13.	-22.	4.1	3.6
	PPM 732360	-25.	-25.	5.1	4.5		A 6783 1747	-15.8	-21.7	1.07	1.15
→	A 6790 1227	-28.5	-23.3	1.17	3.85	→	T 6783 1747	-16.6	-24.2	2.3	1.9
	T 6790 1227	-28.2	-30.0	1.6	2.1		S 6783 1747	-18.	-19.	5.4	5.4
	S 6790 1227	-23.	-24.	5.5	5.5	RXJ 1601.3-2652					
RXJ 1549.0-3102						→	HIP 78483	-12.72	-21.50	1.50	1.31
→	A 7328 1706	-22.5	-23.0	1.21	2.07		PPM 265003	-14.	-26.	3.7	3.3
	T 7328 1706	-31.5	-20.8	3.1	3.5		A 6787 1367	-11.1	-27.2	2.97	2.25
	S 7328 1706	-22.	-21.	5.8	5.8		T 6787 1367	-10.3	-26.1	1.8	2.8
RXJ 1549.3-2600							S 6787 1367	-23.	-20.	4.9	4.9
→	A 6782 878	-16.5	-28.3	1.31	2.61	RXJ 1601.9-2008					
	T 6782 878	-11.5	-31.6	2.2	2.3		PPM 732499	-12.	-23.	5.0	4.8
	S 6782 878	-23.	-30.	5.3	5.3	→	A 6208 1543	-5.4	-23.3	4.32	1.52
RXJ 1550.9-2534							T 6208 1543	-7.0	-22.8	4.8	3.4
	PPM 264766	-17.	-22.	3.1	2.9		S 6208 1543	-12.	-23.	5.3	5.3
	A 6782 178	-13.2	-19.3	4.16	2.13	RXJ 1603.6-2245					
→	T 6782 178	-14.0	-19.9	1.6	2.7		A 6780 56	-20.1	-23.7	5.23	6.05
	S 6782 178	-16.	-19.	5.7	5.7	→	T 6780 56	-26.7	-27.4	1.7	4.4
RXJ 1528.7-3117							S 6780 56	-16.	-21.	6.7	6.7

RXJ 1528.7-3117 Solved as a double star with identical proper motion and parallax in the Hipparcos Catalogue. The entry corresponds to the A-component, and the solution is classified as good.

RXJ 1529.4-2850 Flagged as possibly double in the Hipparcos Catalogue.

RXJ 1530.4-3218 Solved as a double star with identical proper motion and parallax in the Hipparcos Catalogue. The entry corresponds to the A-component, and the solution is classified as good.

RXJ 1535.2-2828 Hipparcos has detected an acceleration of $\mu_\alpha = 6.04 \pm 6.55 \text{ mas/a}^2$ and $\dot{\mu}_\delta = 2.75 \pm 2.08 \text{ mas/a}^2$.

Table A.10: Stars from Table 5.3 (based on the list of Preibisch et al. 1998).

	[mas/a]	μ_α	μ_δ	$\frac{\sigma_{\mu_\alpha}}{\cos \delta}$	σ_{μ_δ}		[mas/a]	μ_α	μ_δ	$\frac{\sigma_{\mu_\alpha}}{\cos \delta}$	σ_{μ_δ}		
GSC 6762 1092						GSC 6213 306							
	A 6762	1092	3.2	-1.1	5.71	4.60		PPM 732645	-20.	-28.	4.6	4.4	
→	T 6762	1092	8.1	-2.3	2.2	1.6		A 6213	306	-15.9	-22.0	2.19	1.47
	S 6762	1092	2.	-4.	5.9	5.9	→	T 6213	306	-15.6	-23.2	2.6	2.7
GSC 6762 602						GSC 6793 819							
	A 6762	602	-23.0	-17.0	2.67	5.34		A 6793	819	-15.0	-22.3	1.60	3.05
→	T 6762	602	-14.4	-17.7	1.8	2.8		T 6793	819	-9.9	-24.0	3.1	3.6
	S 6762	602	-20.2	-17.4	6.3	6.3	→	S 6793	819	-13.	-23.	5.5	5.5
GSC 6771 369						GSC 6797 599							
	A 6771	369	-49.8	-28.5	7.85	1.14		A 6797	599	-22.1	-19.6	1.15	2.65
→	T 6771	369	-49.7	-32.7	5.3	3.6	→	T 6797	599	-14.0	-24.0	1.9	1.6
	S 6771	369	-49.	-32.	5.6	5.6		S 6797	599	-42.	-22.	5.8	5.8
GSC 6768 1212						GSC 6793 1406							
→	PPM 732235	-24.	-13.	4.3	3.8			PPM 265328	-19.	-20.	4.5	4.1	
	A 6768	1212	-24.6	-5.6	3.09	2.54		A 6793	1406	-13.2	-25.5	1.98	2.11
	T 6768	1212	-21.2	-7.9	3.3	4.5	→	T 6793	1406	-10.2	-23.0	1.6	1.9
	S 6768	1212	-23.	-11.	5.0	5.0		S 6793	1406	-9.	-27.	6.0	6.0
GSC 6781 1046						GSC 6214 2006							
	A 6781	1046	-20.3	-23.3	1.15	1.50		PPM 732703	-1.	-24.	5.2	5.0	
→	T 6781	1046	-17.3	-28.7	1.6	2.5	→	A 6214	2006	-1.1	-23.3	1.58	1.25
	S 6781	1046	-15.	-26.	5.1	5.1		T 6214	2006	1.4	-25.3	2.3	1.9
GSC 6198 166						GSC 6210 676							
	A 6198	166	19.5	-54.1	4.79	1.85	→	PPM 265457	-14.	-19.	3.5	3.4	
→	T 6198	166	14.5	-53.0	1.6	3.4		S 6210	676	-15.	-25.	5.1	5.1
	S 6198	166	19.	-54.	6.7	6.7	GSC 6794 156						
GSC 6191 274						GSC 6794 156							
	PPM 231025	-16.	-16.	4.2	4.1			PPM 265501	-16.	-23.	3.4	3.4	
→	A 6191	274	-15.2	-22.1	5.38	2.34		A 6794	156	-17.1	-25.3	2.41	3.39
	T 6191	274	-9.5	-24.9	4.1	2.5	→	T 6794	156	-17.9	-33.9	2.1	2.0
	S 6191	274	-21.	-21.	5.6	5.6		S 6794	156	-13.	-35.	6.7	6.7
GSC 6784 39						GSC 6784 39							
→	A 6784	39	-14.0	-25.5	1.05	1.04							
	T 6784	39	-4.5	-24.0	3.2	1.9							
	S 6784	39	-14.	-30.	5.1	5.1							

Danksagung

An dieser Stelle möchte ich mich gerne bei allen bedanken, die zum Gelingen dieser Arbeit beigetragen haben.

Mein besonderer Dank gilt zunächst Herrn Prof. Dr. Fuchs für die Betreuung dieser Arbeit sowie für die Flexibilität bezüglich des Themas; ohne ihn wäre diese Arbeit sicher nicht zustande gekommen.

Herrn Dr. Röser danke ich ebenfalls herzlich für die Betreuung dieser Arbeit sowie den interessanten Themenvorschlag; ohne entsprechende Vorarbeiten wäre der Start sehr viel schwieriger gewesen.

Bei Herrn Prof. Dr. Wielen bedanke ich mich für die Möglichkeit, meine Doktorarbeit am Astronomischen Rechen-Institut Heidelberg anzufertigen.

Herrn Prof. Dr. Krautter danke ich für die Bereitschaft, das Zweitgutachten anzufertigen.

Allen Doktoranden sowie allen Mitarbeiterinnen und Mitarbeitern des Astronomischen Rechen-Instituts danke ich für die stete Hilfsbereitschaft und angenehme Atmosphäre.

Für zahlreiche Diskussionen, Anregungen und Hilfestellungen nicht nur während der Endphase dieser Arbeit danke ich Holger Baumgardt, Michael Biermann, Heiko Reffert und Stefan Mayr.

Herrn Dr. Bastian danke ich für sein Interesse an meiner Arbeit und für einige wertvolle Hinweise. Herrn Prof. Dr. Schwan bin ich für die Überlassung von Programmen sowie Diskussionen zur Konvergenzpunktmethodologie zu Dank verpflichtet.

Bei Ralph Neuhäuser, Michael Sterzik, Juan Alcalá, Elvira Covino, Wolfgang Brandner, Thomas Preibisch, Rainer Wichmann, Rainer Köhler und Michael Kunkel möchte ich mich für die fruchtbare Zusammenarbeit, gemeinsame Veröffentlichungen, die zum Teil auch Gegenstand dieser Arbeit sind, und/oder die Bereitstellung von noch nicht veröffentlichtem Datenmaterial bedanken.

Der DFG danke ich für die finanzielle Unterstützung im Rahmen des Schwerpunktprogramms *Physik der Sternentstehung*.

An dieser Stelle möchte ich es auch nicht versäumen, meinen Lehrern Herrn Janson, Herrn Dr. Breunig, Herrn Hörter und Herrn Schardt dafür zu danken, daß sie mir die Grundlagen naturwissenschaftlichen Denkens beigebracht und mich zum Physikstudium ermuntert haben.

Schließlich danke ich meinen Eltern, die sich die Mühe gemacht haben, die Tabellen in dieser Arbeit durchzusehen und mich auch sonst immer unterstützt haben!